CHAN YI MIN

B.Sc.(Hons) Chemistry

2024

GREEN SYNTHESIS OF COPPER OXIDE NANOPARTICLES (CuO NPs) USING ORANGE (*Citrus sinensis*) PEEL EXTRACT AND THEIR PHOTOCATALYTIC PERFORMANCE ON ROSE BENGAL B DYE

CHAN YI MIN

BACHELOR OF SCIENCE (HONOURS)
CHEMISTRY

FACULTY OF SCIENCE

UNIVERSITI TUNKU ABDUL RAHMAN

MAY 2024

GREEN SYNTHESIS OF COPPER OXIDE NANOPARTICLES (CuO NPs) USING ORANGE (*Citrus sinensis)* PEEL EXTRACT AND THEIR PHOTOCATALYTIC PERFORMANCE ON ROSE BENGAL B DYE

By

CHAN YI MIN

A project report submitted to the Department of Chemical Science

Faculty of Science

Universiti Tunku Abdul Rahaman

in partial fulfilment of the requirements for the degree of

Bachelor of Science (Hons) Chemistry

May 2024

ABSTRACT

GREEN SYNTHESIS OF COPPER OXIDE NANOPARTICLES (CuO NPs) USING ORANGE (*Citrus sinensis*) PEEL EXTRACT AND THEIR PHOTOCATALYTIC PERFORMANCE ON ROSE BENGAL B DYE

CHAN YI MIN

Copper oxide nanoparticles (CuO NPs) are synthesized through green synthesis, utilizing the natural phytochemicals present in orange (Citrus sinensis) peel as green stabilizing and reducing agents. This synthesis route offers several advantages, including higher sustainability, eco-friendliness, lower cost, reduced generation of toxic chemical waste, and the utilization of a renewable source of stabilizing and reducing agents in the synthesis process. CuO NPs are synthesized using copper (II) nitrate trihydrate and copper (II) acetate monohydrate as precursor salts, along with orange peel extract (OPE) prepared using boiling, soaking, and maceration methods, followed by calcination at 450°C and 500°C for 2 hours. The green-synthesized CuO NPs were characterized by using various analytical tools such as X-ray diffraction (XRD), field emission scanning electron microscopy (FE-SEM), Fourier transform infrared spectroscopy (FTIR), UV-Vis absorption spectroscopy (UV-Vis), and Energy Dispersive X-ray (EDX). The effects of OPE preparation method, calcination temperature, and type of precursor salt on green-synthesized CuO NPs were studied through

a comparison of characterization results of CuO NPs synthesized under different conditions (type of OPE, type of precursor salt, and calcination temperature). The optimized synthesis conditions for CuO NPs were determined. The photocatalytic activity of OPE-mediated CuO NPs under the optimized conditions was studied using an aqueous Rose Bengal B (RBB) dye solution under an 18-Watt UV light, monitored with a UV-Vis spectrophotometer. It was observed that 91.29% of RBB dye was degraded in the presence of OPE-mediated CuO NPs under 18-Watt UV light.

ABSTRAK

SINTESIS ZARAH NANO KUPRUM OKSIDA DENGAN MENGGUNAKAN EKSTRAK KULIT OREN DAN AKTIVITI FOTOKATALITIKNYA DENGAN RBB

CHAN YI MIN

Zarah nano kuprum oksida (CuO NPs) disintesis melalui sintesis hijau, dengan menggunakan fitokimia semula jadi yang terdapat dalam kulit oren sebagai agen penstabilan dan penurun semula jadi. Laluan sintesis ini menawarkan beberapa kelebihan, termasuk kelestarian yang lebih tinggi, kelestarian alam, kos yang lebih rendah, pengurangan pembentukan sisa kimia toksik, dan penggunaan sumber penstabilan dan penurun semula jadi yang boleh dioptimumkan dalam proses sintesis. CuO NPs disintesis menggunakan garam prekursor kuprum (II) nitrat trihidrat dan kuprum (II) asetat monohidrat, bersama-sama dengan ekstrak kulit oren (OPE) yang disediakan menggunakan kaedah mendidih, merendam, dan maserasi, diikuti dengan pengkalsinan pada suhu 450°C dan 500°C selama 2 jam. CuO NPs yang disintesis secara hijau dicirikan oleh XRD, FE-SEM, FTIR, UV-Vis, dan EDX. Kesan kaedah penyediaan OPE, suhu pengkalsinan, dan jenis garam prekursor terhadap CuO NPs yang disintesis secara hijau dikaji melalui pembandingan hasil karakterisasi CuO NPs yang disintesis dalam keadaan yang berbeza (jenis OPE, jenis garam perentang, dan suhu pengkalsinan). Keadaan sintesis yang dioptimumkan bagi CuO NPs

ditentukan. Aktiviti fotokatalisis CuO NPs yang dimediasi oleh OPE dalam keadaan yang dioptimumkan dikaji menggunakan larutan pewarna RBB yang akuatik di bawah cahaya UV 18-Watt, dipantau dengan spektrofotometer UV-Vis. Diperhatikan bahawa 91.29% pewarna RBB telah diuraikan dengan kehadiran CuO NPs yang dimediasi oleh OPE di bawah cahaya UV 18-Watt.

ACKNOWLEDGEMENTS

I am deeply thankful to Dr. Mohammod Aminuzzaman for his invaluable supervision and guidance throughout my final year project. His advice at every stage has been instrumental in shaping the direction of my work. I am also grateful for his support and for granting me the opportunity to undertake this project, which has been a significant learning experience for me.

I extend my sincerest appreciation to Mr. Chan Yu Bin, a PhD student under my supervisor, whose guidance and suggestions have been invaluable throughout the duration of my project. Their expertise has greatly contributed to the successful completion of my final year project.

Furthermore, I wish to express my gratitude to the staff and officers of the UTAR DCS lab for their assistance and guidance in waste management and the operation of various instruments.

Lastly, I am deeply thankful to my family and friends for their unwavering support and encouragement throughout this journey

DECLARATION

I affirm that the project report is a product of my own original efforts, with proper acknowledgment given to any quotations and citations utilized. Furthermore, I confirm that this work has not been submitted for any other degree at UTAR or any other educational institutions, either previously or simultaneously.

Chan Yi Min

Date: MAY 2024

APPROVAL SHEET

The final year project titled **"GREEN SYNTHESIS OF CuO NANOPARTICLES USING ORANGE *(CITRUS SINENSIS)* PEEL AND THEIR PHOTOCATALYTIC PERFORMANCE ON ROSE BENGAL B DYE"** was prepared by CHAN YI MIN and submitted in partial fulfilment of the requirement for the degree of Bachemor of Science (Hons) Chemistry at Universiti Tunku Abdul Rahman

Approved By:

(Ass. Prof. Dr. Mohammad Aminuzzaman) Date: MAY 2024

Supervisor

Department of Chemical Science

Faculty of Science

Universiti Tunku Abdul Rahman

Faculty of Science

Universiti Tunku Abdul Rahman

Date: May 2024

Permission Sheet

It is hereby that **CHAN YI MIN** (ID No: **20ADB01022**) has completed this final year project titled **"GREEN SYNTHESIS OF CuO NANOPARTICLES USING ORANGE *(CITRUS SINENSIS)* PEEL AND THEIR PHOTOCATALYTIC PERFORMANCE ON ROSE BENGAL B DYE"** under the supervision of Asst. Prof. Dr. Mohammod Aminuzzaman from Department of Chemical Science.

I hereby give permission to the University to upload the softcopy of my final year project report in PDF format into the UTAR Institutional Repository, which may be accessible to the UTAR community and public.

Yours truly

(CHAN YI MIN)

TABLE OF CONTENTS

LIST OF TABLES

LIST OF FIGURES

LIST OF ABBREVATIONS

A	Absorption coefficient
A_o	Initial absorbance of dye solution before exposure to UV lamp
A_t	Absorbance of dye solution at different time intervals, t
BOPE	Orange peel extract prepared though boiling method
c	Speed of light
CB	Conduction band
cm^{-1}	Reciprocal centimetre (wavenumber)
Cu	Copper
Cu^0	Copper atom
Cu^{2+}	Copper (II) ion
CuO	Copper (II) oxide
CuO NPs	Copper (II) oxide nanoparticles
D	Crystalline diameter in
e^-	Electron
EDX	Energy Dispersive X-ray spectroscopy
E_g	Energy bandgap
E_{CB}	Conduction band
E_{VB}	Valence band
eV	Electron Volt
FE-SEM	Field Emission- Scanning Electron Microscope
FWHM	Full width half maximum width

FTIR	Fourier Transform Infrared Spectroscopy
g	gram
H	Plank's constant
h^+	Hole
H_2O	Water molecule
H_2O_2	Hydrogen peroxide
$HO_2^{\cdot -}$	Superoxide radical
hv	Incident photon energy
ICDD	International Centre for Diffraction Data
K	Scherrer constant
kV	Kilovolt
mg	Milligram
ml	Millilitre
MOPE	Orange peel extract prepared through maceration method
nm	Nanometre
O	Oxygen
O_2	Oxygen molecule
O_2^-	Superoxide anion
OH^-	Hydroxyl anion
$OH\cdot$	Hydroxyl radical
OPE	Orange Peel Extract
ppm	Parts per million
RBB	Rose Bengal B
SOPE	Orange peel extract prepared through soaking method
UV-Vis	Ultraviolet Visible

VB	Valence band
XRD	X-ray diffraction
π	Pi bonding orbital
π^*	Pi antibonding orbital
$^{\circ}C$	Degree Celsius
$\mu g/m^3$	Microgram per cubic metre
%	Percentage
χ	Absolute electronegativity of CuO NPs
λ	Wavelength
λ_{max}	Wavelength at maximum absorbance

Chapter 1

INTRODUCTION

1.0 Background of study

Although public awareness of the importance of environmental conservation has increased in recent years, it cannot be denied that pollution has already made a significant impact on the environment and continues to bring negative impacts on the environment, humans and other living organisms alike. Water pollution stands out as one of the most pressing issues requiring immediate action to prevent further damage as water is a vital resource for the survival of all living organisms on Earth. Major contributors to water pollution include large-scale industrialization, agricultural activities, sewage water treatment, and more (Lin *et al*., 2022). Dye pollution, in particular, poses a serious threat to the environment, habitats, and human health, as dye molecules often possess toxic and carcinogenic properties.

The Sungai Kim Kim incident that occurred in Johor, Malaysia, back in 2019 showed how dye pollution would affect the air, water, soil, plants and humans alike. The illegal dumping of concentrated dye waste into the river body caused the formation of toxic hydrogen cyanide fumes that easily travels with the wind, causing nearby residents to suffer from varying degrees of poisoning, with symptoms of headaches and nausea. This incident underscored the importance of proper dye effluent

treatment and the urgent need for effective dye removal agents or catalysts. While various methods for dye effluent treatments are available and used in the textile industry, such as dye adsorption, chemical precipitation, chemical oxidation or reduction, and electrochemical treatment, these methods often rely on the use of chemicals or energy, leading to further waste generation.

This study focuses on green synthesis copper oxide nanoparticles (CuO NPs) as a sustainable alternative for treating dye waste. It reduces the reliance on excessive chemicals and energy which lowers the cost of waste treatment. In a study conducted by Karuppannan *et al*. (2021), green-synthesized CuO NPs from *Cardiospernum halicacabum* leaves were able to degrade methylene blue solution with an efficiency of up to 93.6 % in 210 minutes. Another study involving the synthesis of CuO NPs using *Carica papaya* leaves yielded CuO NPs capable of degrading Coomassie brilliant blue dye R-250 with an efficiency of up to 25 % in 90 minutes. Additionally, green-synthesized CuO NPs using papaya peel were capable of degrading palm oil mill effluent (POME) within 3 hours with an efficiency of 66 % (Phang *et al*., 2021). While the application of green-synthesized CuO NPs shows promise as a viable method for dye waste treatment, further research is needed to make dye waste treatment more sustainable and cost-effective while addressing both plant matter and dye waste management issues.

1.1 CuO

Copper, one of the most abundant minerals on Earth's crust, has historically been utilized in various forms for different purposes, such as bronze or alloy products that were utilized in the form of cutlery, coins, and bells (Royal Society of Chemistry, 2024). On the other hand, CuO either in bulk form or nanoparticle form is a metal oxide that finds itself with various functions being able to be applied in the various fields of science. The wide application of CuO is contributed by the physical, magnetic, and optical properties that make it an attractive material to be utilized for catalysts, solar cells, gas sensors, and in field emission (Phiwdang *et al*., 2013).

In recent years, copper oxide nanoparticles (CuO NPs) have emerged as important semiconductors with diverse applications in chemical and biological fields. CuO NPs typically exhibit a relatively narrow bandgap of around 1.2 eV and possess antimicrobial properties, making them attractive for numerous applications (Phiwdang *et al*., 2013). These nanoparticles come in various nanostructures, including nanorods, nanowires, nanoparticles, nanoneedles, and nanoflowers, with nanoparticles being the most synthesized form of CuO NPs, often through green synthesis methods (Phiwdang *et al*., 2013).

1.2 Green Synthesis of Nanoparticles

Green Chemistry is a field of chemistry that follows twelve working principles to reduce or even eliminate the use and generation of toxic substances that pose a threat to humans, animals, and the environment in the manufacturing and synthesis of products. Although chemical and physical synthesis still dominate the field of nanomaterial synthesis in current times, it is slowly and gradually being replaced by green synthesis, which reduces the use of toxic chemicals, excessive energy, and high-end complex machinery in the synthesis of nanomaterials (Ying *et al*., 2022). Green synthesis emphasizes the reduction of toxic chemical use, lowering energy consumption, reducing the involvement of high-end machinery, and increasing the use of renewable and safe raw materials to ease the synthesis process while maintaining sustainability (Singh *et al*., 2018; Ying *et al*., 2022).

Green synthesis offers many benefits when compared to conventional chemical and physical methods, as the process focuses on following the principles of green chemistry which is to ensure the synthesis process is non-toxic, environmentally friendly, cost effective, energy efficient and pollution free (Ying *et al*., 2022). Physical methods often require high-temperature and high-pressure conditions in the synthesis process, while chemical methods usually involve the use of toxic reagents and organic solvents to function as end-capping materials. By utilizing plant materials that are already

rich in polyphenols, flavonoids, and other phytochemicals, these natural sources can act as reducing agents and replace the need for chemicals to reduce the metal ions during the synthesis process (Ying *et al*., 2022).

1.2.1 Nanomaterials

Nanomaterials are a diverse class of materials with sizes ranging from 1 to 100 nanometres, often classified by their morphology and geometry. Nanomaterials currently have found widespread applications across various fields such as electronics, agriculture, and medicine due to their small size and unique properties (Huston *et al*., 2021). Nanoscale metals and metal oxides exhibit physical and chemical properties differing from their bulk counterparts due to the small size effect, interface effect, and quantum effect (Ying *et al*., 2022).

For example, titanium dioxide nanoparticles (TiO_2 NPs) are a form of *n*-type semiconductor with high thermal stability, high optical properties, and exhibits dielectric properties which allows it to be used in photocatalysis, dye-sensitized solar cell (DSSC), and lithium-ion batteries (Amanulla and Sundaram, 2019). The UV absorption capabilities of TiO_2 NPs made them popular in sunscreens, paints to provide protection against UV rays present in sunlight, or antimicrobial coatings that require a high

refractive index against sunlight (Amanulla and Sundaram, 2019). Similarly, zinc oxide nanoparticles (ZnO NPs) find applications in electronics, sensors, and biomedical fields due to their wide energy bandgap, semiconducting properties, and biocompatibility (Doan Thi *et al*., 2020). The versatility and tunability of nanometal oxides make them crucial components in the development of advanced technologies across diverse sectors. However, the distinctive properties of nanomaterials also raise concerns regarding the potential environmental and health impacts of conventional synthesis methods, underscoring the necessity for comprehensive studies to ensure their safe and sustainable use. This concern has led to a growing interest in green synthesis as a sustainable alternative for producing nanometal oxides.

1.2.2 Synthesis of CuO NPs

While CuO NPs have immense potential, their commercial synthesis methods, including chemical precipitation, reduction, electrochemical, hydrothermal, microemulsion, and others, are often energy-intensive, complex, and costly, requiring high-end machinery (Chan *et al*., 2022). This conventional synthesis route possesses sustainability challenges as they often incorporate the use of non-ecological solvents, toxic chemicals, or organic solvents such as ethylene glycol (Siddiqui *et al*., 2019).

In contrast, green synthesis methods using plant materials or waste offer a sustainable alternative. These methods can produce CuO NPs with higher lifespan, conversion rates, and scalability, addressing the limitations of conventional synthesis approaches (Chan *et al*., 2022; Ying *et al*., 2022). By harnessing natural resources and waste materials, green synthesis not only reduces environmental impact but also offers a cost-effective and scalable solution for CuO NP production. Continued research in green synthesis techniques holds promise for advancing the sustainable production of CuO NPs, unlocking their full potential for various applications while minimizing their environmental footprint (Ying *et al*., 2022).

1.3 Orange peel

Orange, scientifically known as *Citrus sinensis*, is a nutritious citrus fruit abundant in vitamin C, folate, and fiber, making it commercially available year-round. The fruit is also packed with various flavonoids and carotenoids, which contribute to its distinct orange colour and aroma (Kubala & Arnarson, 2023). Despite being one of the most sought-after fruits globally, more than 40 % of the fruit is typically considered waste due to the inedible peel, seeds, albedo, and pulp (Zhou, 2023).

Similar to the flesh of the fruit, the orange peel is rich in components such as pectin, cellulose, and hemicellulose, as well as other flavonoids and carotenoids (Ahmadi *et al*., 2014; Kubala & Arnarson, 2023). Constituting up to 20 % of the orange fruit, the peel is abundant in flavonoids, organic acids, polyphenols, natural pigment molecules, essential oils, and pectin (Miera *et al*., 2023). According to a study by Manthey and Grohmann (1996), six flavonoids could be isolated from Valencia, Navel, Amber sweet, and Temple orange peels in higher concentrations, including narirutin 4'-*O* -glucoside, eriocitrin, naurirutin, and hesperidin. In the study conducted by Liew and his collaborators (2018), three general categories of phytochemicals (phenolic acid, organic acid, and flavonoid) were isolated from orange peel extract.

Table 1: Phytochemical content in *Citrus sinensis* peel retrieved from (Liew *et al*., 2018)

Phenolic acid	Gallic acid, Protocatechuic acid, 4- 4-hydroxybenzoic acid, Caffeic acid, Ferulic acid
Organic acid	Lactic acid, Citric acid, L-mallic acid, Kojic acid, Ascorbic acid
Flavonoid	Catechin, Epigallocatechin, Vitexin, Rutin, Luteolin, Apigenin

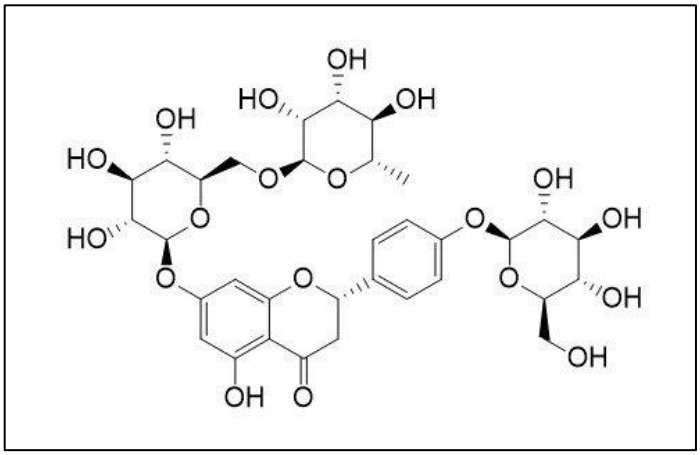

Figure 1: Structure of Narirutin 4'-*o*- glucoside

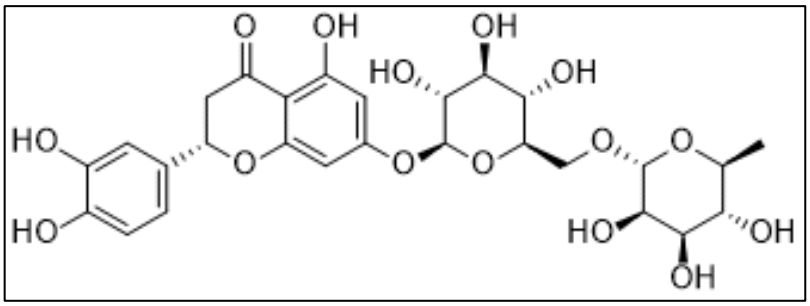

Figure 2: Structure of Eriocitrin

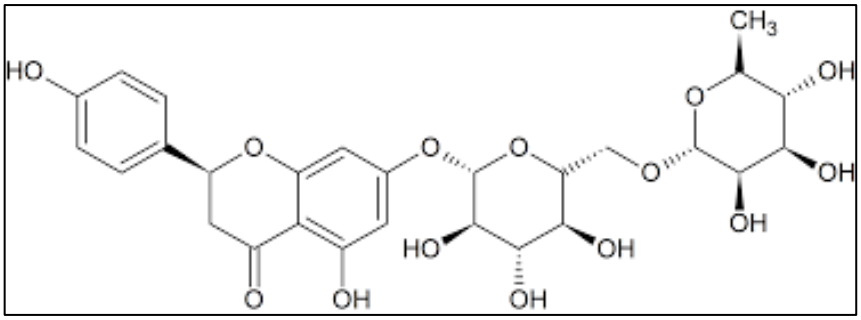

Figure 3: Structure of Naurirutin

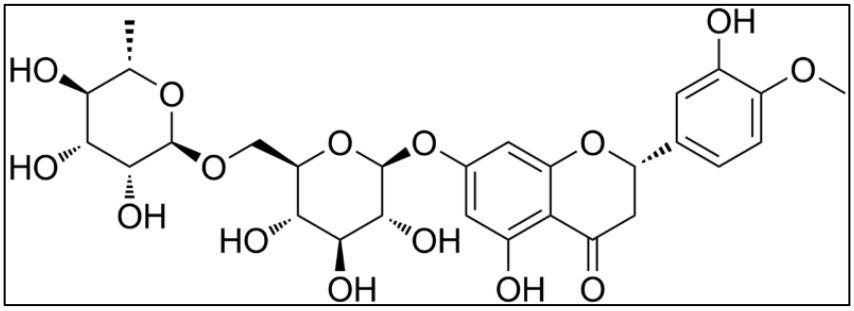

Figure 4: Structure of Hesperidin

These flavonoids are rich with phenolic hydroxyl groups allowing for the orange to poses antioxidant and anti-inflammatory properties and act as green stabilizing and reducing agent in green synthesis process (Aminuzzaman *et al*., 2018; Kubala & Arnarson, 2023). The abundance of valuable compounds in orange peel underscores its potential as a valuable resource rather than just waste left to rot in dumpsites. Once extracted, these compounds can be applied in the manufacturing of various products that poses health benefits which leaves a positive advancement in waste reduction of the citrus industry.

1.4 Dye

In the current world of fast fashion, dye is an essential part of the industry to produce vibrant coloured textiles, cloth, and threads to be made into clothing, accessories, and fabric to be sold to eager consumers. Due to the high demand for vibrant coloured fabric, the textile uses high volumes of synthetic dyes in the process of dyeing fabric which is highly toxic. Though dye molecules would bind to the fabric fibres to give colour to the dyed fabric, the dye molecules that did not bind tightly to the fabric would be discharged as dye effluent with wastewaters into rivers, lakes, streams, ponds even to the ocean when traveling in moving bodies of water (Al-Tohamy *et al*., 2022).

1.4.1 Impact of dye on the environment

The main form of pollution often associated with dye is water pollution as much dye water are often discarded in the form of dye effluent water into bodies of water near the processing or manufacturing factories (Lellis *et al*., 2019; Liu, 2020). Dye molecules are complex, non-biodegradable, and often used in very high concentrations giving a highly saturated colour to the wastewater if not treated prior to disposal, it would pollute the water body and change its colour (Liu, 2020). The wastewaters produced by the textile industry often contains high concentrations of heavy metals (mercury, cadmium, lead) as well as dye molecules such as

azo dyes, sulfur dyes and mordant dyes that are used in the multi-step process of fabric treatment process such as including sizing, softening, de-sizing, brightening, and finishing (Al-Tohamy *et al*., 2022).

The introduction of concentrated dye waste into any body of water will not only change the colour of the water but also significantly decrease the amount of oxygen and sunlight that is able to penetrate the water body, causing aquatic plants and microorganisms living at the bottom of the water body to experience deficiency of sunlight (Al-Tohamy *et al*., 2022). This would then snowball into the death of these bottom-dwelling aquatic plants as the lack of sunlight inhibits these aquatic plants from carrying out photosynthesis, decomposing while using the already limited dissolved oxygen present in the water body and suffocating the other aquatic lifeforms. In addition, some dye molecules would degrade or have carcinogenic and toxic properties that would enter the aquatic lifeforms, eventually traveling up the food chain and poisoning humans who consumed these contaminated fish (Chatterjee, 2020).

Dye pollution caused by the textile industry usually pollutes water bodies, however, the textile industry is also associated with pollutant gas emissions. Dye molecules could vaporize into the air, forming toxic fumes, releasing sulfur dioxide, nitrogen dioxide along with other volatile organic compounds (Lellis *et al*., 2019). Inhalation of these pollutants could lead to various health issues, as the dye molecules can diffuse into the bloodstream through the

alveoli, causing symptoms such as vomiting, nausea, headaches, asthma, and cardiovascular disease (Gupta *et al*., 2017). In countries that is known for their large-scale dye industries such as India and China, the air quality in the surrounding areas is adversely affected by the air emissions from these textile factories. The study conducted by Gupta and his colleagues (2017), collected, and studied air samples from Chatta and Kalikapur which is known for its textile factories showed that the air sample contained much higher concentrations of sulfur dioxide and nitrogen dioxide than the other areas of India around 30 $\mu g/m^3$ and 10 $\mu g/m^3$ respectively.

The textile industry is also involved in many incidents of soil pollution as the dye molecules can leech into the soil through contaminated water bodies (Al-Tohamy *et al*., 2022). Azo dyes in particular are known to be toxic to the microorganisms present in soil and would in turn affect the agriculture productivity of the contaminated area (Meghwal *et al*., 2019). Common categories of dye used in the textile industry includes basic dyes, acid dyes, and direct dyes often carry extremely low or high pH that would disturb the balance of soil pH which decreases soil productivity (Meghwal *et al*., 2019). By altering the pH and microbes present in the soil, germination, and cultivation of crops would become difficult and even affect the growth of the crop as the dye's mutagenic properties would cause mutations that decrease chlorophyll production in the plant cell (Al-Tohamy *et al*., 2022). Similar to the effect of dye in water, the presence of high concentration of dye molecules in the soil

would decrease the presence of dissolved oxygen in the soil further suffocating the microorganism and seedling, disrupting the osmotic balance, stunting plant growth (Al-Tohamy *et al*., 2022).

1.4.2 Impact of dye on human health

Dye molecules often have carcinogenic and toxic properties that can cause a variety of illnesses when exposed, inhaled, or come in contact with the skin. For instance, methylene blue dye which is widely used in the textile and rubber industry can cause stroke, jaundice and narcosis in humans when exposed (Karuppannan *et al*., 2021). Textile industry workers commonly suffer from asthma, allergic conjunctivitis, rhinitis, and dermatitis due to long-term exposure to high concentrations of dye solution or powder as the textile industry is known for its poor working conditions (Lellis *et al*., 2019).

Though it would be often thought that the common folk would not be exposed to dye molecules to a similar degree compared to the workers in the textile industry, the high stability of dye molecules allowed it to travel through the food chain or air pollution eventually reaching the common folk. Dye molecules could remain in the fish, crustaceans or even crops that were harvested that were grown in contaminated waters or soil and can still bring dye molecules into the human body when consumed. Once consumed dye-contaminated foods, the individual would suffer from irritation along the digestive tract or even poisoning at higher concentrations

(Sudarshan *et al*., 2023). The genotoxic and carcinogenic properties of dye would cause mutation of the human genome that would affect ovulation and spermatogenesis in females and male respectively (Al-Tohamy *et al*., 2022; Sudarshan *et al*., 2023). Dye's carcinogenic properties would still remain even if the compound were broken down where in some cases where Basic Red 9 dye, which would break down under anaerobic conditions into carcinogenic amines that would lead to allergic dermatitis and cancer in the liver and bladder when tested in lab rats (Lellis *et al*., 2019).

1.4.3 Dye effluent treatment

Dye effluent treatment is a important process aimed at mitigating environmental pollution caused by wastewater generated by modern industries such as textiles, leather, and paper. In the textile industry, dye treatment methods are generally categorized into three groups: physical, chemical, and biological, each with its own set of drawbacks. Physical methods, such as adsorption and membrane technology, are often considered costly, and the adsorbents may have limited adsorption capacity requiring larger amounts or recycling process to take place (Liu, 2020). Chemical methods, including electrochemical and oxidation methods, often comes with high investments for chemicals and energy to ensure efficient treatment. Biological method though typically employs bacteria and other microorganisms capable of breaking down dye molecules under anaerobic or aerobic conditions, it would require large volumes of

water to dilute the waste as the microbes would be killed off when exposed to high concentrations of dye (Ayele *et al*., 2021).

In this context, photocatalysts such as semiconductor materials emerge as an attractive alternative for dye effluent treatment. They can be excited by green energy sources to initiate the photodegradation treatment process and can be easily synthesized using plant materials and comes with the advantage of scalability (Chan *et al*., 2022). Photocatalyst synthesized through green synthesis are able to act as a green and sustainable alternative that can overcome the disadvantages that are often found in conventional dye treatment methods. Though the utilizing of renewable resources and minimizing energy consumption, photocatalysts present a promising avenue for effective and environmentally friendly dye effluent treatment.

1.5 Objectives

i) To synthesize CuO NPs using *Citrus sinensis* (orange) peel extract acting as a green reducing and stabilizing agent with copper (II) nitrate and copper (II) acetate as precursors.

ii) To study the difference between CuO NPs synthesized through boiling method, maceration method and soaking method.

iii) To study the effect of calcination temperature on synthesized CuO NPs.

iv) To characterize green-synthesized CuO NPs using UV-Vis, SEM, XRD, EDX, and FTIR.

v) To evaluate the rose Bengal B (RBB) dye degradation efficiency of green-synthesized CuO NPs as photocatalysts under UV light through UV-Vis spectroscopy.

1.6 Significance of study

The widespread applications of CuO NPs across various industries highlights the importance of employing sustainable and environmentally friendly synthesis methods in synthesis process of CuO NPs. By utilizing common food waste or agricultural by-products, such as orange peel, for the green synthesis of CuO NPs enhances both the efficiency and sustainability of their production. This study focuses on comparing three common preparation methods for orange peel extract (OPE) in the green synthesis of metal oxide nanoparticles, as well as investigating the effect of calcination temperature on the properties of green-synthesized CuO NPs. This analysis aims to determine the optimal conditions to synthesize CuO NPs to produce CuO NPs able to act as photocatalyst for dye removal with maximum efficiency.

With approximately 17 % to 20 % of industrial wastewater pollution attributed to the textile industry, predominantly in the form of dye waste, the impact on limited freshwater bodies is significant (European Parliament, 2020). By evaluating the dye removal efficiency of CuO NPs synthesized from dye waste, this study aims to mitigate the toxic effects associated with dye pollution, as observed in previous dye pollution incidents such as the Sungai Kim Kim pollution in Malaysia. This environmental disaster led to adverse health effects among nearby civilians, including headaches, nausea, and vomiting, due to exposure to toxic vapours formed from the highly polluted river (Noh, 2020).

Through this research, this study strives to contribute to the development of sustainable solutions for dye effluent treatment, thereby safeguarding both environmental integrity and public health. By optimizing the synthesis of CuO NPs from waste materials and investigating their efficacy in dye removal, this study aims to address the pressing challenges posed by industrial wastewater pollution, particularly in the textile industry.

Chapter 2

LITERATURE REVIEW

2.1 OPE- mediated green synthesis of metal nanomaterial

The global production and consumption of oranges have reached significant levels, with approximately 48.8 million tons of the fruit produced between 2016 to 2017 alone (Skiba and Vorobyova, 2019). Consequently, orange peel waste has become one of the most prevalent fruit waste, making it a readily available resource for various applications. Orange peels have found utility in numerous studies involving the green synthesis of metal oxide nanoparticles, including TiO_2 NPs by Amanulla and Sundaram (2019), ZnO NPs by Doan Thi *et al.*(2020), and Ag NPs by Margarita and Victoria (2019). However, it is noteworthy that the method used for preparing orange peel extract (OPE) can significantly affect the concentration and stability of the extracted phytochemicals due to potential degradation over time or when exposed to high heat. In the studies mentioned, both maceration and boiling methods were employed for OPE preparation. The maceration method involved drying the orange peels in a food dryer for at least 12 hours, followed by grinding into a fine powder and soaking in deionized water at 60 ˚C for 1 hour. Conversely, boiling the collected plant material or fruit peel in deionized water is a conventional approach for OPE preparation. While boiling and maceration methods involve heating to enhance extraction

efficiency, the choice of preparation method may influence the resulting concentration and stability of the extracted phytochemicals.

The utilization of orange peels in nanoparticle synthesis exemplifies an eco-friendly approach to waste management and underscores the potential for sustainable solutions in materials science. As research in this field progresses, further exploration of extraction techniques and their influence on nanoparticle properties will contribute to the advancement of green synthesis methodologies and their applications in diverse fields. The relationship between OPE preparation methods and the morphology of resulting metal oxide nanometarials is summarized in Table 2, providing insights into the impact of preparation techniques on nanoparticle characteristics (adapted from Doan Thi *et al.*, 2020; Amanulla and Sundaram, 2019; Skiba and Vorobyova, 2019).

Table 2: Relationship of OPE preparation method and metal nanomaterial morphology

Preparation method	Metal oxide nanomaterials	Morphology	Reference
Maceration	ZnO NPs	Spherical with average size of 35 – 60 nm	Doan Thi *et al.*, 2020
Maceration	TiO_2 NPs	Irregular and angular with porous network with average 20- 5- nm size	Amanulla and Sundaram, 2019

Boiling	Ag NPs	Spherical and agglomerated with average size of 63 nm	Skiba and Vorobyova, 2019

(a) (b) (c)

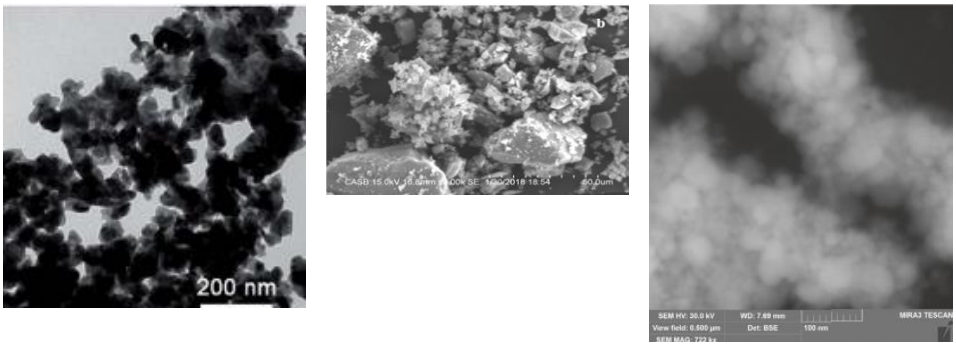

Figure 5 : (a) TEM image of hexagonal wurtzite shaped ZnO NPs and SEM image of (b) irregular and angular shaped TiO_2 NPs and (c) spherical and agglomerated Ag NPs (Retrieved from Doan Thi *et al.*, 2020; Amanulla and Sundaram, 2019; Skiba and Vorobyova, 2019)

In summary, the high availability of orange peels, coupled with their rich phytochemical composition, renders them a valuable resource for green synthesis studies involving metal oxide nanoparticles. Various preparation methods, such as maceration and boiling, have been employed to extract phytochemicals from orange peels for use in nanoparticle synthesis. While these methods involve heating to enhance extraction efficiency, the choice of preparation method may impact the concentration and stability of the extracted phytochemicals. The utilization of orange peels in nanoparticle synthesis exemplifies an eco-friendly approach to waste utilization and underscores the potential for sustainable solutions in materials science. As

research in this field continues to evolve, further exploration of extraction techniques and their influence on nanoparticle properties will contribute to the advancement of green synthesis methodologies and their applications in diverse fields.

2.2 Green synthesis of copper oxide nanoparticles with plant extract

CuO NPs being semiconductor nanoparticles of nano size, hold diverse applications across numerous fields and domains. The green synthesis of CuO NPs presents an innovative approach, achievable through the utilization of various plant materials rich with natural phytochemicals capable of serving as stabilizing and reducing agents throughout the synthesis process. Each plant extract harbours different concentrations and phytochemical compositions, present in varying concentrations, thereby imparting differing degrees of reducing and stabilizing capabilities during the green synthesis process. This would lead to the synthesized CuO NPs to possess different structures and morphology.

Research endeavours have explored the utilization of plant materials that are typically discarded or considered inedible, such as Cavendish banana peel (Amminuzzaman *et al*., 2017), *Carica papaya* peel and leaves (Phang *et al.*, 2021; Sankar *et al.*, 2014), *Garcinia mangostana* leaves (Chan *et al.*, 2022), *Punica granatum* peel, and *Muntingia calabura* leaves (Selvanathan *et al.*, 2021), for the purpose of reducing and stabilizing Cu^{2+} ions during the

green synthesis process. By repurposing these wasted plant materials, a sustainable source of raw material is obtained.

Optimization of the green synthesis process can be achieved through strategic manipulation of variables such as the type of precursor salt utilized, calcination temperature, and the specific type of plant material employed. This approach allows for fine-tuning of the synthesis conditions to maximize the efficiency and reproducibility of CuO NP synthesis, while simultaneously minimizing environmental impact and resource consumption.

Table 3: Summary of relationship of plant extract-mediated CuO NPs and morphology

Plant extract	Precursor salt	Size (nm)	Shape	Reference
Cardiospernum halicacabum leaves	Copper sulfate pentahydrate	~ 14.9	Spherical and agglomerated	Karuppannan *et al.*, 2021
Carica papaya leaves	Cupric sulphate	~ 140	Rod like shape	Sankar *et al.*, 2014
Carica papaya peel	Copper (II) nitrate trihydrate	85-140	Spherical and agglomerated	Phang *et al.*, 2021
Cavendish banana peel	Copper nitrate trihydrate	~ 23	Spherical and agglomerated	Aminuzzaman *et al.*, 2017
Punica granatum peel	Copper acetate monohydrate	10-100	Rough agglomerated spherical shape	Ghidan *et al.*, 2016

In essence, the utilization of inedible or often-discarded plant materials in CuO NP synthesis represents a resource-efficient strategy, tapping into sustainable sources while offering opportunities for process optimization and innovation in green nanotechnology.

2.3 Effect of calcination temperature on green synthesis metal oxide nanomaterials

Calcination is often used in many green synthesis metal oxide nanomaterials as a technique to remove the remaining volatile phytochemicals present and to initiate the oxidation of metal oxides through subjecting the substance of high temperature for a fixed amount of duration (Nordin *et al.,* 2015). The temperature the metal oxide nanomaterials is calcinated would affect the structure, morphology and optical properties of the final synthesized metal oxide nanomaterials (Chan *et al.,* 2022).

In a study conducted by Chan and colleagues (2022), the effects of calcination temperature on the structure, morphology, and optical properties of green-synthesized CuO NPs were investigated. The study encompassed a temperature range from 200 ˚C to 600 ˚C. Notably, the research centred on the green synthesis of CuO NPs employing *Garcinia mangostana* (mangosteen) leaves as the source of green reducing and stabilizing agents during the synthesis process. The plant extract was prepared using the maceration method, wherein mangosteen leaves were dried and ground into powder, followed by heating at 80 ˚C for 20 minutes. Subsequently, the CuO

NPs were synthesized using 2 g of copper (II) nitrate trihydrate and 30 ml of the prepared mangosteen leaf extract. The synthesis process involved heating the mixture to temperatures ranging from 70 ˚C to 80 ˚C, followed by calcination at the specified temperatures for a duration of 2 hours.

The morphological characteristics of the synthesized CuO NPs were investigated, revealing distinct features contingent upon the calcination temperature. At temperatures of 400 ˚C and 500 ˚C, the CuO NPs exhibited a spherical morphology, displaying aggregation with an overall rough surface. In contrast, CuO NPs calcinated at lower temperatures of 200 ˚C and 300 ˚C manifested a nanoflake structure. Notably, at 600 ˚C, the CuO NPs appeared highly bulky, attributed to the elimination of the grain boundary area (Chan *et al.*, 2022). The bandgap energy was also affected which decreases when the calcination temperature increased.

Table 4: Relationship of calcination temperature and crystalline size (Chan *et al.*,2022).

Calcination temperature (˚C)	Crystalline size (nm)
200	12.78
300	14.04
400	18.32
500	19.88
600	28.17

In the investigation led by Doan Thi *et al.*(2020), the impact of calcination on the green synthesis of ZnO NPs utilizing OPE within the temperature range of 300 ˚C to 900 ˚C was examined. The findings exhibited congruence with those reported by Chan *et al.*(2022). Notably, Doan Thi *et*

*al.*concluded that higher calcination temperatures notably enhanced the efficiency of volatile organic compound (VOC) removal, particularly evident from 500 ˚C onwards. Furthermore, they observed that escalating calcination temperatures induced an increase in particle size attributed to crystal growth.

Table 5: Relationship of calcination temperature, appearance and surface morphology (Doan Thi *et al.,* 2020).

Calcination temperature (˚C)	Crystalline size (nm)	Structure	Appearance
Room temperature	-		Dark orange colour and clumpy appearance
300	-		Pale orange colour and fluffy appearance
400	35- 60 nm	hexagonal wurtzite	Pale cream colour and fluffy appearance
500	-		White colour and fluffy appearance
600	-		White colour and fluffy appearance
700	70- 100 nm	hexagonal wurtzite	White colour and fluffy appearance
800	-		White colour and fluffy appearance
900	200- 230 nm	hexagonal wurtzite	White colour and clumpy appearance

The findings from these studies underscore the pivotal role of calcination temperature in green synthesis processes, influencing the structure, appearance, morphology, and optical properties of CuO NPs and ZnO NPs, thus emphasizing the necessity for meticulous temperature control to optimize environmentally benign nanoparticle synthesis.

2.4 Effect of precursor salt on green synthesized metal oxide nanomaterials

Precursors which are typically metal salts are the source of metal ions in the synthesis of metal oxide nanomaterials with precursor salts being acetates, nitrates, chloride and sulfates as shown in **Table 6** below.

Table 6: Comparison of OPE-mediated metal oxide nanomaterials using different precursor salt with other studies

Metal oxide nanomaterials	Precursor salt	Morphology	Reference
CeO_2	Cerium nitrate **$Ce(NO_3)_3 \cdot 6H_2O$**	Cubic nanostructure with particle size around 23 nm	(Sultan Irshad *et al.*, 2019)
CuO	Copper (II) nitrate pentahydrate	Nanorod structure	(Tshireletso, Ateba and Fayemi, 2021)

	$Cu(NO_3)_2 \cdot 5H_2O$		
CuO	Copper (II) acetate monohydrate **$Cu(OOCCH_3)_2 \cdot H_2O$**	Rod and plate shaped particle without uniform size	(Jayaprakash *et al.*, 2020)
MgO	Magnesium nitrate **$Mg(NO_3)_2$**	Spherical shape with particle size less than 10 nm	(Munjal, Singh and Kumar, 2017)
TiO_2	Titanium tetra chloride **$TiCl_4$**	Irregular shape with size ranging from 20- 50 nm	(Amanulla and Sundaram, 2019)
ZnO	Zinc nitrate **$Zn(NO_3)_2 \cdot 6H_2O$**	Spherical shape with size ranging from 35- 60 nm	(Doan Thi *et al.*, 2020)
ZnO	Zinc nitrate **$Zn(NO_3)_2 \cdot 6H_2O$**	Spherical shape with average size of 21 nm	(Aminuzzaman *et al.*, 2018)
CuO	Copper sulfate pentahydrate **$CuSO_4 \cdot 5H_2O$**	Spherical shape with average size of 14.9 nm	(Karuppannan *et al.*, 2021)
CuO	Copper nitrate trihydrate **$Cu(NO_3)_2 \cdot 3H_2O$**	Nanorod structure with	(Sankar *et al.*, 2014)

	average size of 140 nm

Though precursor salt might be initially through as only the source of metal ions during the green synthesis process, it's still had some effect on the final product produced as shown in the studies conducted by Jin *et al.*, (2023) and Wang *et al.*(2017) on the synthesis of CuO-CeO_2 catalysts. Akintelu *et al.* (2021) found that the selection of precursor species would influences the morphological attributes of metal oxide nanomaterials synthesized through green methodologies. Specifically, their investigation revealed that copper chloride salts predominantly formed triangular or tetrahedral shape Cu NPs, while copper acetates yield rod-shaped Cu NPs, and copper sulfates precipitate spherical counterparts. Though some morphology would be more easily formed through the use of certain precursor salts, every type of different structure would still arise despite the trend that was observed in the findings of Akintelu *et al.* (2021) as shown in **Table 6** which suggest that different structure can still be formed by each precursor salt for different plant extract used and metal oxide nanomaterials synthesized.

2. 5 Photocatalytic dye degradation of CuO NPs

CuO NPs serve as versatile materials with applications spanning various fields. One notable application is their utilization as photocatalysts for the degradation of dyes present in effluents. This application presents a sustainable and environmentally friendly alternative to conventional chemical and physical dye treatment processes, which are often characterized by high costs and adverse environmental impacts (Liu, 2020). The unique properties of CuO NPs, including their narrow bandgap and porous surface structure, render them highly effective in maximizing the adsorption of dye molecules. This enhanced adsorption capability, coupled with their photocatalytic activity, facilitates efficient degradation of dyes in effluents. As a result, CuO NPs offer a promising avenue for achieving high dye degradation efficiency while minimizing environmental harm.

Dye pollution poses a significant threat to environmental quality, affecting not only water bodies but also soil and air quality when untreated (Al-Tohamy *et al.*, 2022). By harnessing the capabilities of CuO NPs in photocatalytic dye degradation, it becomes possible to address this pressing environmental concern effectively. Moreover, the synthesis of CuO NPs via green routes further enhances their sustainability profile. Green synthesis methods typically involve the utilization of environmentally benign precursors and reducing agents derived from natural sources. This approach aligns with the principles of green chemistry and promotes the development of eco-friendly technologies. In light of these considerations, the adoption of

green-synthesized CuO NPs represents a win-win solution for promoting sustainability within the textile industry. By integrating these nanoparticles into dye treatment processes, textile manufacturers can achieve effective dye degradation while minimizing their environmental footprint. This shift towards eco-friendly practices not only contributes to environmental conservation but also enhances the long-term viability of the textile industry.

Table 7: Summary of relationship of plant mediated CuO NPs and dye removal efficiency at different duration

Plant Extract	Dye	Duration (min)	Degradation efficiency (%)	Reference
Cavendish banana peel	Congo red	60	90	Aminuzzaman *et al.*, 2017
Cardiospernum halicacabum leaves	Methylene Blue	210	93	Karuppannan *et al.*, 2021
Carica papaya leaves	Coomassie brilliant blue R-250	90	25	Sankar *et al.*, 2014
Carica papaya peel	Palm Oil Mill Effluent	180	66	Phang *et al.*, 2021

The versatility of green-synthesized CuO NPs is evident from research conducted on various dye categories. Across these studies, CuO

NPs have demonstrated remarkable effectiveness in degrading diverse dye molecules, highlighting their robust photocatalytic properties. The degradation process, characterized by its efficiency and rapidity, benefits from the utilization of sunlight as a renewable energy source for the dye removal process. CuO NPs' efficacy extends across different industrial sectors, underscoring their versatility and applicability. Moreover, their expedited degradation kinetics offer a promising solution for timely and efficient treatment of dye-contaminated effluents, addressing dye pollution challenges in a sustainable and environmentally responsible manner. In essence, the combination of CuO NPs' photocatalytic prowess with sunlight as a renewable energy source represents a sustainable approach to dye degradation, positioning green-synthesized CuO NPs as a promising solution for mitigating dye pollution.

Chapter 3

METHODOLOGY

3.1 Chemicals

Copper (II) nitrate trihydrate (**$Cu(NO_3)_2 \cdot 3H_2O$**) and copper (II) acetate (**$Cu(OOCCH_3)_2 \cdot H_2O$**) was purchased from R & M Marketing Essex, UK. *Citrus sinensis* (Orange) was purchased from LOTUS Kampar, Perak. RBB was bought from Carl Roth. All glassware was cleaned with deionized water and dried in an oven prior use to ensure foreign ions are not introduced into OPE that will affect the stabilization of CuO NPs.

3.2 Green synthesis and Characterization of CuO NPs

3.2.1 Preparation of OPE

3.2.1.1 BOPE preparation

50 g of orange peel was collected, washed with deionized water and cut into small pieces. The cut orange peel was added to 250 ml of deionized water in a 500 ml beaker. The mixture was heated up and kept at a temperature range of 60 - 70˚C for 30 minutes with constant stirring. Next, the solution was filtered using vacuum filtration and the OPE was obtained. The process of LPE preparation is shown in the **Figure 6** below.

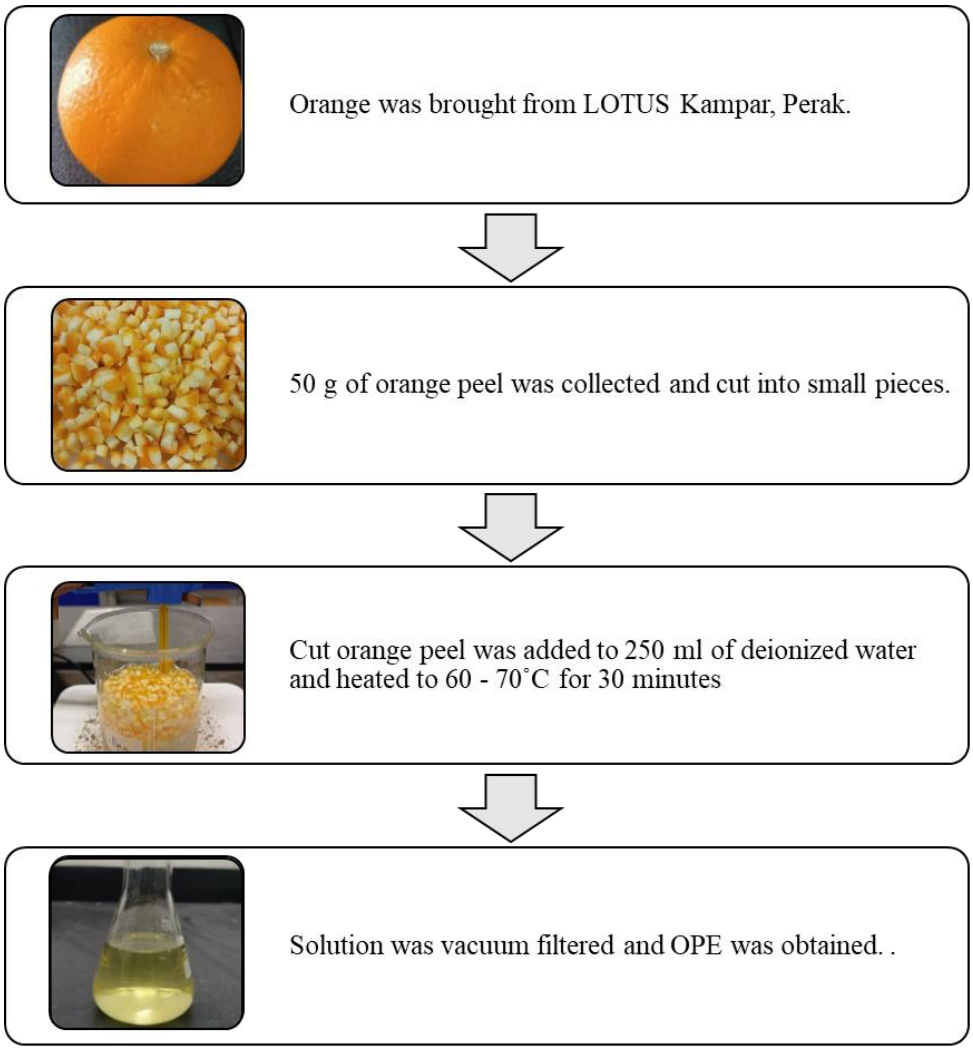

Figure 6: Flowchart of BOPE preparation

3.2.1.2 SOPE preparation

50 g of orange peel was collected, washed with deionized water and cut into small pieces. The cut orange peel was added to 250 ml of deionized water in a 500 ml conical flask and sealed with parafilm. The mixture was left to soak for 1 week at room temperature. After 1 week, the mixture was

filtered through vacuum filtration and OPE was obtained. The process of OPE preparation was shown in the **Figure 7** below.

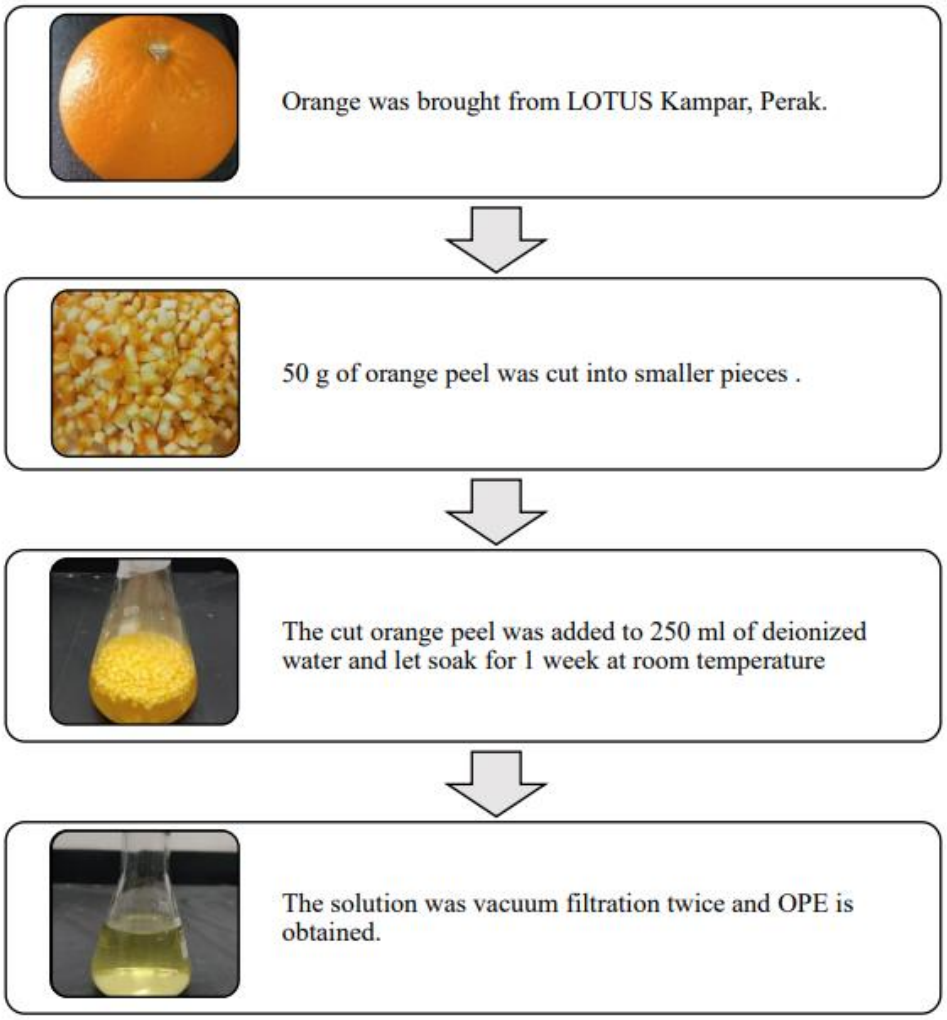

Figure 7: Flow chart of SOPE preparation

3.2.1.3 MOPE preparation

250 g of orange peel was collected, washed with deionized water and cut into small pieces. The orange peel was dried in an oven at 60˚C for 15 hours until completely dried. The dried orange peel was grinded into powder

using grinder. 5 g of the orange peel powder was added into 250 ml of deionized water in a 500 ml conical flask and sealed with parafilm. The mixture was left to soak for one week at room temperature. After 1 week, the mixture was filtered through vacuum filtration twice and OPE is obtained. The process of OPE preparation was shown in the **Figure 8** below.

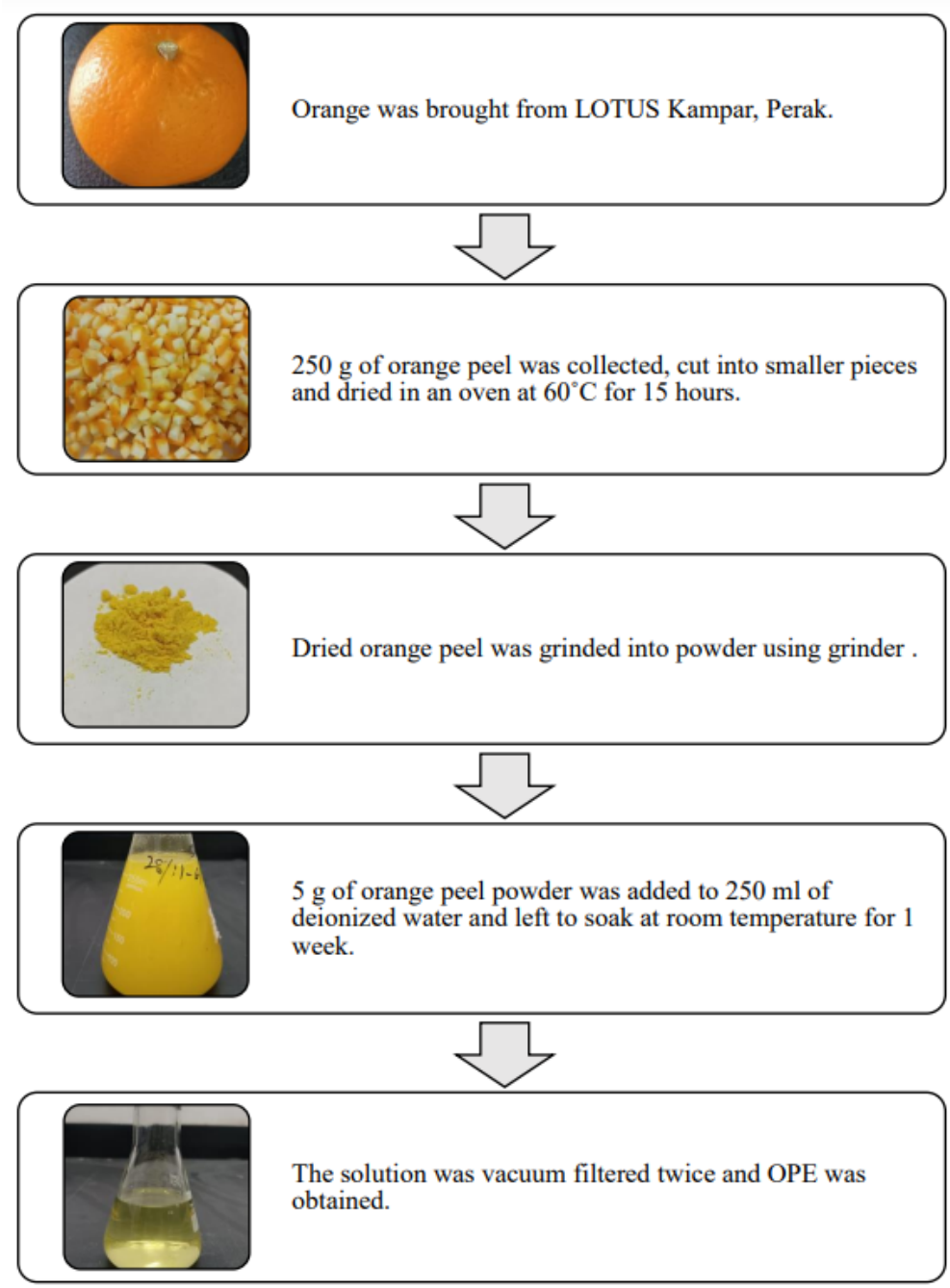

Figure 8: Flow chart of MOPE preparation

3.2.2 Synthesis of CuO NPs using OPE

50 ml of OPE was heated to 60 – 70 ˚C with constant stirring. After the extract had reached 60˚C, 2 g of two different copper precursor salts (copper (II) was used was added to heated OPE. The mixture heated until dark green paste was formed keeping the temperature within 60 - 70˚C. The paste was calcinated in the furnace for 2 hours at two different temperatures (450 and 500˚C). CuO NPs was obtained in the form of black powder.

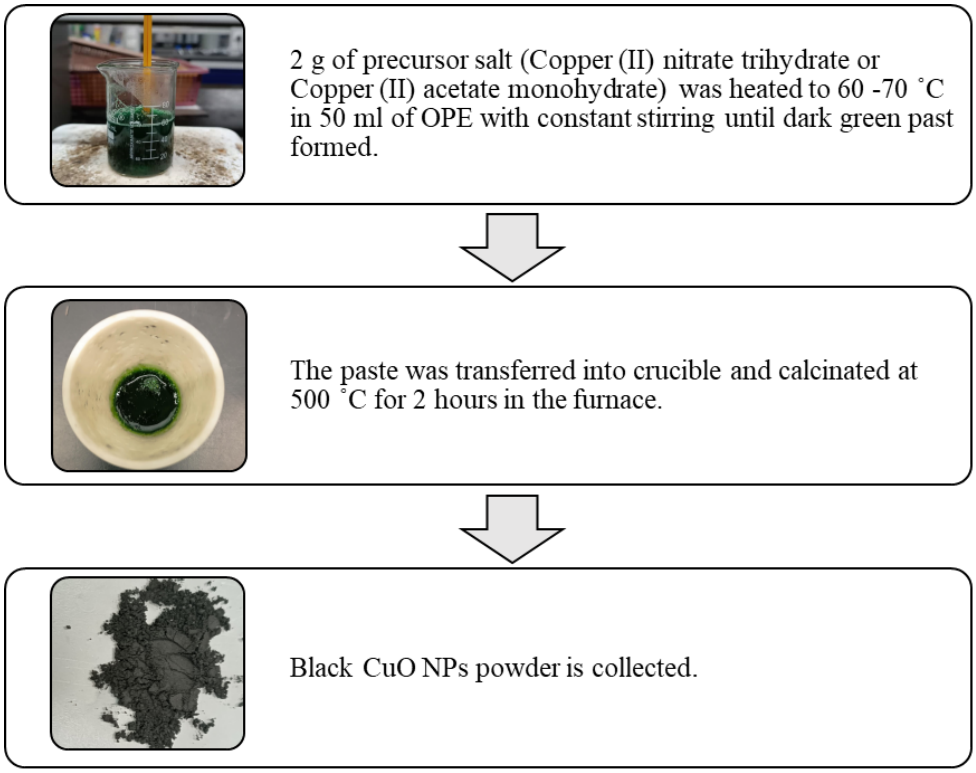

Figure 9: Flowchart of green synthesis process of OPE-mediated CuO NPs

3.2.3 Characterization of CuO NPs

Synthesized CuO NPs were characterized using EDX, FTIR, SEM, UV-Vis and XRD. EDX was used in determining the elemental composition of synthesized CuO NPs with the Oxford Instrument X-max Energy Dispersive Diffractometer model. FTIR was conducted by KBr pellet preparation method with the Perkin Elmer Spectrum RX1 FT-IR spectrometer and scanned within range of 400 – 4000 cm^{-1} . For the study on synthesized CuO NPs surface morphology, SEM was conducted using JEOI JSM-6701F SEM at 3.0 kV. ThermoFisher Scientific Genesys 10s Series UV-Visible Spectrophotometer was used for UV-Vis analysis with the range scanned within 190 – 1100nm. XRD was utilized in determination of crystallinity and crystal phase of CuO NPs using X-Ray diffractometer (Shimidazu XRD 600) with Cu K_α radiation between the 2θ of 20˚- 80 ˚.

3.2.3.1 Calculation of Crystalline Size Using Debye

The crystalline size of green synthesized CuO NPs was calculated using Debye Scherrer equation shown below (Aminuzzaman *et al.*, 2018):

$$D = \frac{k\lambda}{(\beta \cos \theta)}$$

Where:

D = Crystalline diameter

k = Scherrer's constant (always in 0.9)

λ = Wavelength of X-ray source

β = Width of diffraction broadening at full-width half maximum (in radium 2θ)

θ = Bragg's diffraction angle

3.3 Evaluation of Photocatalytic Activity of CuO NPs

3.3.1 Preparation of 15 ppm RBB Dye Solution

15 ppm of RBB dye solution was prepared using 15 mg of Rose Bengal B powder with deionized water in 1000 ml volumetric flask.

3.3.2 Evaluation of Photocatalytic Activity of CuO NPs in Degradation of RBB Dye Solution with Different Time Intervals

40 mg of CuO NPs was added to 200 ml of prepared 15 ppm dye solution in 250 ml beaker. The mixture was allowed to stir on dark condition for 30 minutes. The mixture was then exposed to 18-watt UV lamp with 10 ml of aliquot taken every 30-minute interval. The collected aliquot was subjected to UV-Vis analysis using ThermoFisher Scientific Genesys 10s Series UV-Visible Spectrophotometer by scanning within range of 190 – 1000 nm. Another fixed wavelength scan was conducted based on the maximum wavelength of shown in the previous scan for calculation of the degradation percentage.

3.3.3 Calculation of degradation percentage

Degradation percentage of dye degradation was calculated based on the absorbance values at λ_{max} before and after dye had been subjected to UV radiation using the equation shown below (Aminuzzaman *et al.*, 2018):

$$\text{Degradation percentage} = \frac{A_o - A_t}{A_o} \text{ X } 100\ \%$$

Where:

A_o = Initial absorbance dye solution before UV radiation

A_t = Absorbance of RBB dye solution at various irradiation time intervals (t)

Chapter 4

RESULTS AND DISCUSSION

4.1 Green Synthesis of Copper Oxide Nanoparticles

In this investigation, CuO NPs were synthesized using OPE prepared via various methods (Boiling, Soaking, and Maceration) employing Cu (II) precursor salts, namely $Cu(NO_3)_2 \cdot 3H_2O$ and $Cu(OOCCH_3)_2 \cdot H_2O$, followed by calcination at temperatures of 450 °C and 500 °C. The aim was to assess the impact of different synthesis conditions on CuO NPs using characterization techniques including UV-Vis, FTIR, FE-SEM, EDX, and XRD.

The utilization of OPE, enriched with organic acids, phenolic acids, and flavonoids extracted from orange peel, served as a green source of reducing and stabilizing agents in the eco-friendly synthesis process of CuO NPs. This approach offers the advantage of enhanced sustainability, promoting eco-friendliness by repurposing a common kitchen waste product, namely orange peel (Ghidan, Al-Antary and Awwad, 2016).

4.1.1 Proposed mechanism of OPE- mediated CuO NPs synthesis

The objective of utilizing OPE prepared through various methods in the synthesis of CuO NPs is to leverage the phytochemicals present in orange peel as green reducing and stabilizing agents. These phytochemicals are

involved in two primary routes in the green synthesis process: bio-reduction and chelation (Jabeen *et al.*, 2021; Álvarez-Chimal and Arenas-Alatorre, 2023).

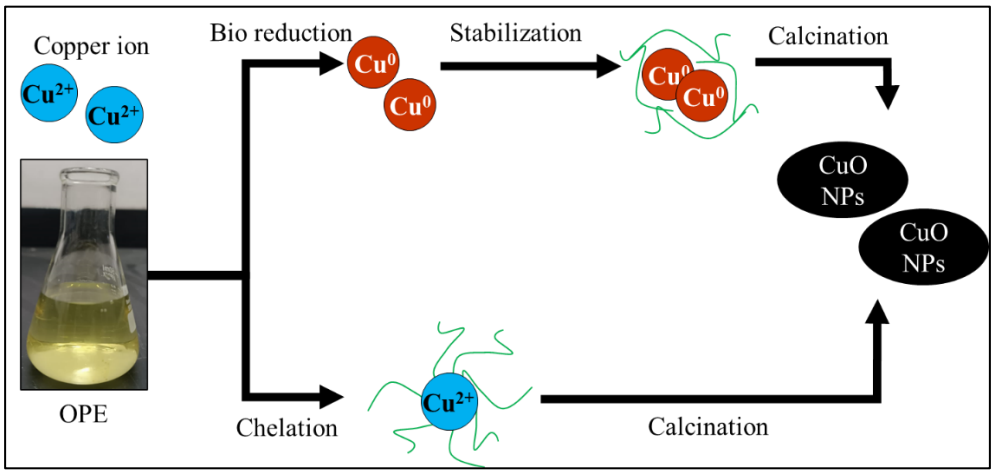

Figure 10: Proposed mechanism of green synthesis of CuO NPs using OPE

Bio-reduction represents the initial route of phytochemical involvement in the synthesis process. Phytochemicals such as organic acids, phenolic acids, and flavonoids found in OPE often contain phenolic hydroxyl (-OH) groups, enabling them to undergo tautomeric transformation and release hydrogen atoms that subsequently reduce Cu^{2+} ions to Cu^{0} (Makarov *et al.*, 2014). For instance, in the chemical reduction process of Ag NPs synthesis, ascorbic acid serves as a reducing agent, yielding Ag NPs with an average size of approximately 20 nm, a compound abundant in orange peel(Liew *et al.*, 2018; Jabeen *et al.*, 2021). Generally, the bio-reduction mechanism of nanometal oxides with plant extracts involves four main stages (Álvarez-Chimal and Arenas-Alatorre, 2023; Makarov *et al.*, 2014),

1) Initial phase: Where the precursor salt is combined with the aqueous plant extract or reaction medium of choice.

2) Activation phase: Where the metal ion form precursor salt is reduced and formed nucleation centre.
3) Growth phase: Where smaller NPs are coated into larger NPs to increase thermodynamic stability of NPs.
4) Termination phase: Where the final shape of NPs is determined.

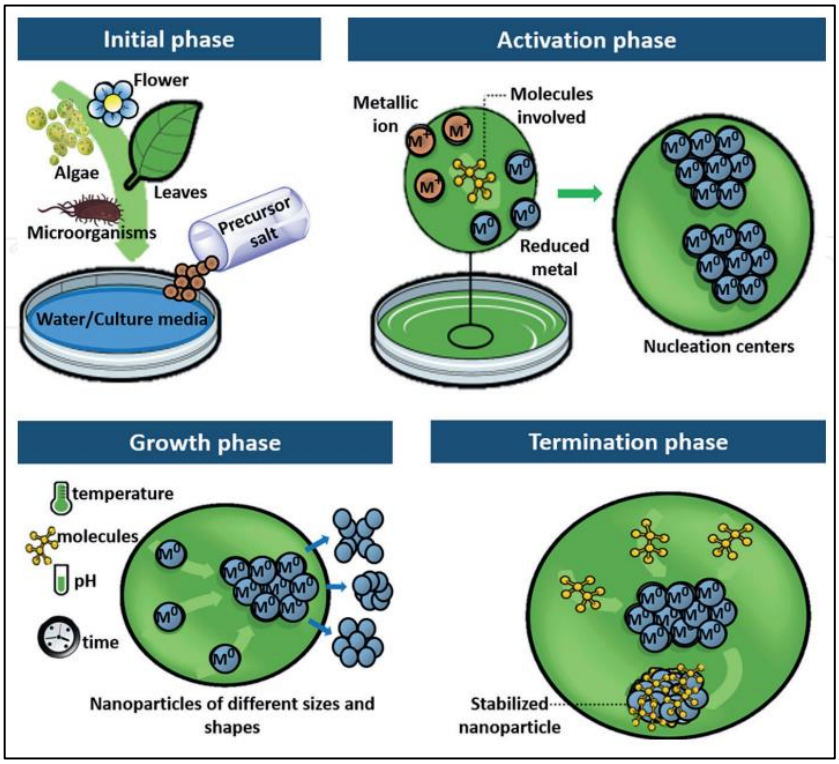

Figure 11: 4 phases of bio reduction synthesis of NPs (Retrieved from Álvarez-Chimal and Ángel Arenas-Alatorre, 2023)

In the nucleation phase, the amount of phytochemical, degree of stabilizing ability of the phytochemical, duration of growth phase will decide the degree of agglomeration of the final product (Makarov *et al.*, 2014). The structure of CuO NPs would favour the structure with the most suitable surface energy which depends on the stabilizing ability of the phytochemical.

The second route entails phytochemicals acting as chelating agents in the green synthesis process. Typically, functional groups such as amine groups, carboxyl groups, hydroxyl groups of organic acids, or their π-electrons present in OPE chelate metal ions. By chelating Cu^{2+} ions from the Cu precursor salt, these phytochemicals prevent superdrive-driven Fenton reactions of Cu^{2+}, which catalyses the formation of metallic NPs (Makarov *et al.*, 2014; Marslin *et al.*, 2018).

4.2 Characterization of Synthesized CuO NPs

4.2.1 X-ray Diffraction XRD

For each precursor salt used, one of the green synthesized CuO NPs with the best overall result in the previous characterization was chosen to conduct XRD characterization. **Table 7** shows the chosen CuO NPs' the synthesis conditions and results of previous characterization result.

Table 8: Summary of characterization of selected CuO NPs and its synthesis condition

Precursor Salt	$Cu(OOCCH_3)_2 \cdot H_2O$	$Cu(NO_3)_2 \cdot 3H_2O$
Calcination Temperature (˚C)	450	500
OPE	SOPE	SOPE
Atomic percentage of Cu (%)	59.01	40.76
Atomic percentage of O (%)	24.26	35.30
Bandgap energy (eV)	3.62	3.26
Size (nm)	55.3	48.1
Structure	Irregular shaped and agglomerated	Spherical and agglomerated

(a) $Cu(NO_3)_2 \cdot 3H_2O$ precursor salt calcinated at 500 ˚C

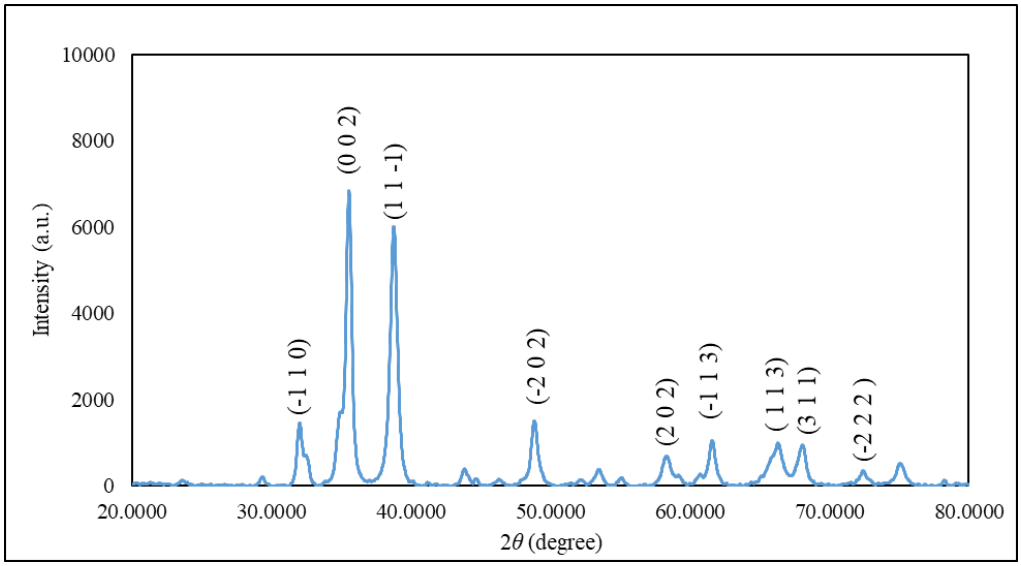

(b) $Cu(OOCCH_3)_2 \cdot H_2O$ precursor salt calcinated at 450 ˚C

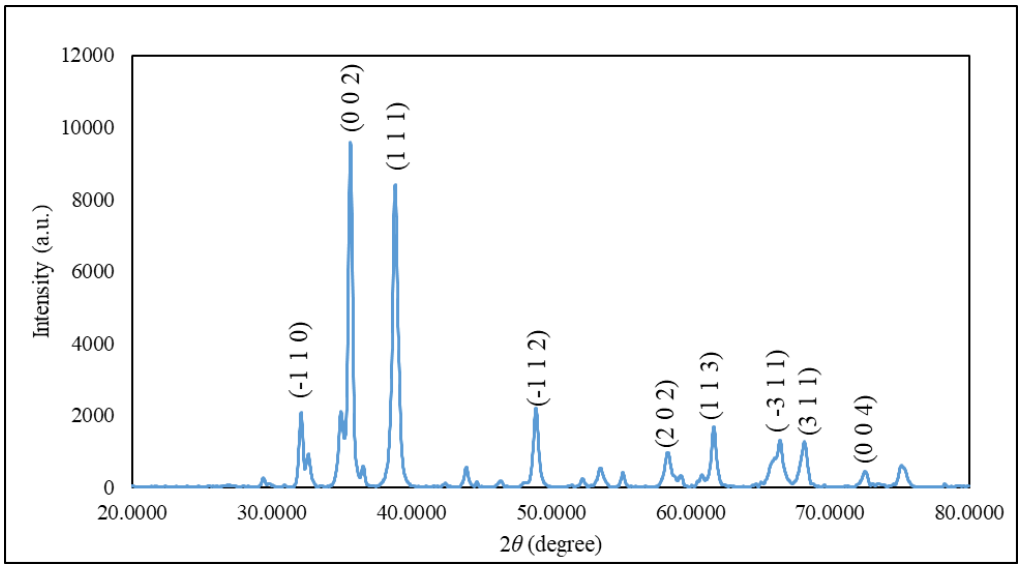

Figure 10 : XRD spectrum of SOPE-mediated CuO NPs synthesized under different experimental condition

The crystallinity of both CuO NPs synthesized under different condition was evaluated through XRD analysis shown in **Figure 10** with each figure displaying 9 distinct peaks. In **Figure 10 (a)**, the Miller indices for 2θ= 32.51 ˚, 35.36 ˚, 38.68 ˚. 4.74 ˚, 58.14 ˚, 61.54 ˚, 66.34 ˚, 68.09 ˚ and 74.94 ˚ were (-1 1 0), (0 0 2), (1 1 -1), (-2 0 2), (2 0 2), (-1 1 3), (-3 1 1),

(3 1 1) and (0 0 4) respectively. In **Figure 10 (b),** the Miller indices for 2θ= 32.45 ˚, 35.49 ˚, 38.68 ˚, 48.68 ˚, 58.46 ˚, 61.53 ˚, 66.25 ˚, 67.94 ˚ and 75.14 ˚ were (-1 1 0), (0 0 2), (1 1 1), (-1 1 2), (2 0 2), (1 1 3), (1 1 3), (3 1 1) and (-2 2 2). In the XRD spectra shown intense peaks at (-1 1 0) and (0 0 2) which indicated the preference of these crystal plane. Both of the XRD spectra had high matching exceeding 90.0 % with ICDD 00-045-00937 shown in **Appendix** with **Figure 10 (a)** having 95.5 % matching rate while **Figure 10 (b)** having 93.1 % matching rate respectively.

Table 9: Degree of crystallinity, average crystalline size and of SOPE - mediated CuO NPs synthesized under different conditions

XRD spectrum CuO NPs	Degree of crystallinity (%)	Average crystalline size (nm)	Crystal system
Figure 10 (a)	19.30	20.16	Monoclinic
Figure 10 (b)	20.87	19.64	Monoclinic

The XRD spectrum of both synthesized SOPE-mediated CuO NPs show presence of contamination as other minor peaks was observed indicating that trace amount of phytochemical or degraded fragments are still present after calcination process which was also reflected in EDX and FTIR analysis in **sections 4.2.2 and 4.2.4**. Despite optimization made in this study, the degree of crystallinity for both SOPE-mediated CuO NPs remains low at only around 20.0 %. This could be further solved through modification in concentration of precursor salt, concentration of plant extract, pH regulation and other factors in the green synthesis process.

4.2.2 Fourier Transform Infrared FTIR

Overall, the CuO NPs FTIR spectra consistently showed the signal of 5 distinct peaks that signified the O-H group, C=C group, C-O group, C=O group, and Cu-O group. At around 3400 cm^{-1} and 1384 cm^{-1} indicated the O-H group presence of O-H group that may had been contributed by adsorbed water molecules on the surface of CuO NPs or from the phenolic phytochemicals that act as stabilizing agent in the synthesis. The presence of C=C group and C-O group at around 1635 cm^{-1} and 1100 cm^{-1} indicates the presence of fatty acids respectively, carbohydrates or phenolic compounds were present in OPE (Amanulla and Sundaram, 2019). Though observing the presence of C=C group and C-O group after calcination process, indicated the phytochemicals have not decomposed completely within the provided calcination duration or temperature (Doan Thi *et al.*, 2020).

The sharp intense peak observed at around 535 cm^{-1} indicated the presence of M-O (metal- oxygen) group which in this study is the Cu-O bond from CuO NPs synthesized. It can be further confirmed through comparison of FTIR spectrum of CuO NPs synthesized using $Cu(NO_3)_2 \cdot 3H_2O$ mediated with SOPE and calcinated at 500 ˚C with all used OPE shown in **Figure 11 (b)** where the presence of peak around 535 cm^{-1} was not observed across all prepared.

(a)

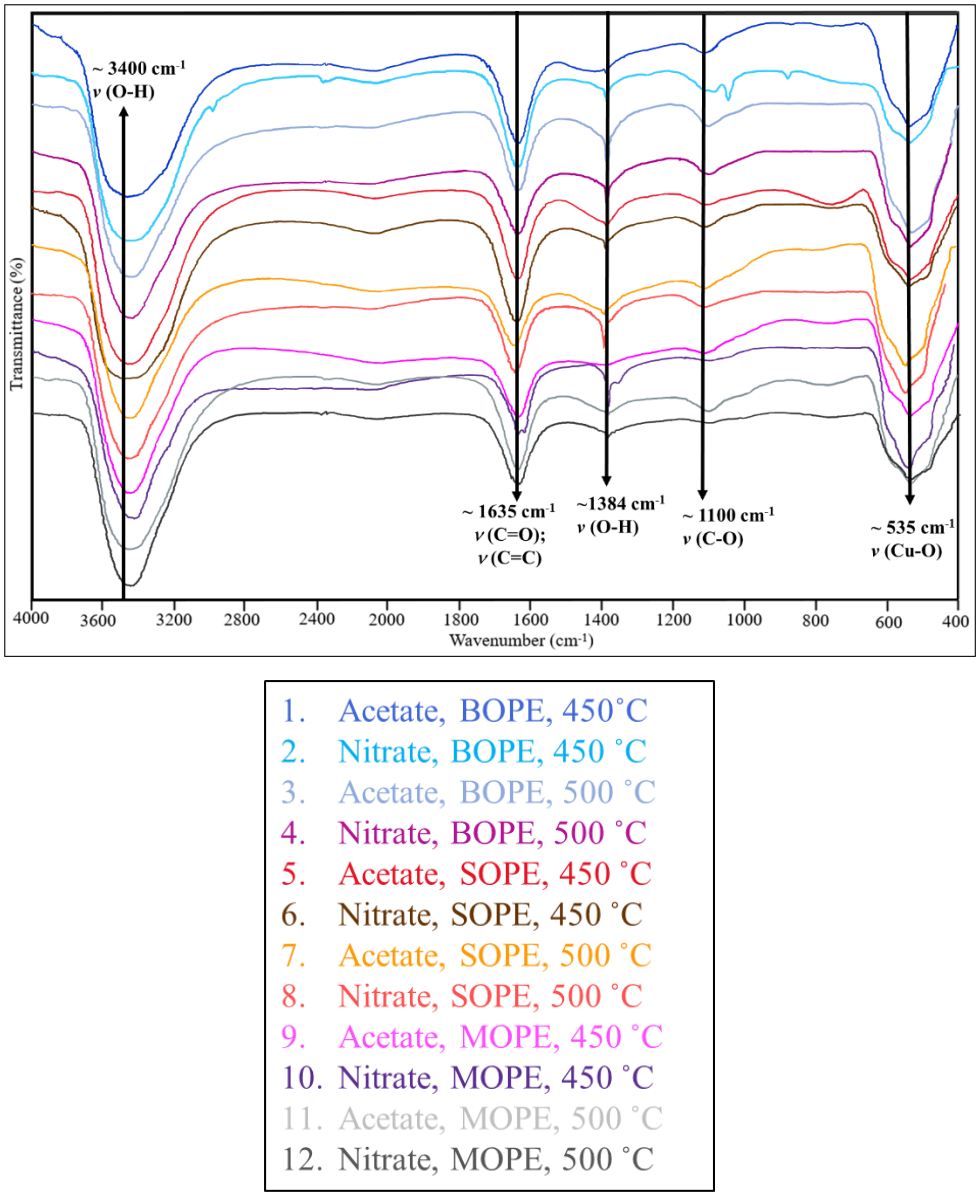

Figure 11: (a) FTIR spectrum of OPE-mediated CuO NPs synthesized under different conditions

(b)

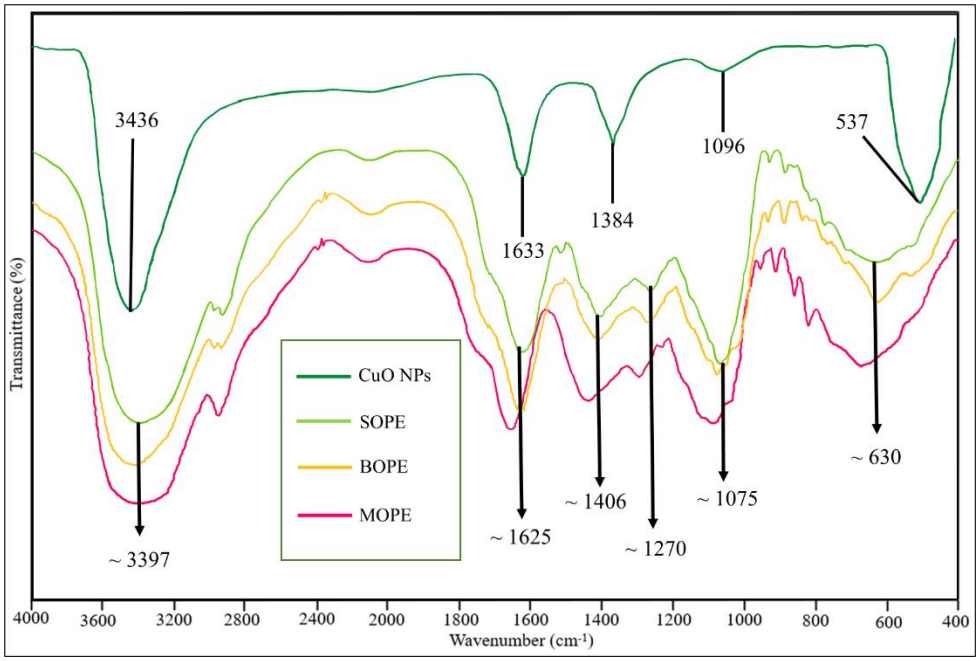

Figure 11: (b) FTIR spectrum of prepared OPE, orange peel and CuO NPs

Table 10: Wavenumber and peak assignment of FTIR spectrum of CuO NPs and OPE

Peak assignment	Wavenumber (cm^{-1})	
	OPE	CuO NPs
ν(O-H)	~ 3397	~3400
ν(C-H)	~1625	-
ν(C=O); ν(C=C)	~1406	~1384
ν (C-O)	~1270	-
ν (C-O)	~1075	~1100
ν(O-H)	~630	-
ν(Cu-O)	-	~537

4.2.3 Field Emission Scanning Electron Microscope FE-SEM

FE-SEM imaging was employed to examine the morphology of CuO NPs mediated by OPE across diverse conditions. As depicted in Figures 12 and 13, the CuO NPs exhibit a predominantly agglomerated structure. This phenomenon stems from various factors, including the inherent high surface area, surface energy, surface tension, and surface reactivity of CuO NPs, as discussed in prior research (Chan *et al*., 2022). Furthermore, the viscosity of the plant extract, attractive forces among CuO NPs, and the oxidation process of CuO NPs contribute to the observed agglomeration (Ramzan *et al*., 2019; Siddiqui *et al*., 2019).

The observed spherical shape of OPE-mediated CuO NPs is attributed to isotropic aggregation at the isoelectronic point region, regulated by dispersive forces and electrostatic interparticle attraction (Baharudin *et al*., 2018). Despite the general expectation that the diameter of metal oxide nanoparticles would increase with higher calcination temperatures, it was noted that the size remained unaffected by the calcination temperature increase of only 50 °C, unlike studies by Chan *et al*. (2022) and Doan Thi *et al*. (2020), which examined the effects of a 100 °C temperature rise.

Based on **Figures 12 and 13**, CuO NPs synthesized with $Cu(OOCCH_3)_2 \cdot H_2O$ displayed more irregular shapes and were highly agglomerated, with generally larger average sizes compared to CuO NPs synthesized with $Cu(NO_3)_2 \cdot 3H_2O$ precursor salt, which exhibited a more spherical structure and lesser agglomeration.

(a) BOPE, 450 ˚C

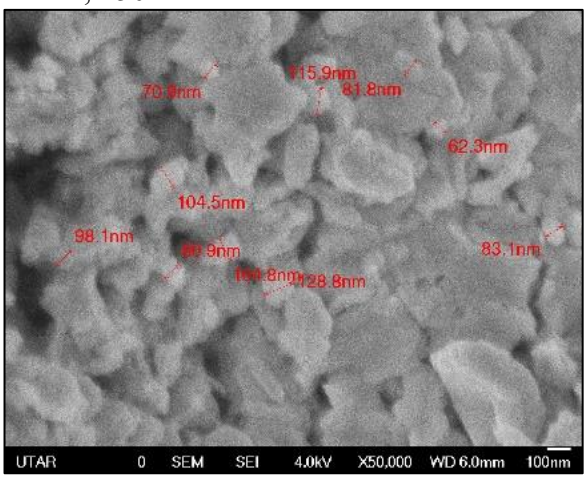

(b) BOPE 500 ˚C

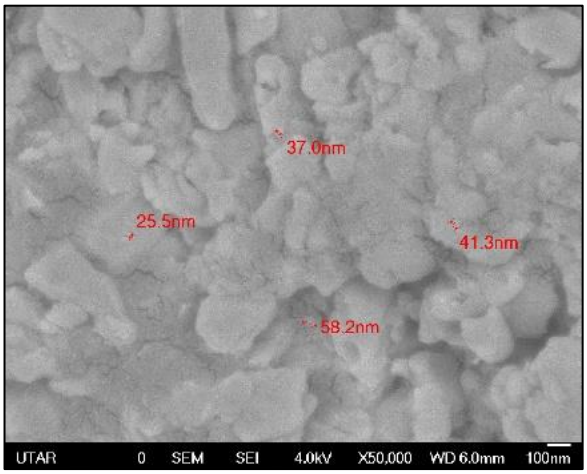

(c) SOPE, 450 ˚C

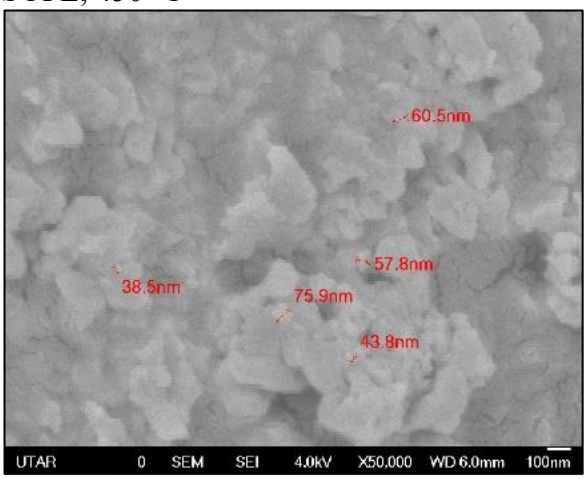

(d) SOPE, 500 ˚C

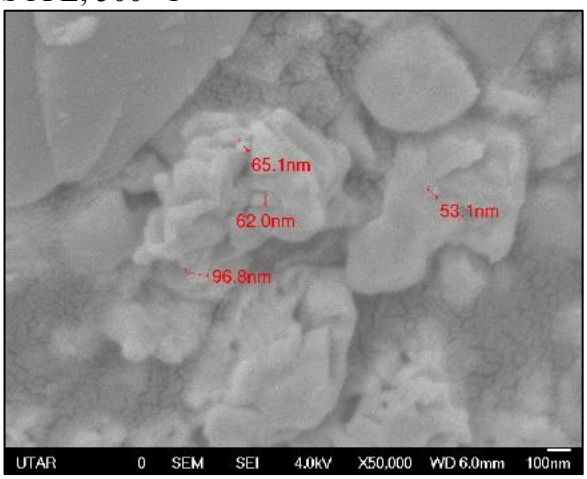

(e) MOPE, 450 ˚C

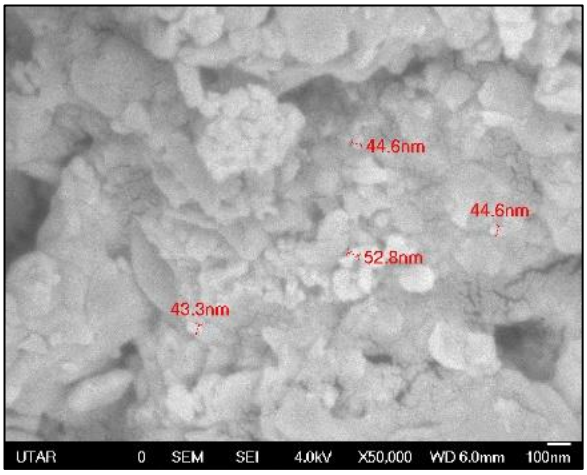

(f) MOPE, 500 ˚C

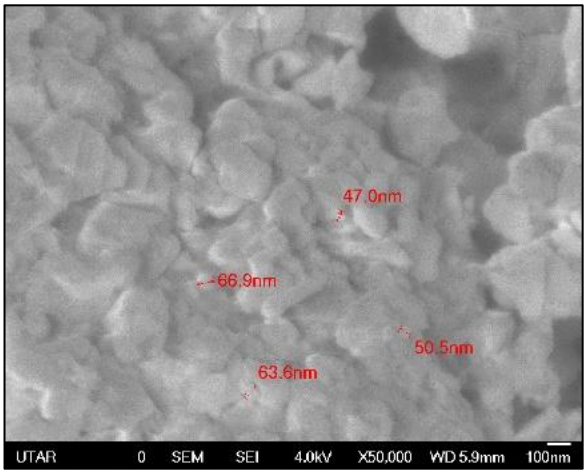

Figure 12 (a)- (f): SEM images at x50000 of OPE-mediated OPE CuO NPs synthesized using $Cu(OOCCH_3)_2 \cdot H_2O$ under different conditions

(a) BOPE, 450 ˚C

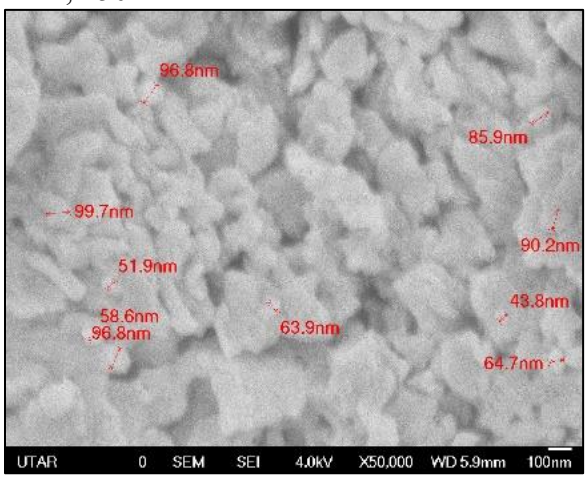

(b) BOPE, 500 ˚C

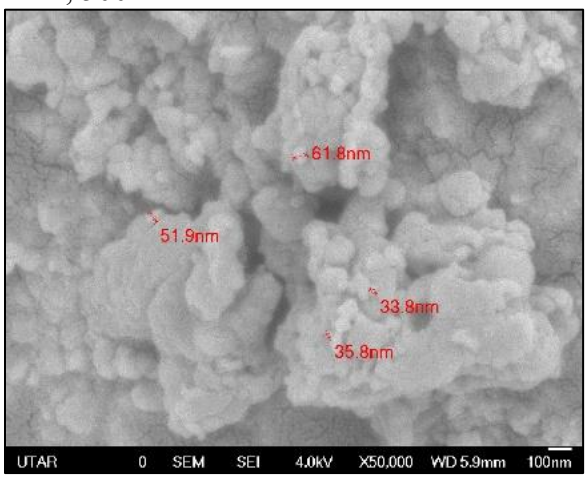

(c) SOPE, 450 ˚C

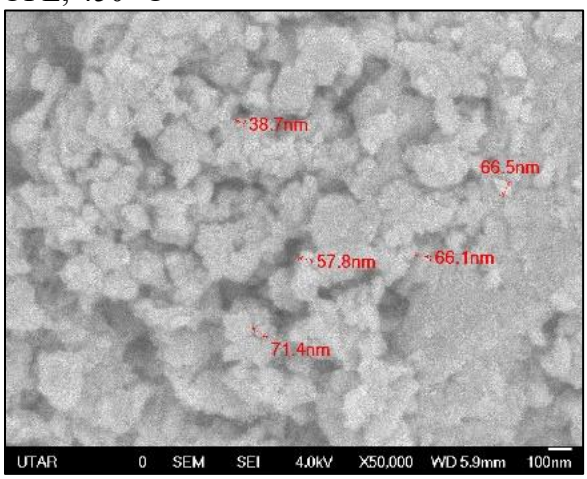

(d) SOPE, 500 ˚C

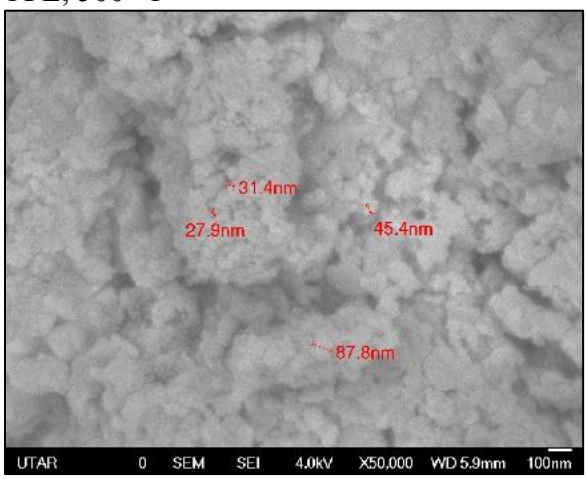

(e) MOPE, 450 ˚C

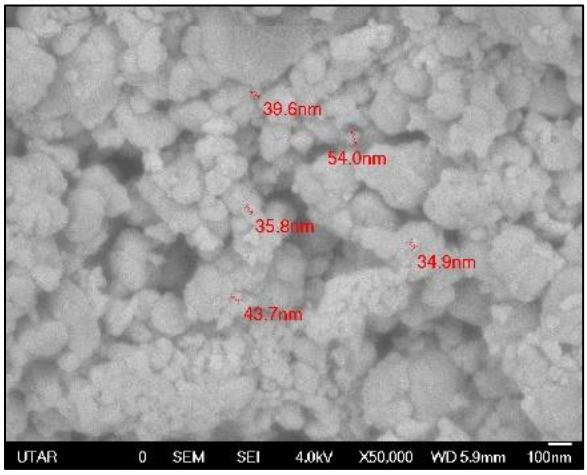

(f) MOPE, 500 ˚C

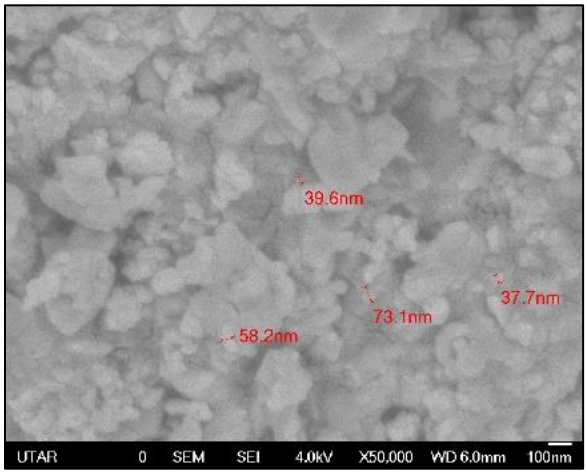

Figure 13 (a)- (f): SEM images at x50000 of OPE-mediated OPE CuO NPs synthesized using $Cu(NO_3)_2 \cdot 3H_2O$ under different conditions

Table 11: Summary of size and morphology of OPE-mediated CuO NPs synthesized under different conditions

Precursor salt	OPE	Calcination temperature (˚C)	Size (nm)	Morphology
$Cu(OOCCH_3)_2 \cdot H_2O$	BOPE	450	84.1	Irregular shaped and agglomerated
	BOPE	500	40.5	Irregular shaped and highly agglomerated
	SOPE	450	55.3	Irregular shaped and agglomerated
	SOPE	500	69.3	Irregular shaped and highly agglomerated
	MOPE	450	46.3	Irregular shaped and agglomerated
	MOPE	500	57.0	Irregular shaped and agglomerated
$Cu(NO_3)_2 \cdot 3H_2O$	BOPE	450	81.6	Irregular shaped and agglomerated
	BOPE	500	45.8	Irregular shaped and highly agglomerated
	SOPE	450	60.1	Spherical and agglomerated
	SOPE	500	48.1	Spherical and agglomerated

	MOPE	450	41.6	Spherical and agglomerated
	MOPE	500	52.2	Irregular shaped and agglomerated

4.2.4 Energy Dispersive X-ray Spectroscopy (EDX)

EDX was carried out to determine the elemental composition of OPE-mediated CuO NPs synthesized under different conditions. In all the EDX spectrum for OPE-mediated CuO NPs under different conditions presence of Cu, oxygen and carbon was observed, the presence of carbon signal may be attributed to presence of impurities which is from the remaining phytochemicals from the OPE that was degraded in the calcination process (Nguyen *et al.*, 2023).

The atomic percentage of Cu, O and C present in each OPE-mediated synthesized CuO NPs was observed and listed in **Table 12** and shown in **Figure 14 and 15**. Based on **Table 12**, it was generally observed that at high calcination temperature of 500 ˚C, the signal for carbon is relatively lower for all OPE preparation method using $Cu(OOCCH_3)_2 \cdot H_2O$ precursor salt while for OPE-mediated CuO NPs synthesized using $Cu(NO_3)_2 \cdot 3H_2O$, carbon signal was relatively similar. Trace amount of potassium was present as orange peel contain relatively high amount of potassium that may had been extracted into the OPE during preparation process (Czech *et al.*, 2020). It was observed that relatively high signal for carbon is present in CuO NPs synthesized using BOPE usually around the range of 35- 45% indicating high amount of decomposed phytochemicals remaining after calcination due to the low reducing ability of phytochemicals (Chan *et al.*, 2022; Nguyen *et al.*, 2023).

(a) BOPE, 450 ˚C

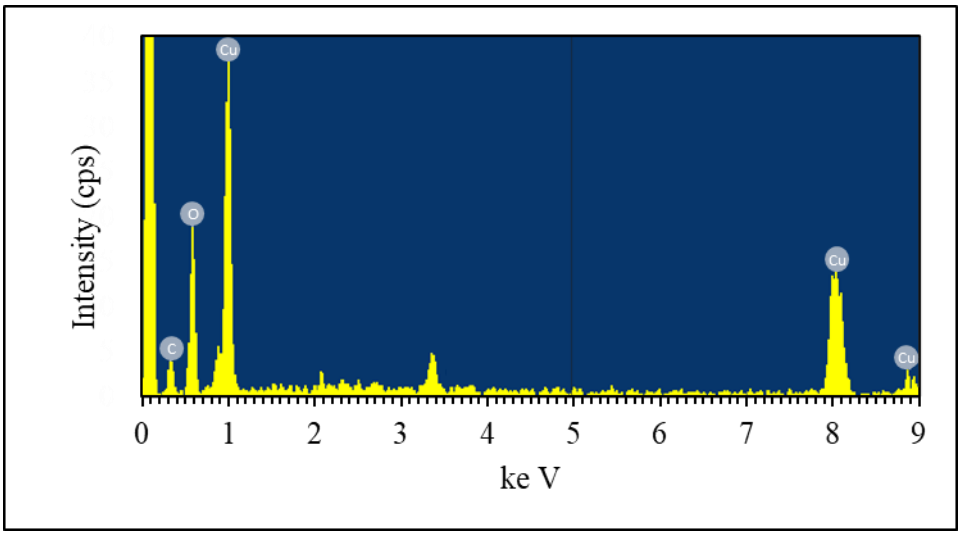

(b) BOPE, 500 ˚C

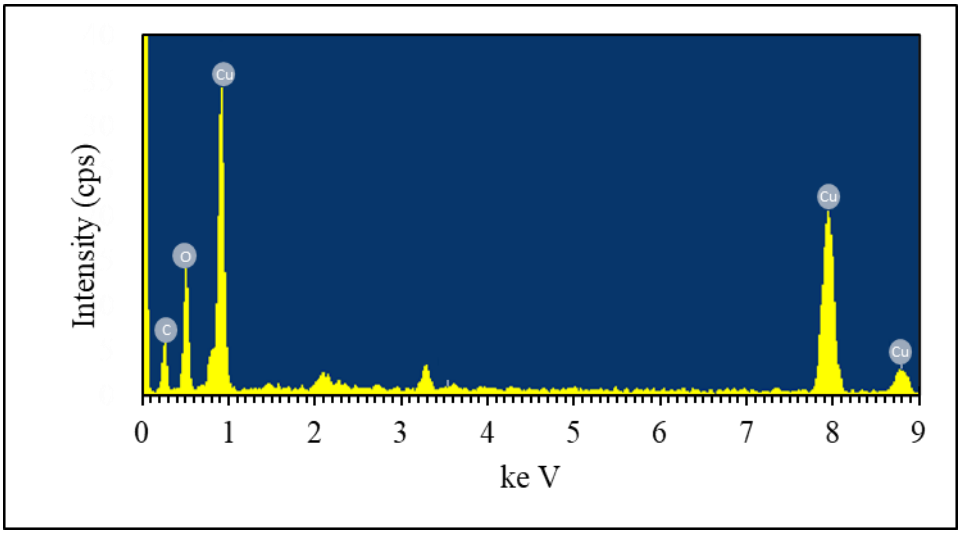

(c) SOPE, 450 ˚C

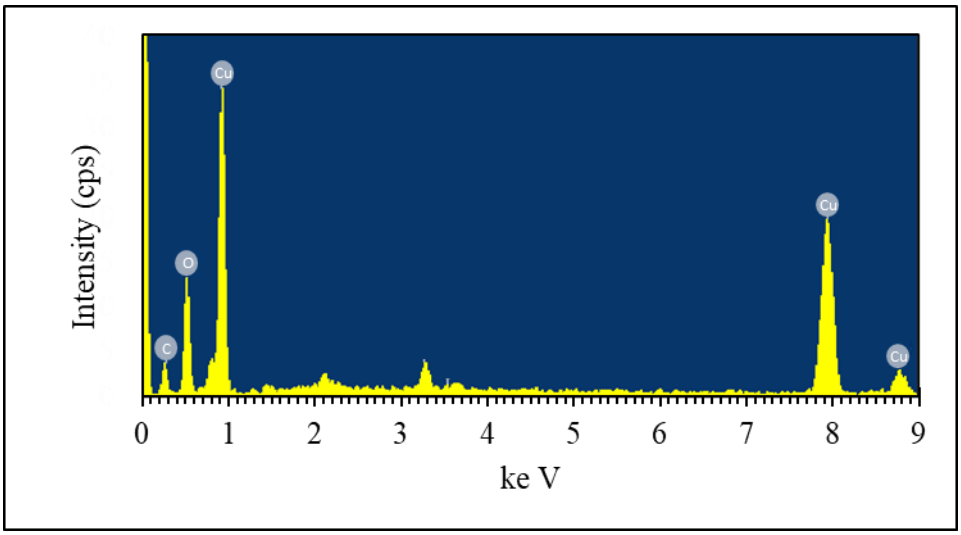

(d) SOPE, 500 ˚C

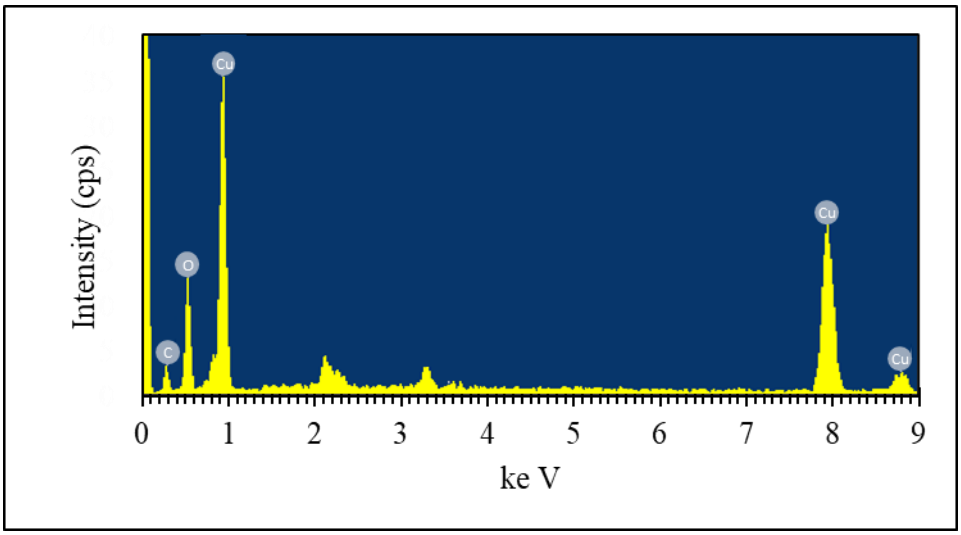

(e) MOPE, 450 ˚C

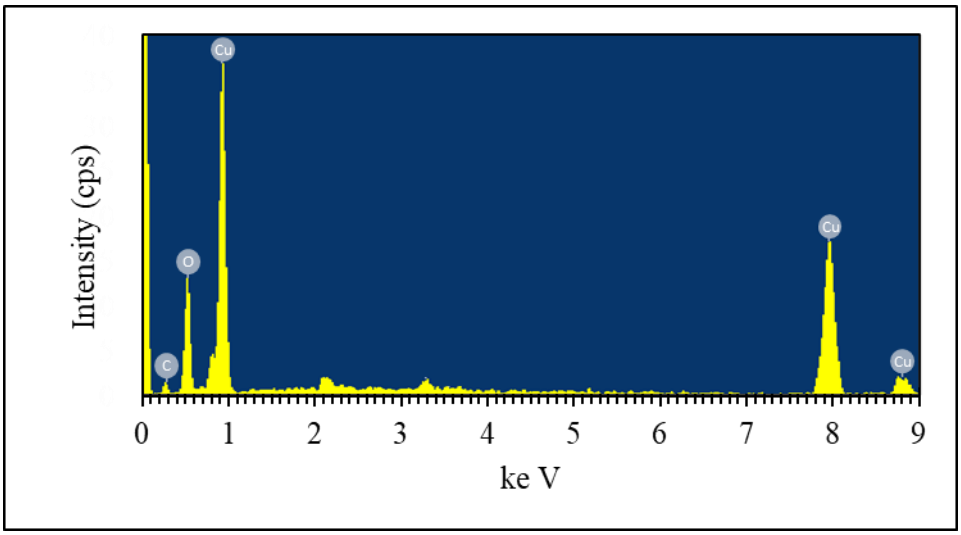

(f) MOPE, 500 ˚C

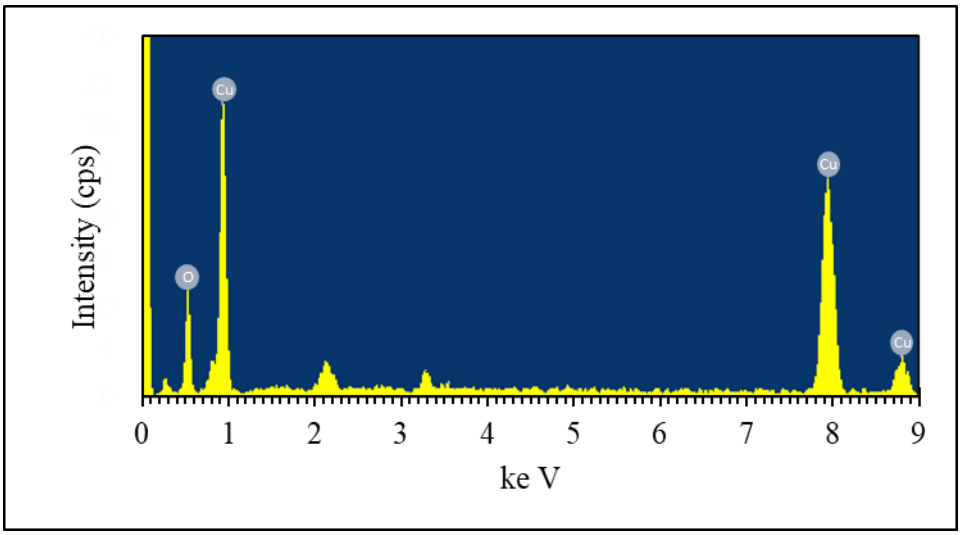

Figure 14 a) – f): EDX spectrum of OPE- mediated CuO NPs synthesized using $Cu(OOCCH_3)_2 \cdot H_2O$ precursor salt

(a) BOPE, 450 ˚C

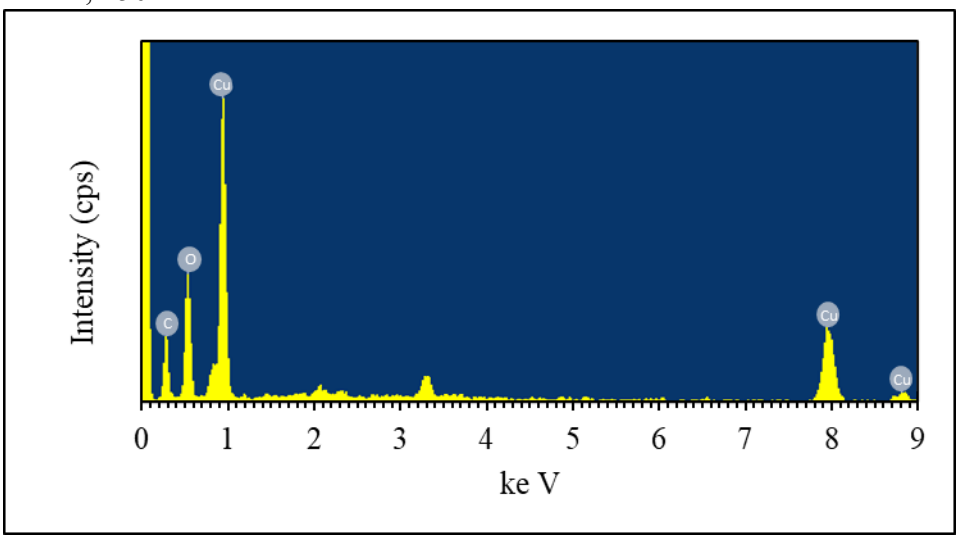

(b) BOPE, 500 ˚C

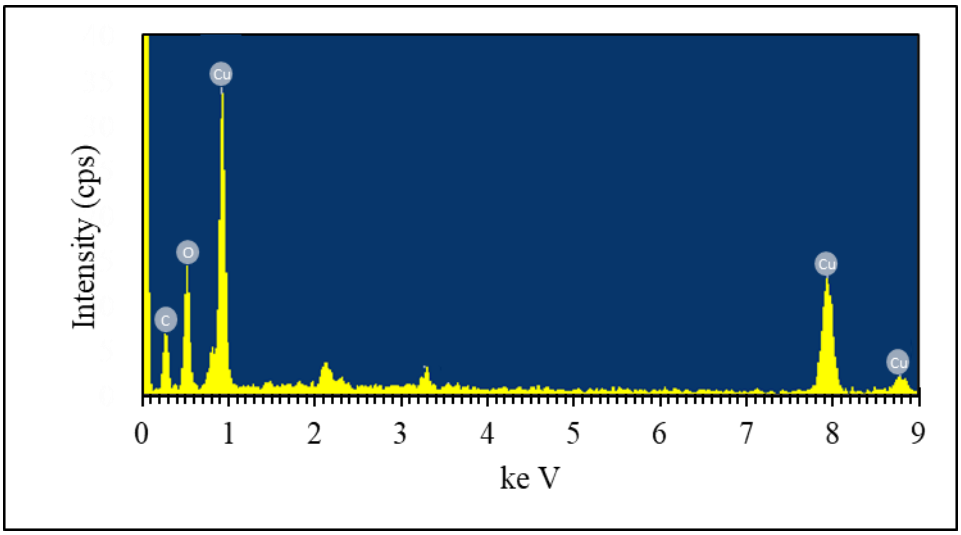

(c) SOPE, 450 ˚C

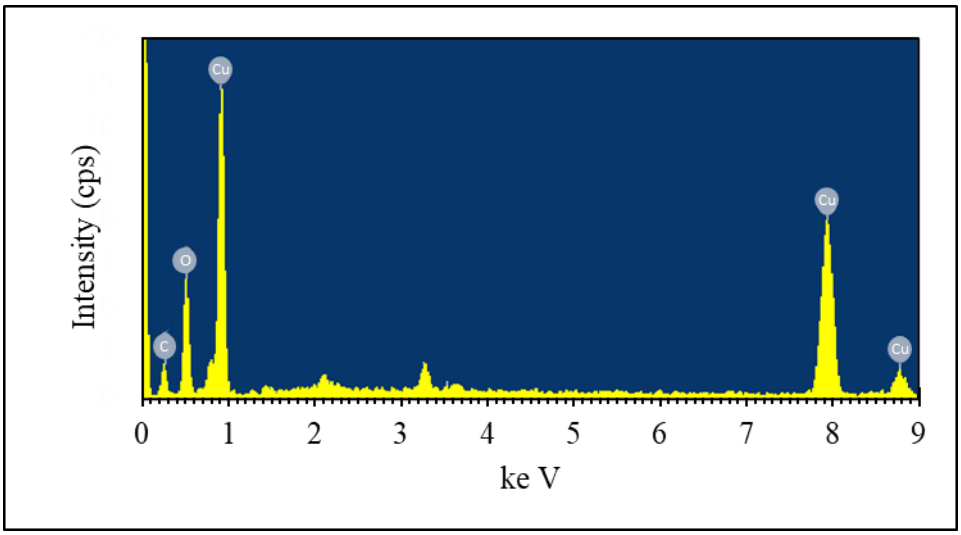

(d) SOPE, 500 ˚C

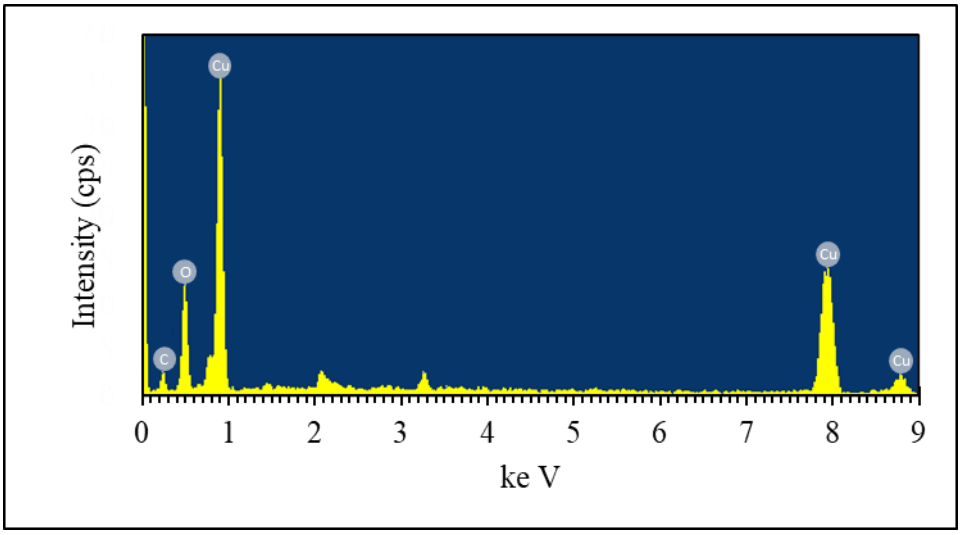

(e) MOPE, 450 ˚C

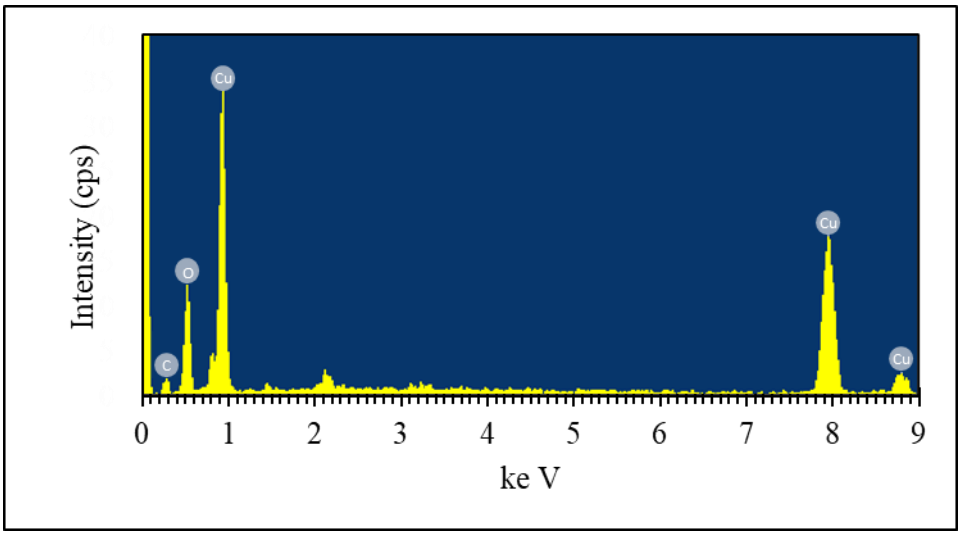

(f) MOPE, 500 ˚C

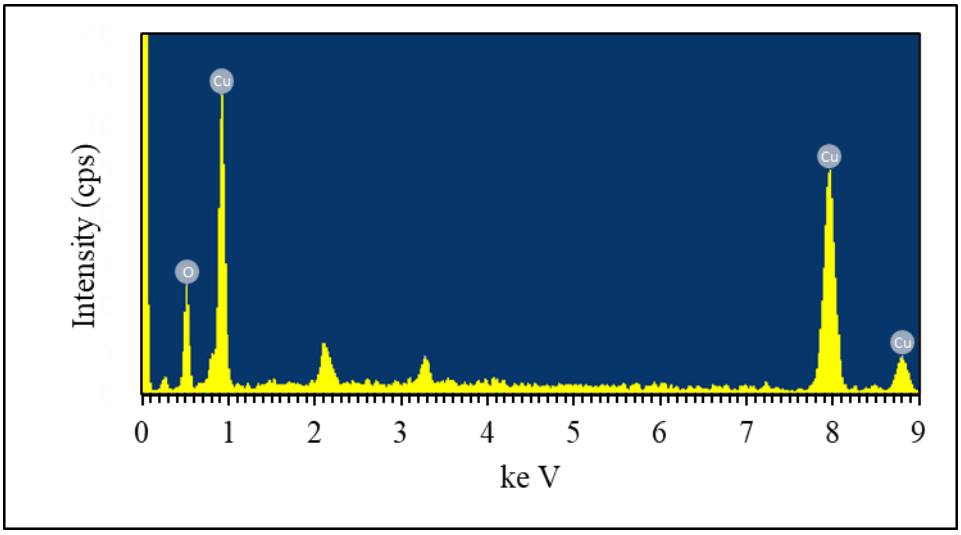

Figure 15 (a)- (f): EDX spectrum of OPE- mediated CuO NPs synthesized using $Cu(NO_3)_2 \cdot 3H_2O$ precursor salt

Table 12: Summary of atomic percentage of Cu and O in OPE-mediated CuO NPs synthesized under different conditions

Precursor salt	OPE	Calcination temperature (˚C)	Atomic percentage (%)		
			Cu	O	C
$Cu(OOCCH_3)_2 \cdot H_2O$	BOPE	450	16.99	40.84	41.22
	BOPE	500	35.24	30.30	33.56
	SOPE	450	59.01	24.26	15.66
	SOPE	500	60.24	22.66	15.31
	MOPE	450	49.6	35.37	14.44
	MOPE	500	70.90	27.72	-
$Cu(NO_3)_2 \cdot 3H_2O$	BOPE	450	12.34	42.26	44.50
	BOPE	500	25.58	35.81	37.85
	SOPE	450	45.68	32.68	20.30
	SOPE	500	40.76	35.30	22.88
	MOPE	450	47.81	32.60	19.59
	MOPE	500	69.99	28.09	-

4.2.5 Ultra-violet Visible Spectroscopy (UV-Vis)

While heating the Cu precursor salt in 50 ml of OPE, a shift in colour from light green to dark green paste was noted, indicating the formation of CuO NPs. This colour change can be attributed to both the reductio of Cu^{2+} to Cu^{0} and the excitation of surface plasmon vibrations associated with them (Ghidan *et al*., 2016). UV-Vis spectrum analysis was conducted with the aim of studying the optical properties of OPE-mediated CuO NPS synthesized under different conditions. From **Figure 16 and 17,** distinct absorbance peaks were at around 380 nm -390 nm was only observed in CuO NPs synthesized with SOPE and MOPE. This observation is due to the Surface Plasmon Resonance (SPR) of CuO NPs that is influenced by the shape, size, concentration and degree of dispersion of CuO NPs (Karuppannan *et al*., 2021). The resonance effect caused by the interaction of conduction electron with the incident photon in the CuO NPs lead to the manifestation of SPR (Jana, Ganguly and Pal, 2016).

It was observed that there was an absence of distinct absorbance peak at 380 nm- 490 nm in CuO NPs synthesized with BOPE which is attributed by high agglomeration of CuO NPs that would lead to band broadening phenomenon (Jana, Ganguly and Pal, 2016). Denatured phytochemical structure and low extraction efficiency of BOPE would reduce the stabilizing ability of phytochemical in nucleation process lead to high agglomeration. In addition, BOPE involves heating the 50 g peel in 150 ml of deionized water for 20 minutes which would lead to higher viscosity

for BOPE compared to SOPE and MOPE that does not heating the final aqueous extract prior to vacuum filtration due to evaporation of water during the heating process. High viscosity of plant extract would lead to high agglomeration of CuO NPs mediated by BOPE that affects the SPR which is reflected by the absence of peak in **Figure 16 (a),(b) and Figure 17(a),(b)** (Jana, Ganguly and Pal, 2016). Another potential factor that attributed to this phenomenon is the non-uniformed size distribution amongst the synthesized CuO NPs that would contribute to band broadening as well (Baharudin, Abdullah and Derawi, 2018).

(a) BOPE, 450 ˚C

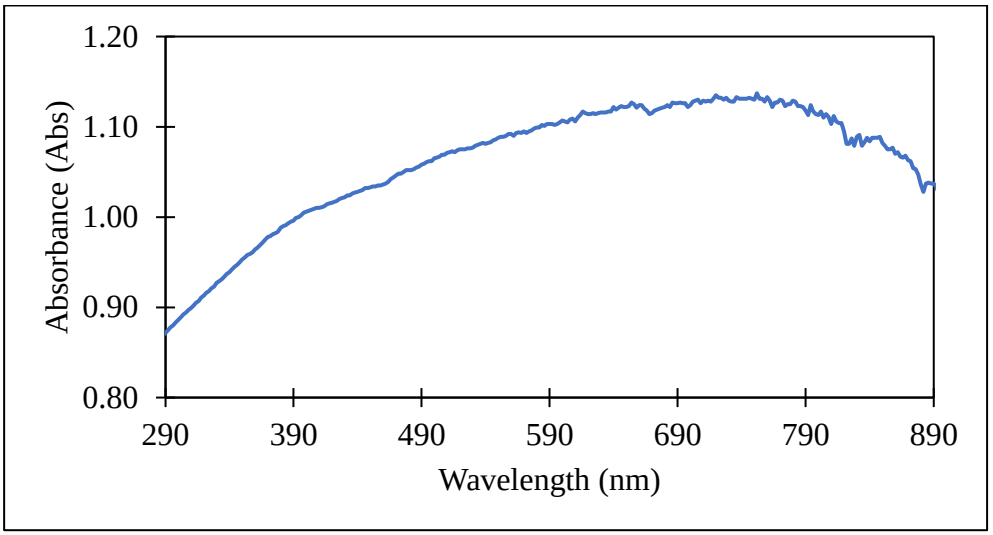

(b) BOPE, 500 ˚C

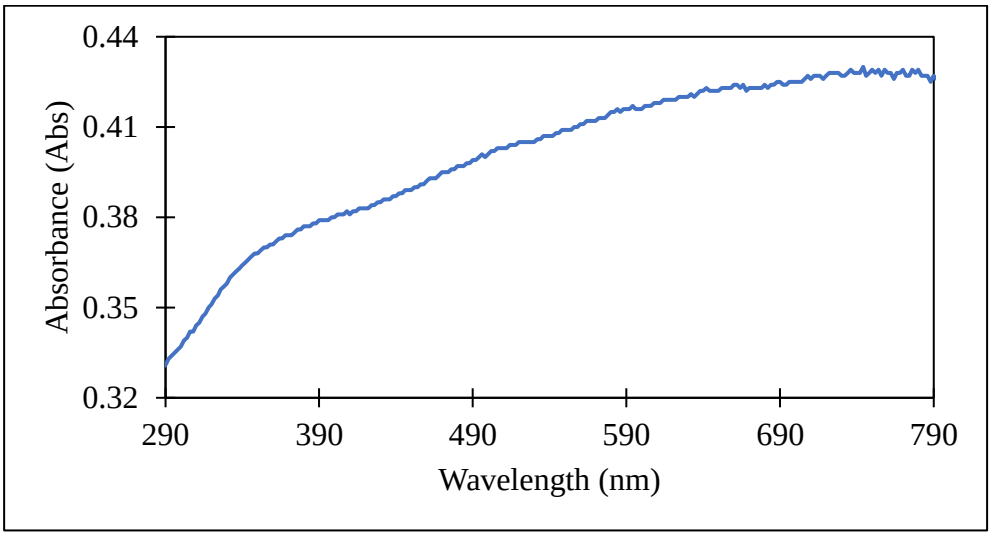

(c) SOPE, 450 ˚C

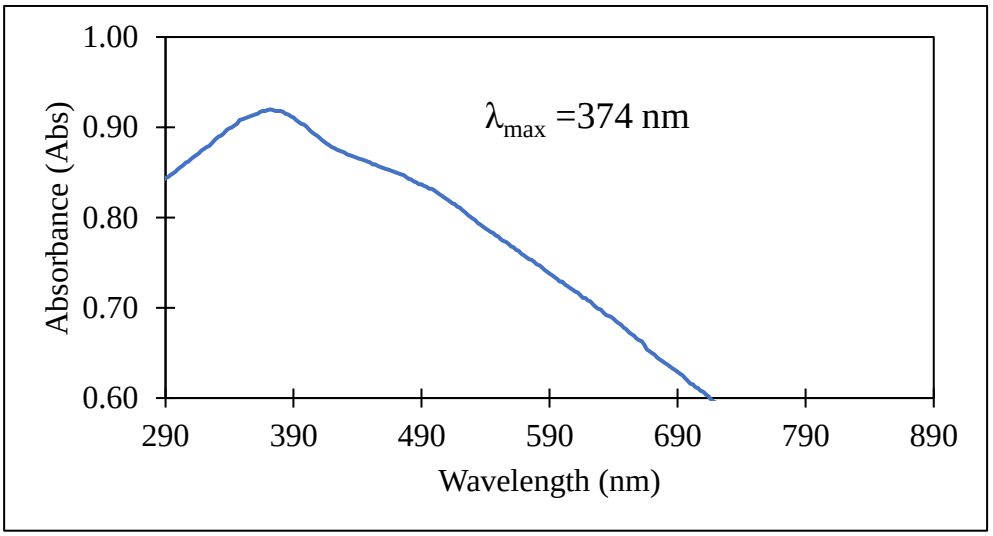

(d) SOPE, 500 ˚C

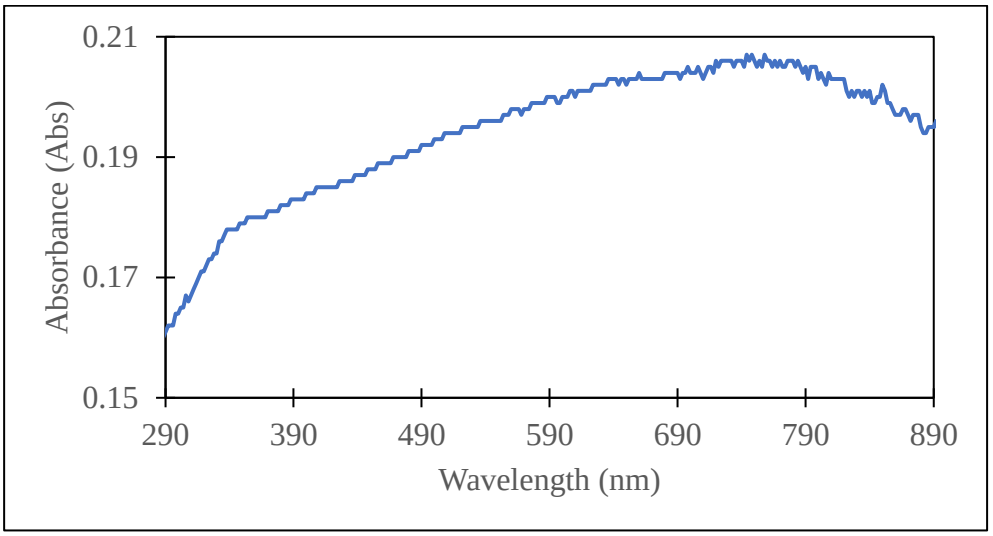

(e) MOPE, 450 ˚C

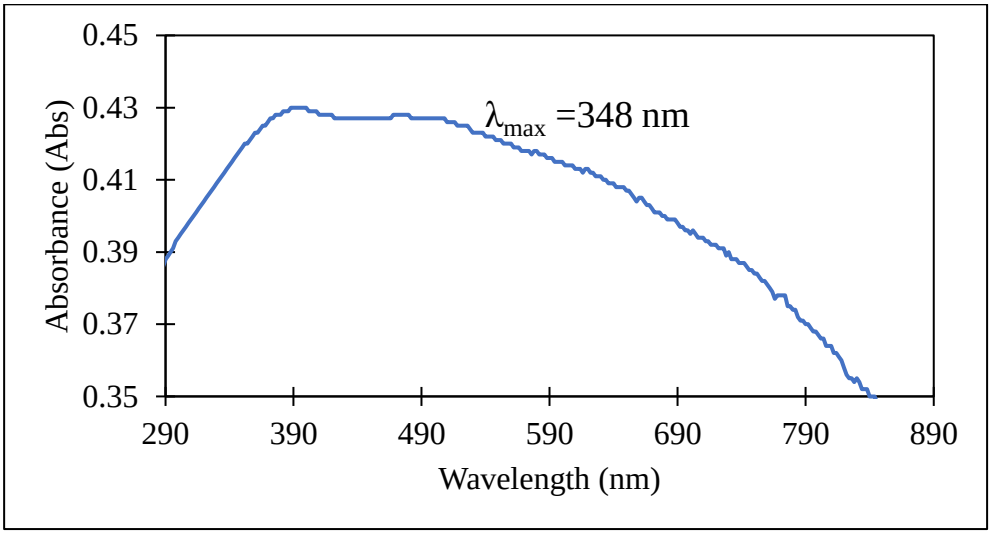

(f) MOPE, 500 ˚C

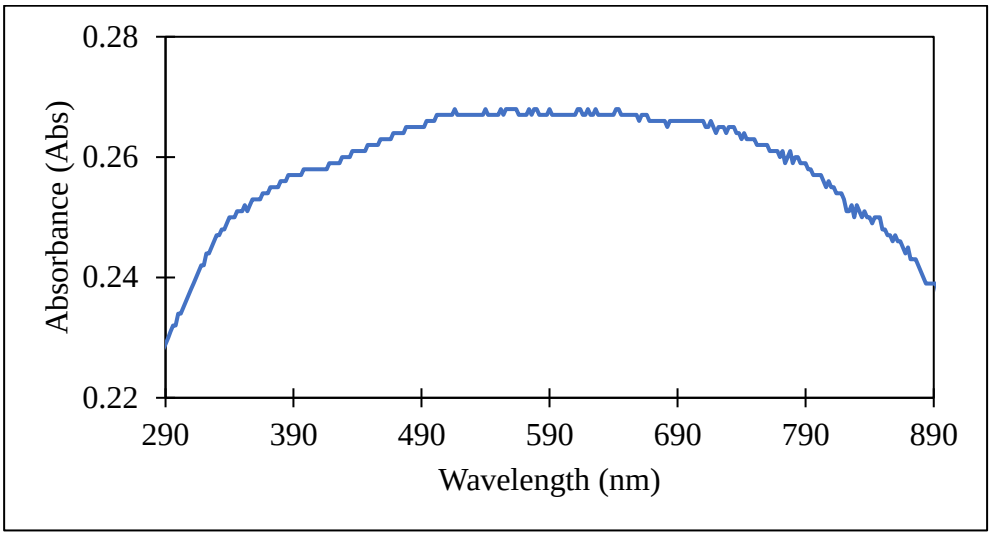

Figure 16 (a)- (f): UV-Vis spectrum of OPE-mediated CuO NPs synthesized using $Cu(OOCCH_3)_2 \cdot H_2O$ under different conditions

(a) BOPE, 450 ˚C

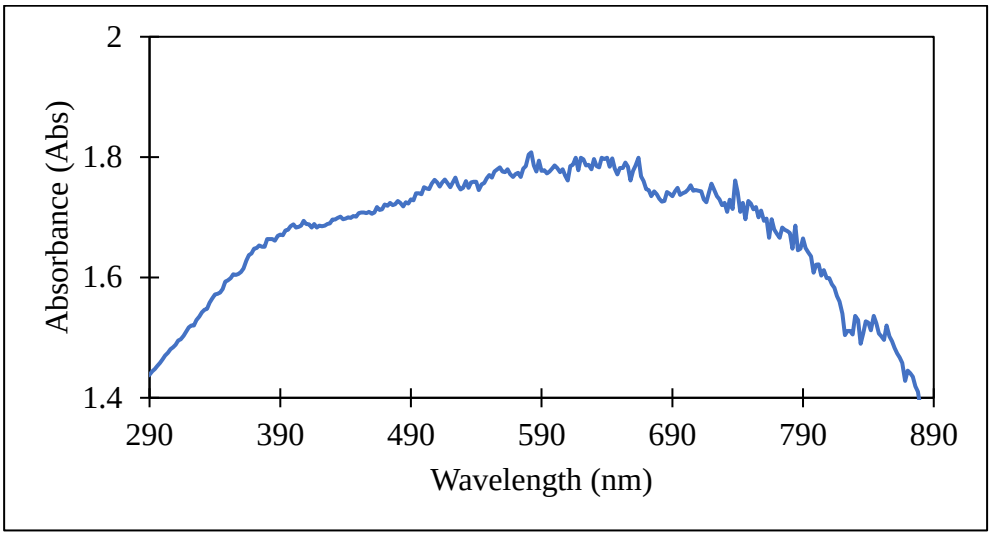

(b) BOPE, 500 ˚C

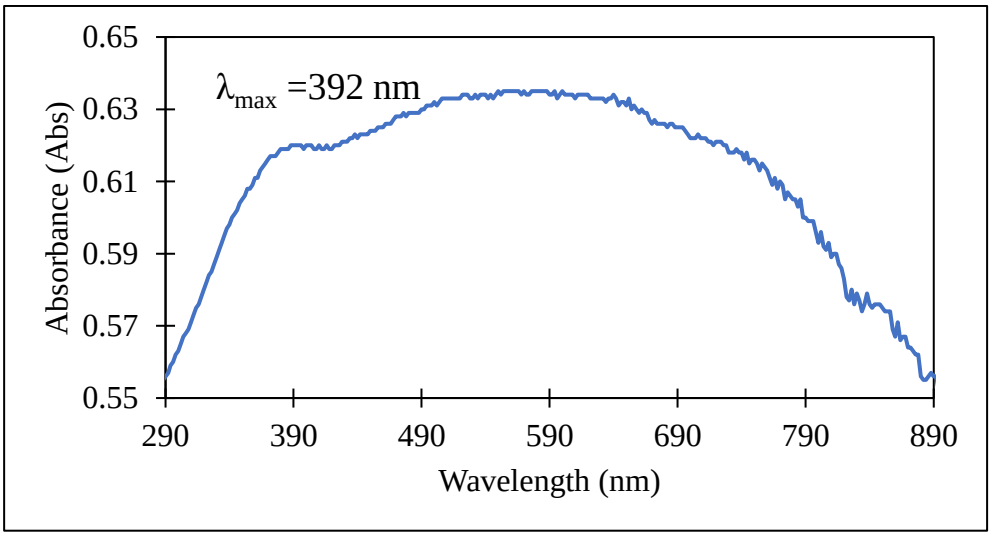

(c) SOPE, 450 ˚C

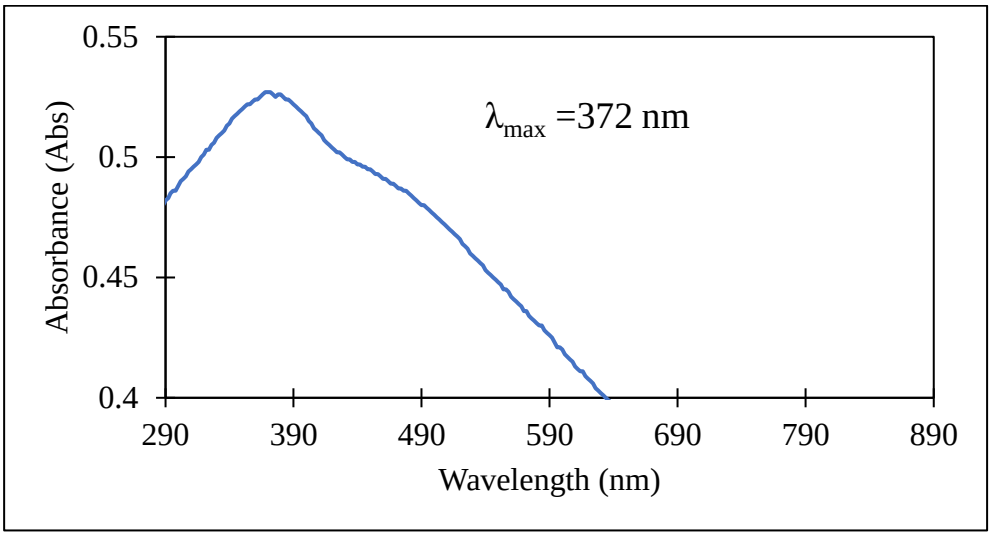

(d) SOPE, 500 ˚C

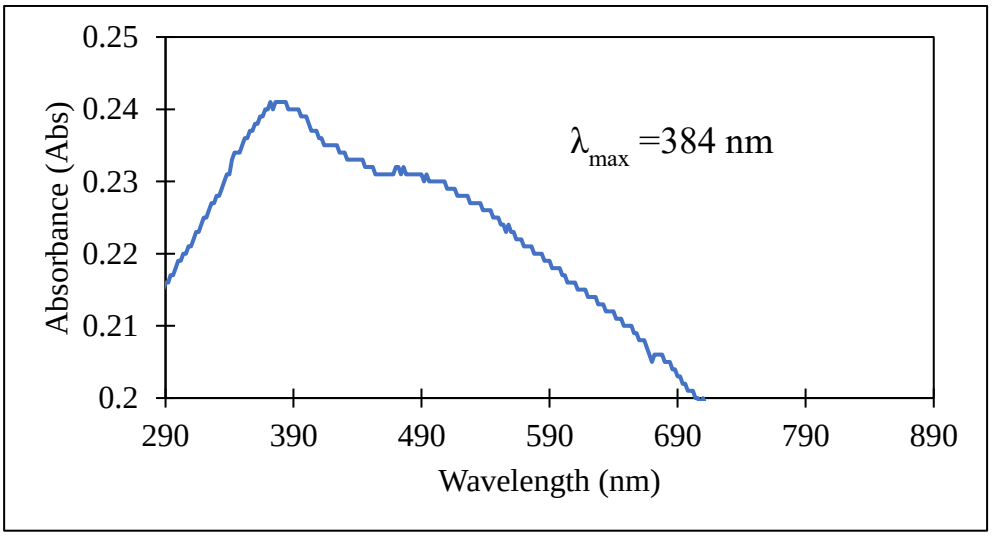

(e) MOPE, 450 ˚C

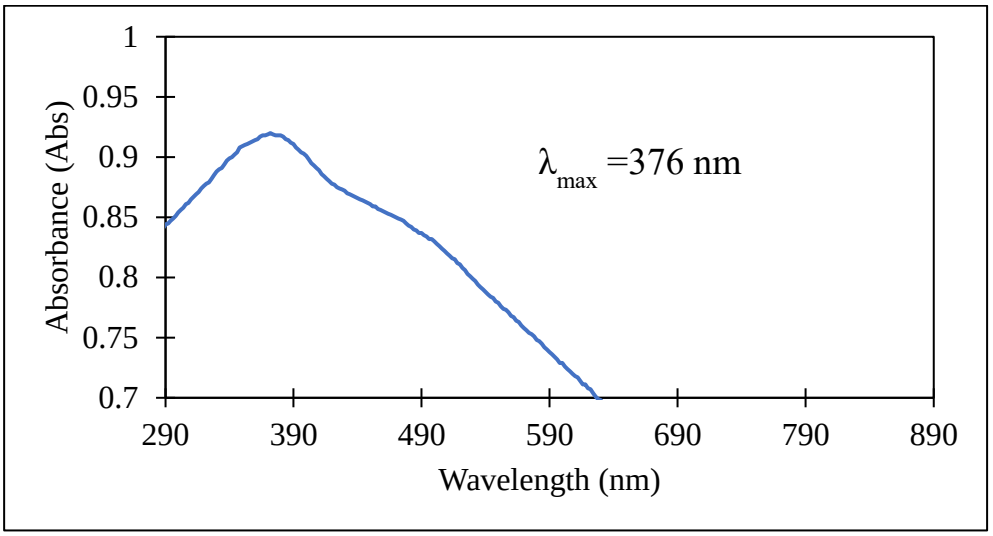

(f) MOPE, 500 ˚C

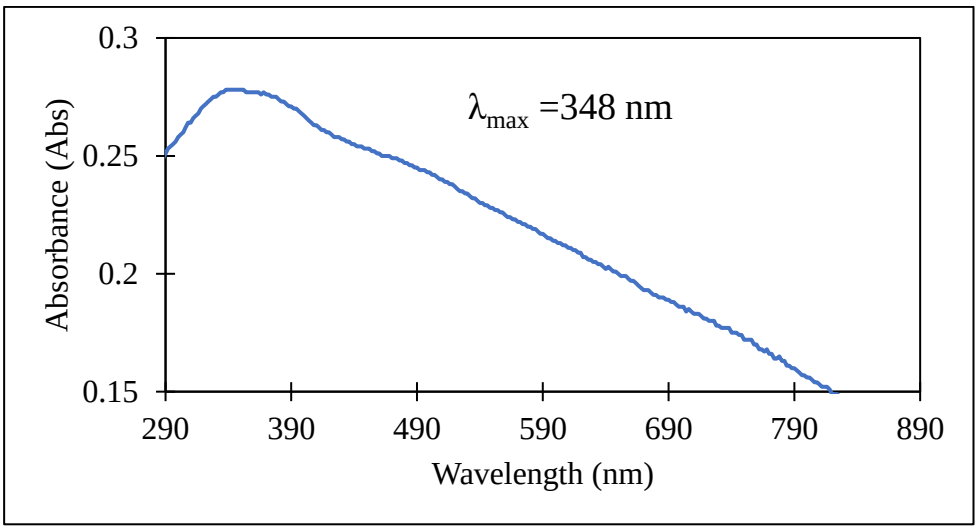

Figure 17: UV-Vis spectrum of OPE-mediated CuO NPs synthesized using $Cu(NO_3)_2 \cdot 3H_2O$ under different conditions

The determination of the energy bandgap for CuO NPs mediated by OPE, synthesized under different conditions, was accomplished through Tauc's plot methodology.

Using Tauc's plot equation ,

$$E_g = \frac{hc}{\lambda}$$

Where

Eg = Energy bandgap (eV)

h = Plank's constant

= 4.135 x 10^{-15} eV•s^{-1}

c = Speed of light

= 2.998 x 10^{8} m•s^{-1}

λ = maximum absorption wavelength (m)

The findings are summarized in **Table 13** below, wherein the direct and indirect bandgap energy was calculated to generate the Tauc's plot which is shown in **Figure 18**. On average, the E_g of OPE-mediated CuO NPs was within the range of 3.2 eV- 3.7 eV which is due to quantum confinement effect.

Table 13: Summary of E_g and λ_{max} of OPE-mediated CuO NPs synthesized under different conditions

Precursor salt	OPE	Calcination temperature (˚C)	E_g (eV)	λ_{max} (nm)
$Cu(OOCCH_3)_2 \cdot H_2O$	BOPE	450	3.56	-
	BOPE	500	3.62	-
	SOPE	450	3.62	374
	SOPE	500	3.56	-
	MOPE	450	3.66	348
	MOPE	500	3.66	-
$Cu(NO_3)_2 \cdot 3H_2O$	BOPE	450	3.43	-
	BOPE	500	3.31	392
	SOPE	450	3.56	372
	SOPE	500	3.26	384
	MOPE	450	3.73	376
	MOPE	500	3.49	348

(a) BOPE, 450 ˚C

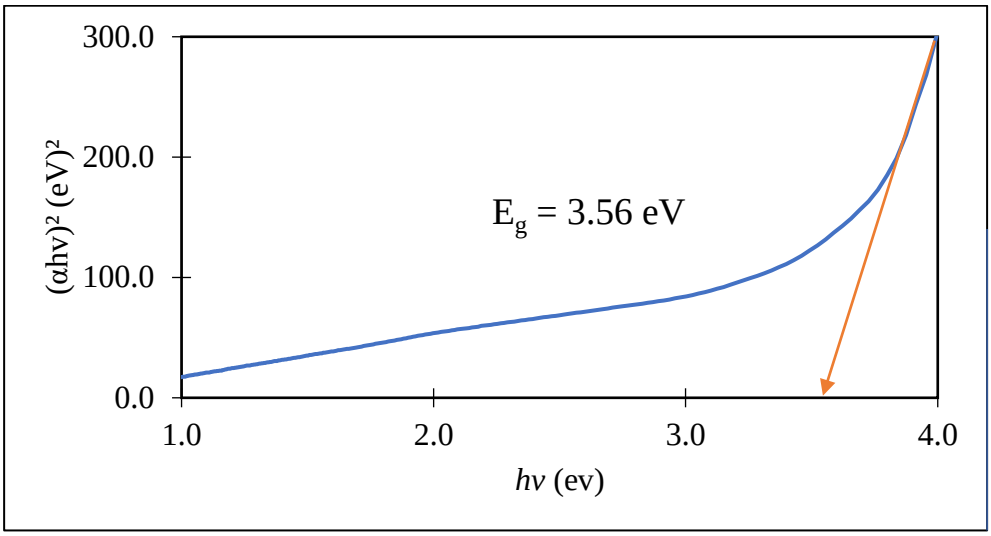

(b) BOPE, 500 ˚C

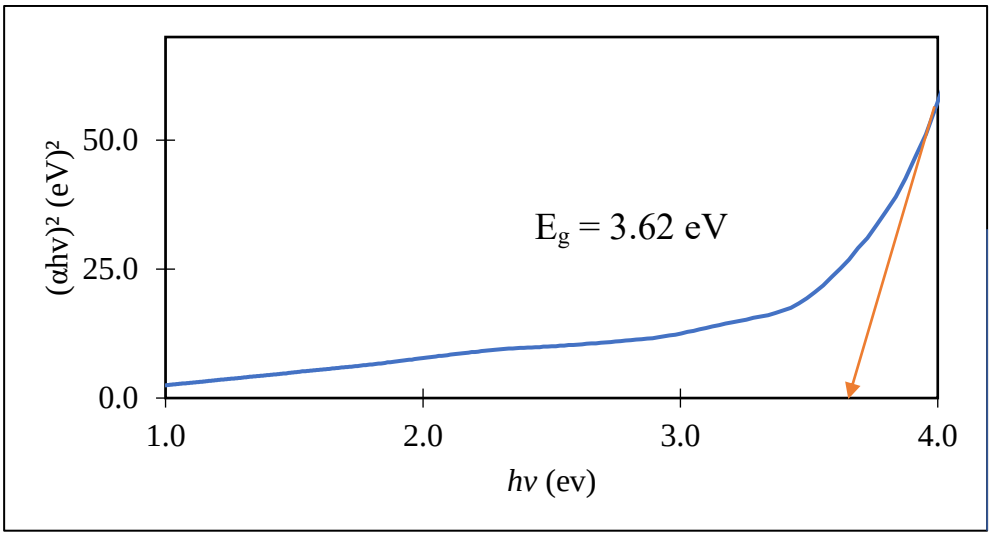

(c) SOPE, 450 ˚C

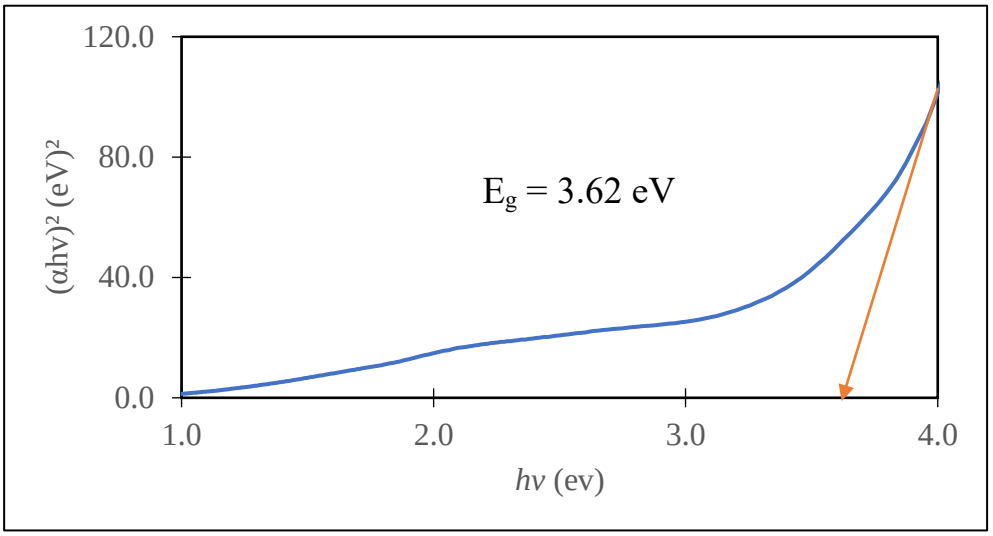

(d) SOPE, 500 ˚C

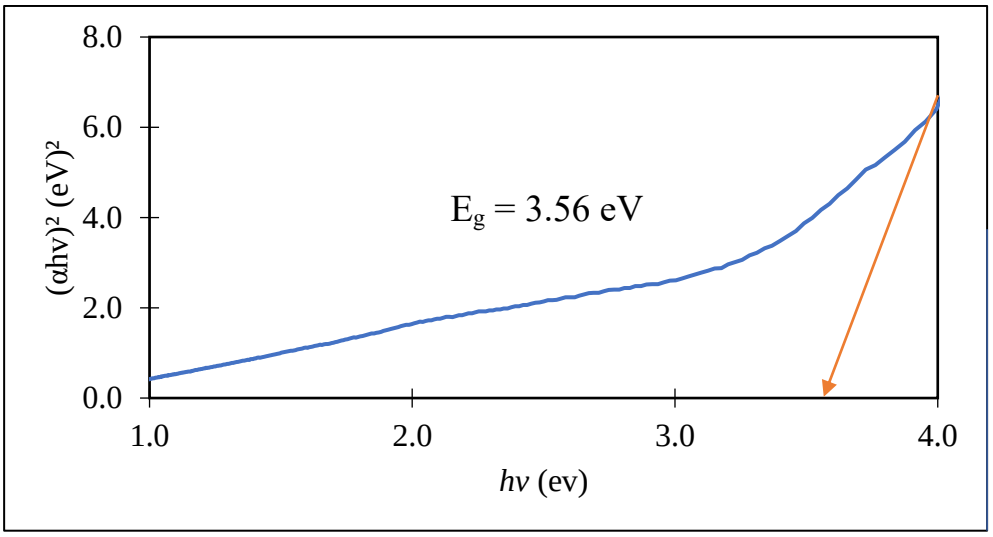

(e) MOPE, 450 ˚C

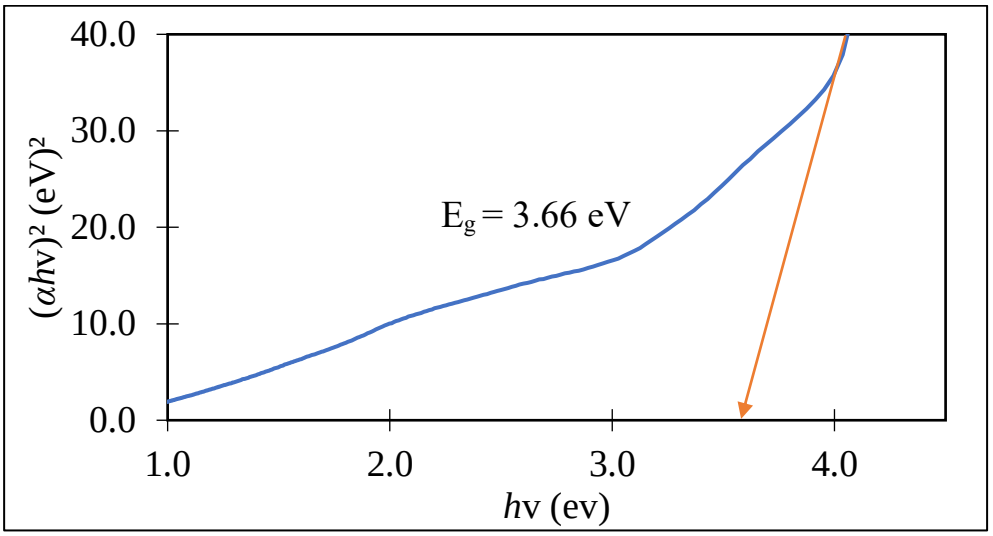

(f) MOPE, 500 ˚C

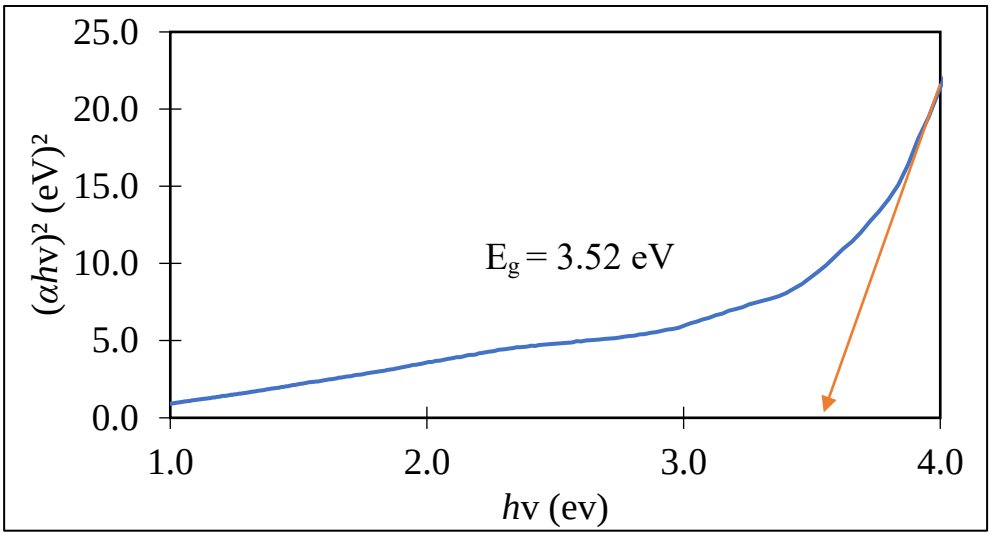

Figure 18: Tauc's plot of OPE-mediated CuO NPs synthesized using $Cu(OOCCH_3)_2 \cdot H_2O$ under different conditions

(a) BOPE, 450 ˚C

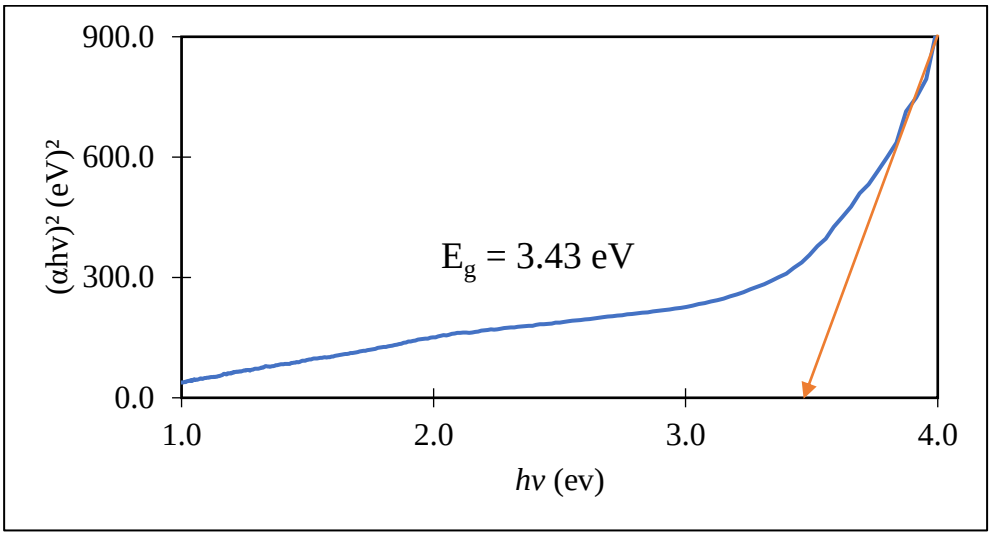

(b) BOPE, 500 ˚C

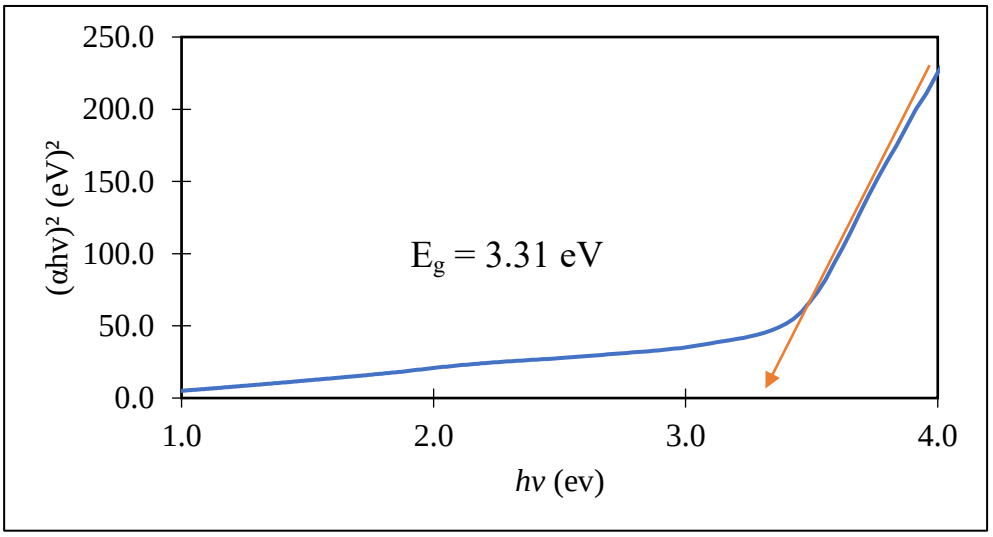

(c) SOPE, 450 ˚C

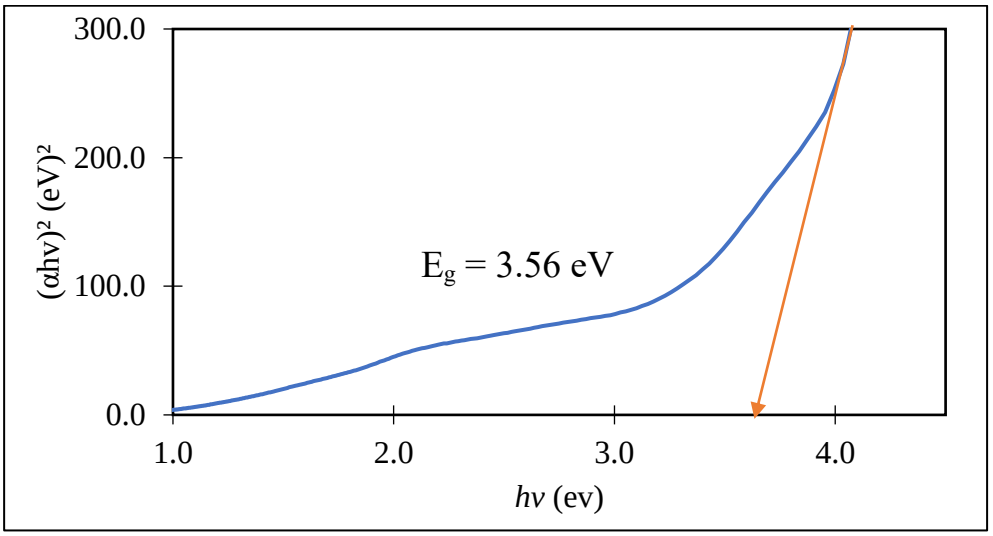

(d) SOPE, 500 ˚C

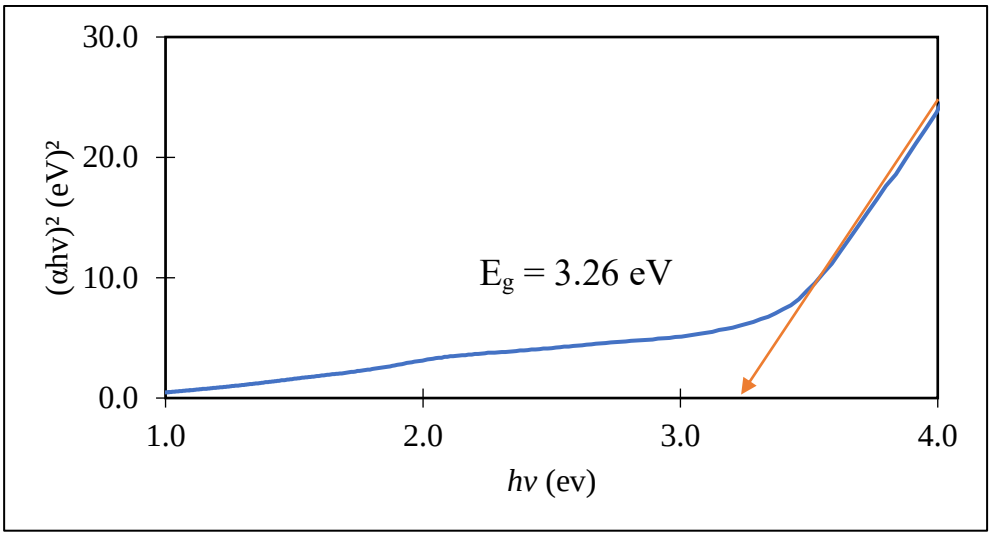

(e) MOPE, 450 ˚C

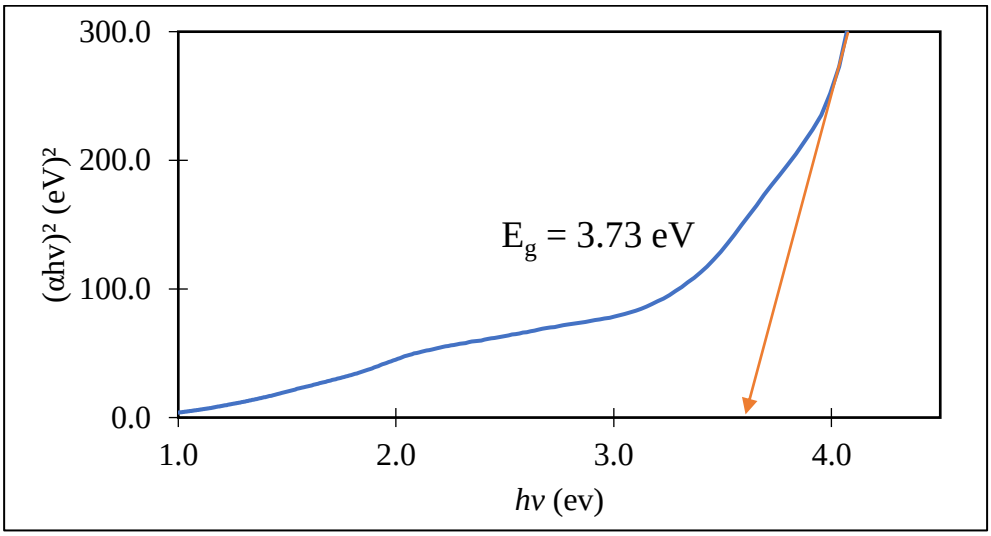

(f) MOPE, 500 ˚C

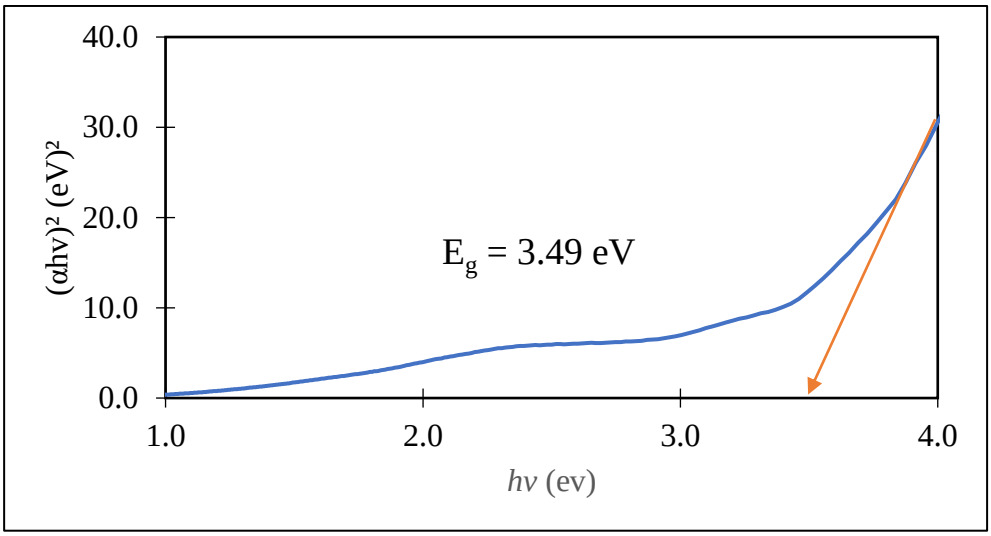

Figure 19: Tauc's plot of OPE-mediated CuO NPs synthesized using $Cu(NO_3)_2 \cdot 3H_2O$ under different conditions

4.3.1 Effect of OPE preparation method

In this study, BOPE, SOPE and MOPE was prepared and used to synthesis CuO NPs. Characterization result in **4.2** were compared to determine the most suitable method OPE for green synthesis of CuO NPs. It was found that SOPE yielded the most successful synthesised CuO NPs. Soaking method does not involve any form of heating in the OPE preparation process which enable more proper preservation of the phytochemicals of the orange peel for the purpose of acting as stabilizing and reducing agent in green synthesis process.

The preparation of BOPE involved the heating of freshly minced orange peel in deionized water, a process resulting in higher viscosity compared to SOPE and MOPE due to evaporation. Additionally, this heating process induces alterations in the secondary and tertiary structures of phytochemicals, thereby diminishing their functionality in the green synthesis process, as evidenced by the highly agglomerated and irregularly shaped CuO NPs observed in **Figures 12 (a),(b) and Figures 13 (a),(b)** (Marslin *et al*., 2018). The weakened stabilizing ability of BOPE is further evident in the UV-vis analysis presented in **Figures 16 (a),(b)** and **Figures 17(a),(b),** where pronounced agglomeration leads to band broadening, rendering distinct absorbance peaks indistinguishable within the range of 380 nm to 390 nm, indicative of CuO NPs formation (Jana *et al*., 2016). Moreover, as depicted in **Table 12**, elevated levels of carbon are detected in BOPE-mediated CuO NPs, suggesting the diminished stabilizing capacity of

phytochemicals, which lead to their conversion into soot or other degraded fragments during calcination. (Chan *et al.*, 2022; Nguyen *et al.*, 2023).

Maceration stands as a prevalent and widely employed method of extraction. In this process, the orange peel undergoes a drying phase within an oven for 15 hours at 60 °C. Unlike certain plant materials such as leaves or dry stems, which can readily be ground into powder form sans prior treatment, the orange peel's high moisture content necessitates drying to prevent paste formation upon grinding. Following drying, the orange peel is ground into a powder, a step pivotal in enhancing extraction efficiency (Rasul, 2018). The powdered orange peel boasts a significantly heightened surface area-to-volume ratio, thereby facilitating more efficient extraction processes. While conventional extraction methodologies, as observed in prior studies such as that by Doan Thi *et al*. (2020), commonly involve heating the powdered orange peel in deionized water within a water bath to expedite the extraction process, the maceration process in this project underwent modification to optimize the preservation of phytochemical integrity and minimize secondary degradation. Unlike BOPE, it is noted that phytochemicals in MOPE retain their reducing and stabilizing capabilities to a degree comparable to that of SOPE.

SOPE was formulated following a comprehensive review of maceration and boiling methods, aiming to curtail energy consumption in OPE preparation. Among the three studied preparation methods, the formulation of SOPE emerges as the most environmentally sustainable, aligning with the principles of green chemistry. This is primarily attributed to the absence of solvents, ensuring the generation of minimal chemical

waste. Furthermore, the utilization of solely orange peel waste contributes to cost reduction, while the entire preparation process conducted at room temperature further enhances its eco-friendliness. The pronounced presence of stabilizing and reducing agents in SOPE is exemplified in the UV-Vis analysis, where distinct peaks within the range of 380 nm to 390 nm were observed for both precursor salts used, as delineated in **Table 13**. Notably, both MOPE and SOPE exhibited comparable reducing and stabilizing capabilities, evidenced by the phytochemical removal efficiency post-calcination, with atomic percentages of carbon (C) below 25%, as depicted in **Table 12**.

4.3.2 Comparison of Cu precursor salt

In this study, two precursor salts, $Cu(OOCCH_3)_2 \cdot H_2O$ and $Cu(NO_3)_2 \cdot 3H_2O$, were employed for the synthesis of CuO NPs. Characterization results in Section **4.2** indicated that CuO NPs synthesized using $Cu(NO_3)_2 \cdot 3H_2O$ exhibited superior characteristics compared to those synthesized with $Cu(OOCCH_3)_2 \cdot H_2O$.

Interestingly, $Cu(OOCCH_3)_2 \cdot H_2O$ demonstrated higher effectiveness when the calcination temperature was set at 450 °C, as evidenced by UV-Vis analysis and SEM imaging. Although the removal efficiency at 500 °C was higher, it resulted in significant agglomeration and the formation of larger particle sizes, as illustrated in **Figure 12** and **Table 12**. Moreover, according to the trend observed in **Table 13**, the E_g of CuO

NPs synthesized with $Cu(OOCCH_3)_2 \cdot H_2O$ was higher than those synthesized with $Cu(NO_3)_2 \cdot 3H_2O$ under the same conditions. The increase in E_g is attributed to the heightened agglomeration of CuO NPs, leading to larger particle sizes and consequently a larger E_g. This phenomenon is ascribed to the quantum confinement effect, which is size-dependent (Sami and Abdulkarim, 2021).

$Cu(NO_3)_2 \cdot 3H_2O$ has demonstrated notable efficacy when utilized in conjunction with OPE, particularly with SOPE and MOPE preparations. In employing this precursor salt, the calcination temperature exhibited minimal influence on the UV-vis spectrum. Previous studies, as delineated in **Table 7 in section 2.4**, have predominantly employed nitrate precursors for synthesizing green nanometal oxide NPs with OPE, although chloride and acetate precursors have also been utilized. Characterization results have consistently indicated that $Cu(NO_3)_2 \cdot 3H_2O$ yields superior outcomes when paired with OPE compared to $Cu(OOCCH_3)_2 \cdot H_2O$ under equivalent conditions. This superiority is evidenced by reduced agglomeration, smaller diameter sizes, and lower E_g values. However, a drawback associated with $Cu(NO_3)_2 \cdot 3H_2O$ is its requirement for higher calcination temperatures relative to $Cu(OOCCH_3)_2 \cdot H_2O$ to effectively eliminate phytochemicals and mitigate observed agglomeration, as indicated by EDX analysis (**Table 12**) and FE-SEM imaging (**Figure 13**).

4.3.3 Effect of calcination temperature on OPE-mediated CuO NPs

The calcination temperature represents a critical parameter in the green synthesis process, exerting significant influence over the structural, morphological, and optical properties of CuO NPs. Moreover, it serves as the pivotal stage where phytochemicals are decomposed to eliminate them from the final product.

The impact of a 50 °C increment in calcination temperature (450 °C and 500 °C) on the synthesis of OPE-mediated CuO NPs was investigated. Notably, at 500 °C, enhanced removal efficiency was observed, consistent with findings reported by Chan *et al*. (2022), Doan Thi *et al*. (2020), and Baharudin *et al*. (2018). This is underscored by a discernible trend of decreased atomic percentage of carbon in the EDX analysis summarized in **Table 12**, particularly pronounced when MOPE was employed. At 500 °C, the absence of carbon presence in MOPE indicates complete removal of phytochemicals.

Traditionally, higher calcination temperatures are anticipated to yield larger CuO NPs, as elucidated in previous studies concerning ZnO NPs and CuO NPs (Section **2.3**). This phenomenon is attributed to an increase in crystalline size, facilitated by the reduction in defects within the grain boundary. However, in this project, it is noteworthy that the 50 °C increment in calcination temperature did not significantly impact the size and morphology of CuO NPs, as compared to the effect observed from the choice of precursor salt as shown in **Table 11**.

4.4 Evaluation of Photocatalytic Activity of Green synthesized CuO NPs

4.4.1 Degradation of RBB Dye in Aqueous Solution Using CuO NPs under UV light

The CuO NPs synthesized using $Cu(NO_3)_2 \cdot 3H_2O$ with OPE prepared through the soaking method and calcinated at 500 °C were selected as the photocatalyst for degrading 15 ppm RBB dye solution, based on its optimal characterization outcomes among all CuO NPs synthesized under varied conditions. The RBB dye exhibited a notable absorbance peak at 537 nm, with absorbance steadily declining over the 240-minute duration, as depicted in Figure 19. This observed reduction in absorbance signifies the successful degradation of the RBB dye facilitated by the CuO NPs photocatalyst. This selection underscores the efficacy of CuO NPs synthesized via the soaking method using $Cu(NO_3)_2 \cdot 3H_2O$ and calcination at 500 °C as a potent photocatalyst for the degradation of RBB dye solution.

Two controls were conducted with the aim to study the dye removal efficiency of synthesized CuO NPs. One blank being only 15 ppm RBB dye solution exposed under UV light with constant stirring to examine if RBB dye would degrade in presence of UV light. The other being 40 mg of CuO NPs in 15 ppm RBB dye solution stirred in dark condition to examine if the CuO NPs still exhibited dye removal properties without light source. The colour of dye molecules are contributed by its chromophore which are often complex in structure and hard to degrade. The pink reddish colour observed

in RBB is contributed by the anthracene chromophore shown in **Figure 21** below.

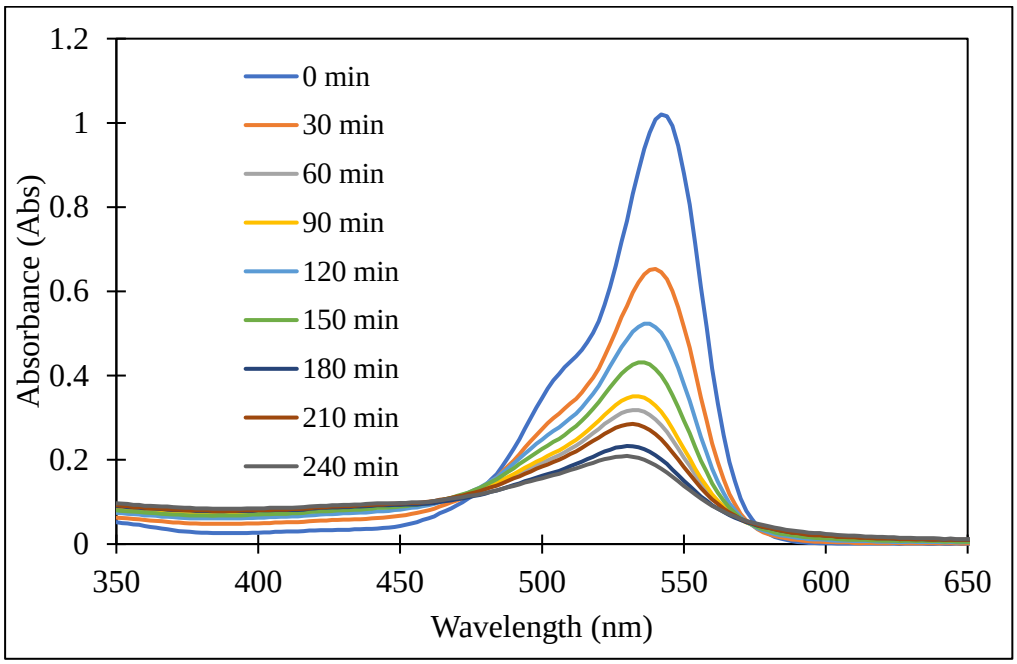

Figure 19: Photodegradation of RBB dye by 18- Watt UV light using OPE-mediated CuO NPs as photocatalyst

Figure 20: Colour change of RBB dye solution over 240 minutes under UV lamp

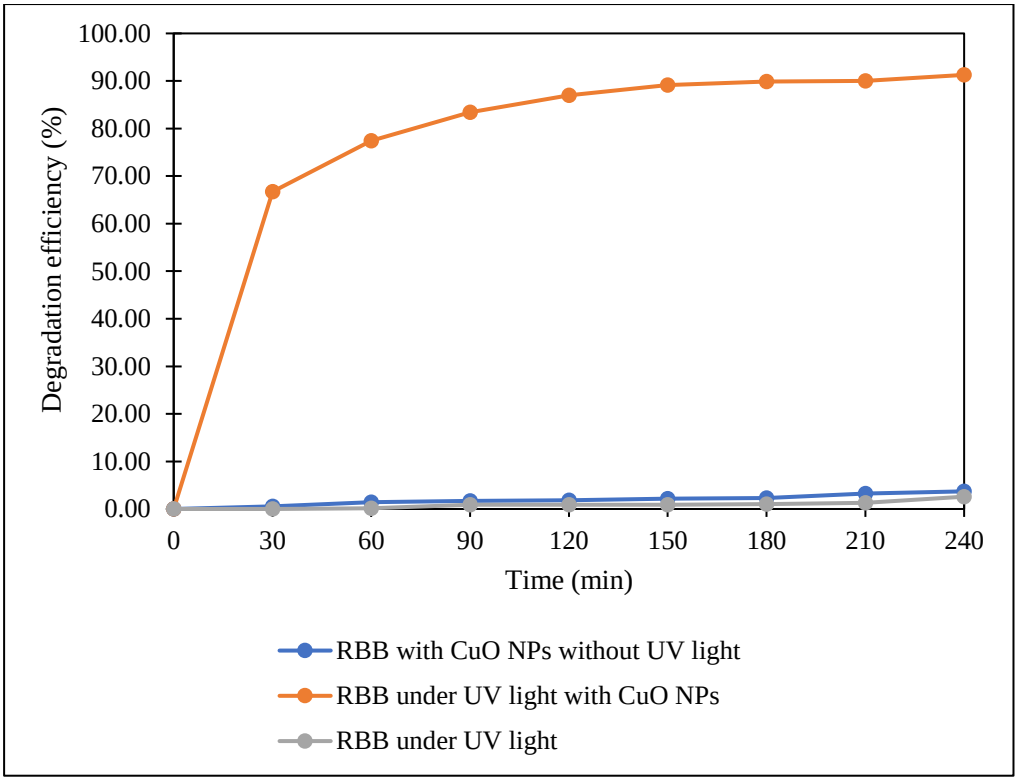

Figure 20: Comparison of percentage degradation efficiency of RBB dye under different conditions

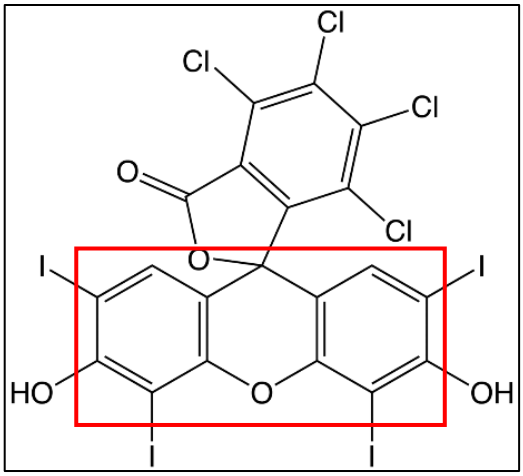

Figure 21: Structure of RBB dye molecule and its chromophore outlined in red

In **Figure 20**, it was observed that the degradation efficiency of RBB in the presence of CuO NPs under UV light was exceptionally high, reaching 91.29%. However, when CuO NPs were removed, the degradation efficiency of RBB drastically decreased to only 2.59% after 240 minutes of exposure under UV light, indicating the crucial role of CuO NPs in the degradation process. Furthermore, in the absence of UV light, with CuO NPs present, the degradation efficiency remained relatively low at 3.71%, highlighting the significance of UV light in enhancing the photocatalytic activity of CuO NPs for RBB degradation as a form green energy source. The 3.71 % removal is due to the adsorption of RBB molecule on the surface of CuO NPs after stirring for 240 minutes.

4.4.2 Proposed mechanism of photocatalytic degradation of CuO NPs

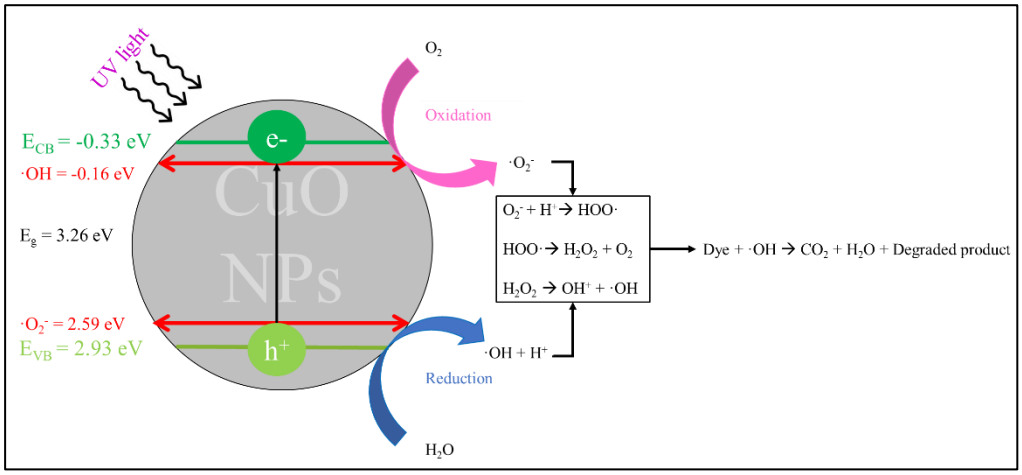

Figure 21: Proposed mechanism of the degradation of RBB dye using CuO NPs under UV lamp irradiation

The photocatalytic RBB degradation in presence of OPE- mediated CuO NPs was studied under 18- Watt UV light for 240 minutes. The photocatalytic mechanism mainly relies on the generation of free radical using O_2 and H_2O (Tammina *et al.*, 2018). The position of E_{CB} and E_{VB} was calculated utilizing the Mulliken electronegative theory shown below (Nguyen *et al.*, 2023),

$$E_{CB} = \chi - E_e - 0.5E_g = -0.33 \text{ eV}$$

$$E_{VB} = \chi - E_e + 0.5E_g = 2.93 \text{ eV}$$

Where χ = Absolute electronegativity of CuO NPs

= 5.8 eV

E_e= Free electron energy

= 4.5 eV

E_g = Energy bandagp of CuO NPs

= 3.26 eV

The redox potential of ·OH and $\cdot O_2^-$ is 2.59 eV and -0.16 eV respectively in normal hydrogen electrode (NHE) condition which is the similar condition conducted in the project (Mrabet *et al*., 2023).Based on the calculation shown above, the CuO NPs synthesized exceeded the redox potential enable the reduction and oxidation of H_2O and O_2 to kick start the photocatalytic mechanism.

Upon exposure to UV light, SPR induces the excitation of electrons (*e*-) from the VB to the CB, resulting in the generation of positively charged holes (h^+) in the VB (Karuppannan *et al.*, 2021). This initial excitation sets off a series of redox reactions. Each mole of water (H_2O) at the VB undergoes reduction to yield one mole of H^+ and one mole of ·OH, while each mole of oxygen (O_2) at the CB undergoes oxidation to produce one mole of $\cdot O_2^-$. These reactions continue, leading to the formation of reactive species such as HOO·, which further reacts with H^+ to form hydrogen peroxide (H_2O_2) and oxygen (O_2). The reduction of H_2O_2 at the CB generates hydroxyl radicals (OH·) and hydroxide anions (OH-). The hydroxide ions subsequently undergo oxidation to generate additional OH· radicals. These highly reactive OH· radicals play a crucial role in oxidizing the RBB dye molecules, predominantly targeting the anthracene chromophore. This oxidative process leads to the breakdown of the dye molecules into benign byproducts, including carbon dioxide (CO_2), water (H_2O), and residual fragments (Tammina, Mandal and Kadiyala, 2018).

Chapter 5

CONCLUSION

CuO NPs were synthesized successfully using *Citrus sinensis* peel extract acting natural source of reducing and stabilizing agent prepared though three methods (Boiling, Soaking and Maceration), using two different precursor salt (Copper (II) acetate monohydrate and Copper (II) nitrate trihydrate) and calcinated at two different calcination temperature (450 ˚and 500 ˚C). The CuO NPs synthesized under different conditions were characterized with UV-Vis, EDX, SEM and FTIR. The optimum CuO NPs for each precursor salt used determined and chosen for XRD analysis. The most optimum condition for CuO NPs using OPE was using copper (II) nitrate trihydrate, with OPE prepared through soaking method and calcinated at 500 ˚C.

The XRD analysis of CuO NPs synthesized through the most optimum condition showed the formation of monoclinic crystalline phase structure with average crystalline size of 20.16 nm when calculated using Debye-Scherrer's equation. Under FE-SEM imaging, the CuO NPs appeared agglomerated with spherical shape and the average particle size was calculated at 53.55 nm. Based on the UV-Vis spectrum of CuO NPs, the maximum absorbance peak was located at 382 nm with a energy bandgap of 3.26 eV. The RBB degradation efficiency of CuO NPs synthesized in optimized condition was conducted for 240 minutes under UV light and obtained an efficiency of 91.29 % when added to 15 ppm RBB dye. The high degradation efficiency proven that synthesized CuO NPs works as an efficient photocatalyst.

The degradation mechanism of RBB dye in the presence of CuO NPs could be studied in depth through the use of LC-MS to understand the degradation mechanism of RBB dye. The effects of calcination temperature on structure, morphology and crystallinity on CuO NPs can be conducted using larger increments of calcination temperature as well as different time intervals to further study and determine for optimizations that can be conducted to fine tune synthesized CuO NPs.

Chapter 6

FURTHER STUDIES

i) The degradation mechanism of Rose Bengal B dye in the presence of CuO NPs will be studied with liquid chromatography-mass spectrometry (LCMS)

ii) The effect of calcination temperature on morphology, energy bandgap, and crystallinity on CuO NPs will be studied using various calcination duration

Reference

Akintelu, S.A., Oyebamiji, A.K., Olugbeko, S.C. and Latona, D.F. (2021) 'Green chemistry approach towards the synthesis of copper nanoparticles and its potential applications as therapeutic agents and environmental control', Current Research in Green and Sustainable Chemistry. Elsevier B.V. Available at: https://doi.org/10.1016/j.crgsc.2021.100176.

Al-Tohamy, R., Ali, S.S., Li, F., Okasha, K.M., Mahmoud, Y.A.G., Elsamahy, T., Jiao, H., Fu, Y. and Sun, J. (2022) 'A critical review on the treatment of dye-containing wastewater: Ecotoxicological and health concerns of textile dyes and possible remediation approaches for environmental safety', Ecotoxicology and Environmental Safety. Academic Press. Available at: https://doi.org/10.1016/j.ecoenv.2021.113160.

Álvarez-Chimal, R. and Arenas-Alatorre, J.Á. (2023) 'Green Synthesis of Nanoparticles: A Biological Approach', Green Chemistry For Enviromental Sustainability- Prevention-Assurance-Sustainability(P-A-S) Approach [Preprint]. Available at: https://doi.org/http://dx.doi.org/10.5772/intechopen.1002203.

Amanulla, A.M. and Sundaram, R. (2019) Green synthesis of TiO2 nanoparticles using orange peel extract for antibacterial, cytotoxicity and humidity sensor applications. Available at: www.sciencedirect.com.

Aminuzzaman, M., Kei, L.M. and Liang, W.H. (2017) 'Green synthesis of copper oxide (CuO) nanoparticles using banana peel extract and their photocatalytic activities', in AIP Conference Proceedings. American Institute of Physics Inc. Available at: https://doi.org/10.1063/1.4979387.

Aminuzzaman, M., Ying, L.P., Goh, W.S. and Watanabe, A. (2018) 'Green synthesis of zinc oxide nanoparticles using aqueous extract of Garcinia mangostana fruit pericarp and their photocatalytic activity', Bulletin of Materials Science, 41(2). Available at: https://doi.org/10.1007/s12034-018-1568-4.

Anastas, P.T. and Warner, J.C. (1998) Green Chemistry: Theory and Practice , American Chemical Society. Available at: https://www.acs.org/greenchemistry/principles/12-principles-of-green-chemistry.html (Accessed: 26 February 2024).

Ayele, A., Getachew, D., Kamaraj, M. and Suresh, A. (2021). Phycoremediation of Synthetic Dyes: An Effective and Eco-Friendly Algal Technology for the Dye Abatement. Journal of Chemistry, [online] 2021, pp.1–14. doi:https://doi.org/10.1155/2021/9923643.

Baharudin, K.B., Abdullah, N. and Derawi, D. (2018) 'Effect of calcination temperature on the physicochemical properties of zinc oxide nanoparticles synthesized by coprecipitation', Material Research Express [Preprint]. Available at: https://doi.org/10.1088/2053.

Chan, Y. Bin, Selvanathan, V., Tey, L.H., Akhtaruzzaman, M., Anur, F.H., Djearamane, S., Watanabe, A. and Aminuzzaman, M. (2022) 'Effect of Calcination Temperature on Structural, Morphological and Optical Properties of Copper Oxide Nanostructures Derived from Garcinia mangostana L. Leaf Extract', Nanomaterials, 12(20). Available at: https://doi.org/10.3390/nano12203589.

Chatterjee, B. (2020) "'Textile finishing dye turns Ulhas River water turquoise,'" The Hindustan Times, 13 June. Available at: https://www.hindustantimes.com/mumbai-news/textile-finishing-dye-turns-ulhas-river-water-turquoise/story-vPDfGlKIAQGNS0g5yRAHUO.html (Accessed: July 28, 2023).

Czech, A., Zarycka, E., Yanovych, D., Zasadna, Z., Grzegorczyk, I. and Kłys, S. (2020) 'Mineral Content of the Pulp and Peel of Various Citrus Fruit Cultivars', Biological Trace Element Research, 193(2), pp. 555–563. Available at: https://doi.org/10.1007/s12011-019-01727-1.

Doan Thi, T.U., Nguyen, T.T., Thi, Y.D., Ta Thi, K.H., Phan, B.T. and Pham, K.N. (2020) 'Green synthesis of ZnO nanoparticles using orange fruit peel extract for antibacterial activities', RSC Advances, 10(40), pp. 23899–23907. Available at: https://doi.org/10.1039/d0ra04926c.

Ghidan, A.Y., Al-Antary, T.M. and Awwad, A.M. (2016) 'Green synthesis of copper oxide nanoparticles using Punica granatum peels extract: Effect on green peach Aphid', Environmental Nanotechnology, Monitoring and Management, 6, pp. 95–98. Available at: https://doi.org/10.1016/j.enmm.2016.08.002.

Jabeen, S., Qureshi, R., Munazir, M., Maqsood, M., Munir, M., Shah, S.S.H. and Rahim, B.Z. (2021) 'Application of green synthesized silver nanoparticles in cancer treatment - A critical review', Materials Research Express. IOP Publishing Ltd. Available at: https://doi.org/10.1088/2053-1591/ac1de3.

Jana, J., Ganguly, M. and Pal, T. (2016) 'Enlightening surface plasmon resonance effect of metal nanoparticles for practical spectroscopic application', RSC Advances. Royal Society of Chemistry, pp. 86174–86211. Available at: https://doi.org/10.1039/c6ra14173k.

Jayaprakash, N., Suresh, R., Rajalakshmi, S., Sundaravadivel, E. and Raja, S. (2020) 'One-step synthesis of CuO nanoparticles and their effects on H9c2 cardiomyoblasts cells', Inorganic and Nano-Metal Chemistry,

50(8), pp. 644–653. Available at: https://doi.org/10.1080/24701556.2020.1723628.

Jin, W., Liu, Y., Yu, J., Guo, X. and Mao, D. (2023) 'Effect of copper precursors on CO oxidation catalyzed by CuO-CeO2 prepared by solvothermal method', Journal of Rare Earths, 41(12), pp. 1953–1962. Available at: https://doi.org/10.1016/j.jre.2022.10.005.

Karuppannan, S.K., Ramalingam, R., Mohamed Khalith, S.B., Dowlath, M.J.H., Darul Raiyaan, G.I. and Arunachalam, K.D. (2021) 'Characterization, antibacterial and photocatalytic evaluation of green synthesized copper oxide nanoparticles', Biocatalysis and Agricultural Biotechnology, 31. Available at: https://doi.org/10.1016/j.bcab.2020.101904.

Kubala, J. and Arnarson, A. (2023) Oranges 101: Health Benefits and nutrition facts, Healthline. Available at: https://www.healthline.com/nutrition/oranges#beneficial-plant-compounds (Accessed: 30 March 2024).

Lellis, B., Fávaro-Polonio, C.Z., Pamphile, J.A. and Polonio, J.C., 2019. Effects of textile dyes on health and the environment and bioremediation potential of living organisms. Biotechnology Research and Innovation, 3(2), pp.275–290.

Liew, S.S., Ho, W.Y., Yeap, S.K. and Bin Sharifudin, S.A. (2018) 'Phytochemical composition and in vitro antioxidant activities of Citrus sinensis peel extracts', PeerJ, 2018(8). Available at: https://doi.org/10.7717/peerj.5331.

Lin, L., Yang, H. and Xu, X., 2022. Effects of Water Pollution on Human Health and Disease Heterogeneity: A Review. Frontiers in Environmental Science, 10.

Liu, Q., 2020. Pollution and Treatment of Dye Waste-Water. IOP Conference Series: Earth and Environmental Science. 2 July 2020 IOP Publishing Ltd.

Makarov, V. V, Love, A.J., Sinitsyna, O. V, Makarova, S.S., Yaminsky, I. V, Taliansky, M.E. and Kalinina, N.O. (2014) 'Green' Nanotechnologies: Synthesis of Metal Nanoparticles Using Plants.

Manthey, J.A. and Grohmann, K., 1996. Concentrations of Hesperidin and Other Orange Peel Flavonoids in Citrus Processing Byproducts. Journal of Agricultural ad Food Chemistry , pp.811–814. Available at: https://pubs.acs.org/sharingguidelines.

Marslin, G., Siram, K., Maqbool, Q., Selvakesavan, R.K., Kruszka, D., Kachlicki, P. and Franklin, G. (2018) 'Secondary metabolites in the

green synthesis of metallic nanoparticles', Materials. MDPI AG. Available at: https://doi.org/10.3390/ma11060940.

Meghwal, K., Kumawat, S., Ameta, C. and Jangid, N.K., 2019. Effect of dyes on water chemistry, soil quality, and biological properties of water. In: Impact of Textile Dyes on Public Health and the Environment. IGI Global, pp. 90–114.

Miera, B.S. de, Cañadas, R., González-Miquel, M. and González, E.J., 2023. Recovery of Phenolic Compounds from Orange Peel Waste by Conventional and Assisted Extraction Techniques Using Sustainable Solvents. Frontiers in Bioscience - Elite, 15(4).

Mrabet, C., Jaballah, R., Mahdhi, N., Boukhachem, A. and Amlouk, M. (2023) 'CuO-ZnO nanocomposites-based thin films: Characterization, physical properties and sunlight photocatalytic degradation of organic pollutants', Journal of Alloys and Compounds, 968. Available at: https://doi.org/10.1016/j.jallcom.2023.172252.

Munjal, S., Singh, A. and Kumar, Vipin. (2017) 'Synthesis and Characterization of MgO Nanoparticles by Orange Fruit Waste through Green Method', International Journal of Advanced Research in Chemical Science, 4(9), pp. 36–42. Available at: https://doi.org/10.20431/2349-0403.0409005.

Nguyen, Thuy Thi Thanh, Nguyen, Y.N.N., Tran, X.T., Nguyen, Tam Thi Thanh and Tran, T. Van (2023) 'Green synthesis of CuO, ZnO and CuO/ZnO nanoparticles using Annona glabra leaf extract for antioxidant, antibacterial and photocatalytic activities', Journal of Environmental Chemical Engineering, 11(5). Available at: https://doi.org/10.1016/j.jece.2023.111003.

Noh, M. F. (2020) "Once polluted Sungai Kim Kim now rehabilitated; water clean and clear," New Straits Times . Available at: https://www.nst.com.my/news/nation/2020/10/635765/once-polluted-sungai-kim-kim-now-rehabilitated-water-clean-and-clear (Accessed: August 2, 2023).

Nordin, N., Hamzah, Z., Hashim, O., Hafiz Kasim, F. and Abdullah, R. (2015) EFFECT OF TEMPERATURE IN CALCINATION PROCESS OF SEASHELLS (Kesan Suhu Dalam Proses Pengkalsinan Kulit Kerang), Malaysian Journal of Analytical Sciences.

Phang, Y.K., Aminuzzaman, M., Akhtaruzzaman, M., Muhammad, G., Ogawa, S., Watanabe, A. and Tey, L.H. (2021) 'Green synthesis and characterization of CuO nanoparticles derived from papaya peel extract for the photocatalytic degradation of palm oil mill effluent (POME)', Sustainability (Switzerland), 13(2), pp. 1–15. Available at: https://doi.org/10.3390/su13020796.

Phiwdang, K., Suphankij, S., Mekprasart, W. and Pecharapa, W., 2013. Synthesis of CuO nanoparticles by precipitation method using different precursors. Energy Procedia, 34, pp.740–745.

Rasul, M.G. (2018) Conventional Extraction Methods Use in Medicinal Plants, their Advantages and Disadvantages, International Journal of Basic Sciences and Applied Computing.

Royal Society of Chemistry (2024) Copper - element information, properties and uses: Periodic Table, Copper - Element information, properties and uses | Periodic Table. Available at: https://www.rsc.org/periodic-table/element/29/coppLin, L., Yang, H. and Xu, X., 2022. Effects of Water Pollution on Human Health and Disease Heterogeneity: A Review. Frontiers in Environmental Science, 10.

Sami, S.A. and Abdulkarim, N.A. (2021) 'Energy gaps of Si nanoparticles using size-dependent Debye-Waller factors', Materials Research Bulletin, 142. Available at: https://doi.org/10.1016/j.materresbull.2021.111428.

Sankar, R., Manikandan, P., Malarvizhi, V., Fathima, T., Shivashangari, K.S. and Ravikumar, V. (2014) 'Green synthesis of colloidal copper oxide nanoparticles using Carica papaya and its application in photocatalytic dye degradation', Spectrochimica Acta - Part A: Molecular and Biomolecular Spectroscopy, 121, pp. 746–750. Available at: https://doi.org/10.1016/j.saa.2013.12.020.

Singh, J., Dutta, T., Kim, K.H., Rawat, M., Samddar, P. and Kumar, P. (2018) '"Green" synthesis of metals and their oxide nanoparticles: Applications for environmental remediation', Journal of Nanobiotechnology. BioMed Central Ltd. Available at: https://doi.org/10.1186/s12951-018-0408-4.

Skiba, M.I. and Vorobyova, V.I. (2019) 'Synthesis of Silver Nanoparticles Using Orange Peel Extract Prepared by Plasmochemical Extraction Method and Degradation of Methylene Blue under Solar Irradiation', Advances in Materials Science and Engineering, 2019. Available at: https://doi.org/10.1155/2019/8306015.

Sudarshan, S., Harikrishnan, S., RathiBhuvaneswari, G., Alamelu, V., Aanand, S., Rajasekar, A. and Govarthanan, M. (2023) 'Impact of textile dyes on human health and bioremediation of textile industry effluent using microorganisms: current status and future prospects', Journal of applied microbiology. NLM (Medline). Available at: https://doi.org/10.1093/jambio/lxac064.

Sultan Irshad, M., Hamamd Aziz, M., Fatima, M., Rehman, S.U., Idrees, M., Rana, S., Shaheen, F., Ahmed, A., Javed, M.Q. and Huang, Q. (2019) 'Green Synthesis, Cytotoxicity, Antioxidant and Photocatalytic

Activity of CeO2 Nanoparticles Mediated via Orange Peel Extract (OPE)'. Available at: https://doi.org/10.1088/2053.

Tammina, S.K., Mandal, B.K. and Kadiyala, N.K. (2018) 'Photocatalytic degradation of methylene blue dye by nonconventional synthesized SnO2 nanoparticles', Environmental Nanotechnology, Monitoring and Management, 10, pp. 339–350. Available at: https://doi.org/10.1016/j.enmm.2018.07.006.

Tshireletso, P., Ateba, C.N. and Fayemi, O.E. (2021) 'Spectroscopic and antibacterial properties of CuONPs from orange, lemon and tangerine peel extracts: Potential for combating bacterial resistance', Molecules, 26(3). Available at: https://doi.org/10.3390/molecules26030586.

Wang, J., Pu, H., Wan, G., Chen, K., Lu, J., Lei, Y., Zhong, L., He, S., Han, C. and Luo, Y. (2017) 'Promoted the reduction of Cu2+ to enhance CuO–CeO2 catalysts for CO preferential oxidation in H2-rich streams: Effects of preparation methods and copper precursors', International Journal of Hydrogen Energy, 42(34), pp. 21955–21968. Available at: https://doi.org/10.1016/j.ijhydene.2017.07.122.

Ying, S., Guan, Z., Ofoegbu, P.C., Clubb, P., Rico, C., He, F. and Hong, J. (2022) 'Green synthesis of nanoparticles: Current developments and limitations', Environmental Technology and Innovation. Elsevier B.V. Available at: https://doi.org/10.1016/j.eti.2022.102336.

Zhou, M. (2023) From Orange Waste to a green future, MNEXT. Available at: https://www.mnext.nl/en/projecten/from-orange-waste-to-a-green-future/#:~:text=Around%2040%25%20of%20the%20fruit,and%20pulp%20of%20the%20oranges. (Accessed: 21 March 2024).

APPENDIX

APPENDIX A

Calculation of crystalline size by using Debye Scherrer equation

For CuO NPs synthesized using

Calculation of β

$$\beta = \frac{FWHMM\ in\ 2\theta \text{ x } \pi}{180°}$$

$$\beta = \frac{0.483 \text{ x } \pi}{180°}$$

β = 0.00843

Calculation of crystalline size using Debye Scherrer equation

$$D = \frac{k\lambda}{\beta \cos \theta}$$

$$D = \frac{0.9 \text{ x } (1.54 \text{ x } 10^{-10}\ m)}{0.00768 \cos 35.5923°}$$

D = 20.16 nm

For CuO NPs synthesized using

Calculation of β

$$\beta = \frac{FWHMM\ in\ 2\theta \text{ x } \pi}{180°}$$

$$\beta = \frac{0.483 \text{ x } \pi}{180°}$$

β = 0.00768

Calculation of crystalline size using Debye Scherrer equation

$$D = \frac{k\lambda}{\beta \cos\theta}$$

$$D = \frac{0.9 \text{ x } (1.54 \text{ x } 10^{-10}\ m)}{0.00768 \cos 33.1615°}$$

D = 19.64 nm

Appendix B

*** Basic Data Process ***

Group : Standard
Data : CYM_W

Strongest 3 peaks

no.	peak no.	2Theta (deg)	d (A)	I/I1	FWHM (deg)	Intensity (Counts)	Integrated Int (Counts)
1	6	35.5248	2.52499	100	0.47360	6840	169191
2	7	38.7524	2.32179	88	0.59160	6015	203827
3	5	34.9200	2.56733	25	0.62620	1718	64052

Peak Data List

peak no.	2Theta (deg)	d (A)	I/I1	FWHM (deg)	Intensity (Counts)	Integrated Int (Counts)
1	13.9948	6.32304	4	0.56740	279	12515
2	29.3239	3.04327	3	0.39870	205	5010
3	32.0265	2.79236	21	0.49260	1467	31206
4	32.4400	2.75771	11	0.53240	723	19157
5	34.9200	2.56733	25	0.62620	1718	64052
6	35.5248	2.52499	100	0.47360	6840	169191
7	38.7524	2.32179	88	0.59160	6015	203827
8	39.6000	2.27403	4	0.35580	285	14374
9	43.8740	2.06190	6	0.55600	391	15084
10	48.8429	1.86312	22	0.54270	1504	44551
11	49.3800	1.84411	5	0.32660	316	9329
12	53.4404	1.71317	5	0.64670	372	19964
13	58.3235	1.58083	10	0.71290	687	26005
14	59.1600	1.56045	4	0.58400	247	8670
15	60.7400	1.52359	4	0.66000	273	10598
16	61.5877	1.50464	15	0.54940	1053	32472
17	65.1200	1.43130	3	0.44000	229	7697
18	65.9200	1.41585	10	0.98000	690	21618
19	66.3200	1.40828	14	0.80260	990	31665
20	67.9929	1.37765	14	0.73540	948	41404
21	72.4414	1.30361	5	0.63710	344	16271
22	75.1075	1.26381	8	0.70200	533	24490

Figure 1: Information of XRD analysis of green synthesized CuO NPs in Figure 12 (a) (Part I)

Appendix B

*** Basic Data Process ***

Group : Standard
Data : CYM_450

Strongest 3 peaks

no.	peak no.	2Theta (deg)	d (A)	I/I1	FWHM (deg)	Intensity (Counts)	Integrated Int (Counts)
1	6	35.6366	2.51733	100	0.34650	9590	180138
2	8	38.8558	2.31585	88	0.44060	8413	224597
3	10	48.9321	1.85994	23	0.39800	2202	55443

Peak Data List

peak no.	2Theta (deg)	d (A)	I/I1	FWHM (deg)	Intensity (Counts)	Integrated Int (Counts)
1	14.0762	6.28666	8	0.55400	742	28648
2	15.2560	5.80304	3	0.57000	302	12783
3	32.0988	2.78624	22	0.32710	2082	35962
4	32.6200	2.74290	10	0.34460	927	19738
5	34.9600	2.56448	22	0.39540	2122	54466
6	35.6366	2.51733	100	0.34650	9590	180138
7	36.5234	2.45821	6	0.34220	593	16023
8	38.8558	2.31585	88	0.44060	8413	224597
9	43.9452	2.05873	6	0.32470	558	12444
10	48.9321	1.85994	23	0.39800	2202	55443
11	53.5727	1.70925	6	0.47450	532	17139
12	55.1648	1.66363	4	0.29080	418	7494
13	58.3858	1.57929	10	0.51160	972	29488
14	58.8800	1.56721	3	0.00000	313	0
15	59.3000	1.55710	4	0.35260	341	9059
16	60.8200	1.52178	4	0.45720	349	11225
17	61.6772	1.50267	18	0.38680	1691	39168
18	65.8200	1.41776	7	0.51480	678	24925
19	66.4200	1.40640	14	0.47280	1309	36402
20	68.1325	1.37516	13	0.55310	1265	41243
21	72.5188	1.30241	5	0.46770	449	15179
22	75.2110	1.26233	6	0.62440	617	23663

Figure 2: Information of XRD analysis of green synthesized CuO NPs in Figure 12 (b) (Part I)

Appendix C

```
          ***  Basic Data Process  ***

# Data Infomation
          Group                : Standard
          Data                 : CYM_W
          Sample Nmae          : W
          Comment              :
          Date & Time          : 03-21-24 12:17:16

# Measurement Condition
    X-ray tube
          target               : Cu
          voltage              : 40.0 (kV)
          current              : 30.0 (mA)
    Slits
          Auto Slit            : not Used
          divergence slit      :   1.00000 (deg)
          scatter slit         :   1.00000 (deg)
          receiving slit       :   0.30000(mm)
    Scanning
          drive axis           : Theta-2Theta
          scan range           :   10.0000 - 80.0000 (deg)
          scan mode            : Continuous Scan
          scan speed           :    2.0000 (deg/min)
          sampling pitch       :    0.0200 (deg)
          preset time          :    0.60 (sec)

# Data Process Condition
    Smoothing                  [ AUTO ]
          smoothing points     : 25
    B.G.Subtruction            [ AUTO ]
          sampling points      : 27
          repeat times         : 30
    Ka1-a2 Separate            [ MANUAL ]
          Ka1 a2 ratio         : 50 (%)
    Peak Search                [ AUTO ]
          differential points  : 25
          FWHM threhold        : 0.050 (deg)
          intensity threhold   : 30 (par mil)
          FWHM ratio  (n-1)/n  : 2
    System error Correction    [ NO ]
    Precise peak Correction    [ NO ]
```

Figure 3: Information of XRD analysis of green synthesized CuO NPs in Figure 12 (a) (Part II)

Appendix C

```
          ***  Basic Data Process  ***

# Data Infomation
          Group                : Standard
          Data                 : CYM_450
          Sample Nmae          : 450
          Comment              :
          Date & Time          : 03-21-24 14:09:49

# Measurement Condition
    X-ray tube
          target               : Cu
          voltage              : 40.0 (kV)
          current              : 30.0 (mA)
    Slits
          Auto Slit            : not Used
          divergence slit      :   1.00000 (deg)
          scatter slit         :   1.00000 (deg)
          receiving slit       :   0.30000(mm)
    Scanning
          drive axis           : Theta-2Theta
          scan range           :   10.0000 - 80.0000 (deg)
          scan mode            : Continuous Scan
          scan speed           :    2.0000 (deg/min)
          sampling pitch       :    0.0200 (deg)
          preset time          :    0.60 (sec)

# Data Process Condition
    Smoothing                  [ AUTO ]
          smoothing points     : 19
    B.G.Subtruction            [ AUTO ]
          sampling points      : 21
          repeat times         : 30
    Ka1-a2 Separate            [ MANUAL ]
          Ka1 a2 ratio         : 50 (%)
    Peak Search                [ AUTO ]
          differential points  : 19
          FWHM threhold        : 0.050 (deg)
          intensity threhold   : 30 (par mil)
          FWHM ratio  (n-1)/n  : 2
    System error Correction    [ NO ]
    Precise peak Correction    [ NO ]
```

Figure 4: Information of XRD analysis of green synthesized CuO NPs in Figure 12 (b) (Part II)

Appendix D

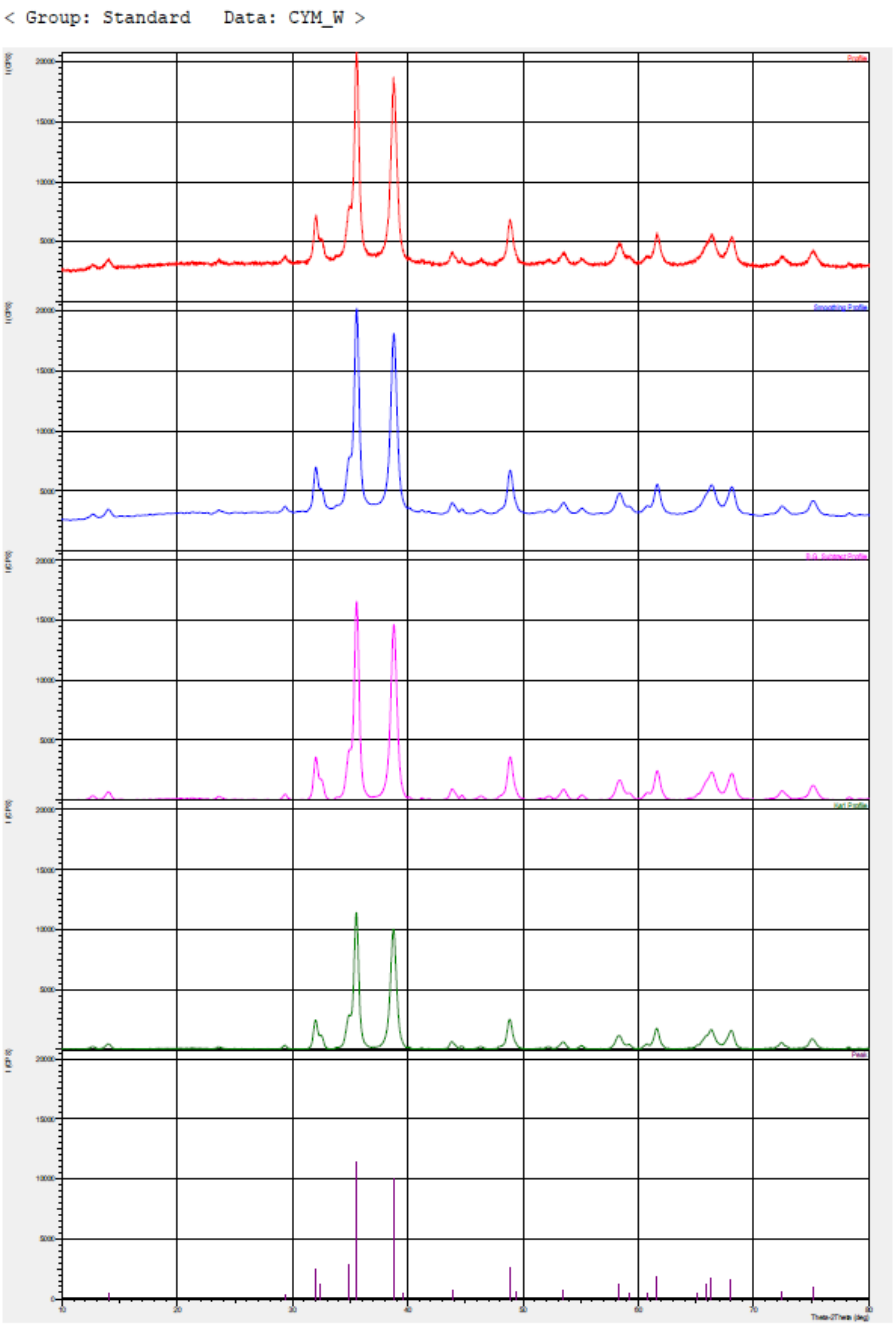

Figure 5: Information of XRD analysis of green synthesized CuO NPs in Figure 12 (a) (Part III)

Appendix D

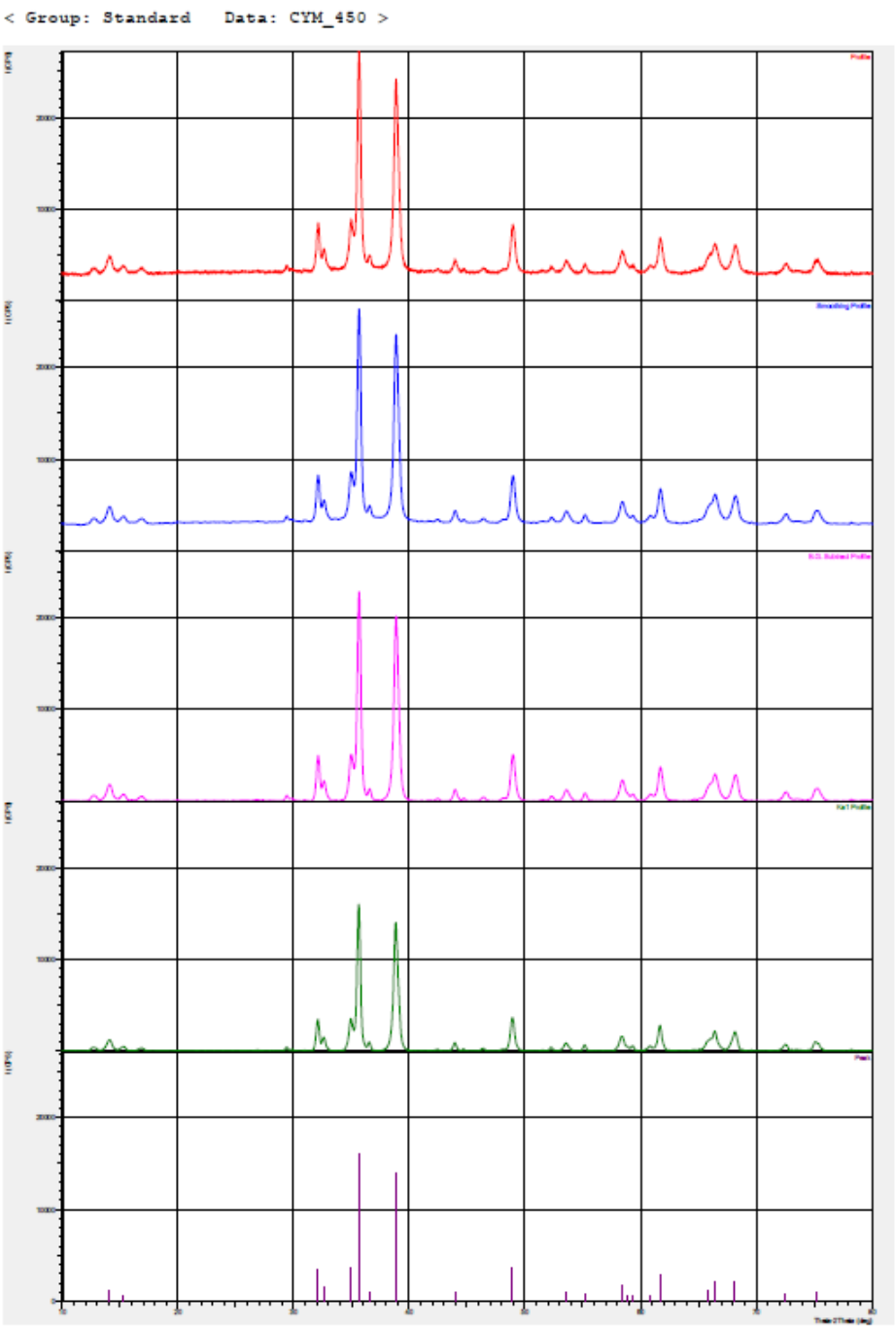

Figure 6: Information of XRD analysis of green synthesized CuO NPs in Figure 12 (b) (Part III)

Appendix E

Match! Phase Analysis Report

Universiti Tunku Abdul Rahman, Faculty of Science

Sample: W ()

Sample Data

File name	CYM_W.RAW
File path	C:/xddat/Standard/CYM_W
Data collected	Mar 21, 2024 12:54:12
Data range	9.980° - 79.980°
Original data range	10.000° - 80.000°
Number of points	3501
Step size	0.020
Rietveld refinement converged	No
Alpha2 subtracted	No
Background subtr.	No
Data smoothed	No
2theta correction	-0.02°
Radiation	X-rays
Wavelength	1.540600 Å

Matched Phases

Index	*Amount (%)*	*Name*	*Formula sum*
A	95.5	Copper Oxide Tenorite, syn	Cu O
	4.5	*Unidentified peak area*	

A: Copper Oxide Tenorite, syn (95.5 %)

Formula sum	Cu O
Entry number	01-089-5896
Figure-of-Merit (FoM)	0.891159
Total number of peaks	71
Peaks in range	71
Peaks matched	15
Intensity scale factor	0.82
Space group	C2/c
Crystal system	monoclinic
Unit cell	a= 4.6830 Å b= 3.4240 Å c= 5.1290 Å β= 99.440 °
I/Ic	3.76
Calc. density	6.513 g/cm³
Reference	Massarotti, V., Capsoni, D., Bini, M., Altomare, A., Moliterni, A.G.G., Z. Kristallogr. **213**, 259 (1998)

Figure 7: XRD match analysis report of green-synthesized CuO NPs with ICDD 00-045-0937 Figure 12 (a) (Part I)

Appendix E

Match! Phase Analysis Report

Universiti Tunku Abdul Rahman, Faculty of Science

Sample: 450 ()

Sample Data	
File name	CYM_450.RAW
File path	C:/xddat/Standard/CYM_450
Data collected	Mar 21, 2024 14:46:45
Data range	9.820° - 79.820°
Original data range	10.000° - 80.000°
Number of points	3501
Step size	0.020
Rietveld refinement converged	No
Alpha2 subtracted	No
Background subtr.	No
Data smoothed	No
2theta correction	-0.18°
Radiation	X-rays
Wavelength	1.540600 Å

Matched Phases

Index	*Amount (%)*	*Name*	*Formula sum*
A	93.1	Copper Oxide Tenorite, syn	Cu O
	6.9	*Unidentified peak area*	

A: Copper Oxide Tenorite, syn (93.1 %)	
Formula sum	Cu O
Entry number	00-045-0937
Figure-of-Merit (FoM)	0.888756
Total number of peaks	38
Peaks in range	18
Peaks matched	14
Intensity scale factor	0.57
Space group	C2/c
Crystal system	monoclinic
Unit cell	a= 4.6853 Å b= 3.4257 Å c= 5.1303 Å β= 99.549 °
I/Ic	2.50
Meas. density	6.450 g/cm³
Calc. density	6.507 g/cm³
Color	Black
Reference	Martin, K., McCarthy, G., North Dakota State Univ., Fargo, ND, USA., ICDD Grant-in-Aid (1991)

Figure 8: XRD match analysis report of green-synthesized CuO NPs with ICDD 00-045-0937 Figure 12 (a) (Part I)

Appendix F

Search-Match

Settings

Reference database used	PDF-2 Release 2016 RDB
Automatic zeropoint adaptation	Yes
Minimum figure-of-merit (FoM)	0.60
2theta window for peak corr.	0.30 deg.
Minimum rel. int. for peak corr.	1
Parameter/influence 2theta	0.50
Parameter/influence intensities	0.50
Parameter multiple/single phase(s)	0.50

Selection Criteria

Elements:

Elements that must be present:	O, Cu
Elements that may be present:	All elements not mentioned above

Peak List

No.	*2theta [°]*	*d [Å]*	*I/I0*	*FWHM*	*Matched*
1	14.05	6.2994	44.24	0.2800	
2	31.90	2.8031	201.71	0.3200	
3	32.51	2.7516	113.91	0.4400	A
4	34.84	2.5730	255.75	0.6000	
5	35.46	2.5295	1000.00	0.4400	A
6	38.68	2.3260	891.76	0.5200	A
7	43.81	2.0646	55.49	0.4000	
8	48.74	1.8668	201.27	0.3600	A
9	53.54	1.7103	53.37	0.2800	A
10	58.14	1.5854	80.35	0.4000	A
11	58.46	1.5775	93.89	0.3200	
12	61.54	1.5057	145.82	0.4800	A
13	65.97	1.4148	91.77	0.8000	A
14	66.34	1.4078	134.56	0.7200	A
15	66.54	1.4042	108.61	0.4000	A
16	68.09	1.3759	125.90	0.5200	A
17	74.94	1.2662	63.24	0.4400	A

Rietveld Refinement using FullProf

Figure 9: XRD match analysis report of green-synthesized CuO NPs with ICDD 00-045-0937 Figure 12 (a) (Part II)

Appendix F

Search-Match

Settings

Reference database used	PDF-2 Release 2016 RDB
Automatic zeropoint adaptation	Yes
Minimum figure-of-merit (FoM)	0.60
2theta window for peak corr.	0.30 deg.
Minimum rel. int. for peak corr.	1
Parameter/influence 2theta	0.50
Parameter/influence intensities	0.50
Parameter multiple/single phase(s)	0.50

Selection Criteria

Elements:

Elements that must be present:	O, Cu
Elements that may be present:	All elements not mentioned above

Peak List

No.	*2theta [°]*	*d [Å]*	*I/I0*	*FWHM*	*Matched*
1	12.49	7.0817	23.51	0.2400	
2	12.67	6.9787	19.96	0.2800	
3	13.89	6.3721	68.96	0.4800	
4	16.62	5.3284	20.00	0.2400	
5	29.24	3.0520	27.16	0.2000	
6	31.88	2.8049	190.39	0.3200	
7	32.45	2.7566	93.54	0.3600	A
8	34.74	2.5802	196.47	0.3600	
9	35.49	2.5271	1000.00	0.3600	A
10	38.68	2.3257	878.31	0.4400	A
11	43.79	2.0658	53.07	0.2400	
12	48.68	1.8690	176.32	0.4000	A
13	52.13	1.7533	22.56	0.2400	
14	54.96	1.6693	34.40	0.2800	
15	58.26	1.5825	96.23	0.5200	A
16	61.53	1.5059	156.40	0.3600	A
17	66.25	1.4097	117.61	0.6400	A
18	67.94	1.3786	102.95	0.4800	A
19	72.44	1.3036	37.22	0.3200	A
20	74.90	1.2668	50.54	0.2800	
21	75.14	1.2633	58.36	0.4000	A

Figure 10: XRD match analysis report of green-synthesized CuO NPs with ICDD 00-045-0937 Figure 12 (a) (Part II)

Appendix G

Degree of crystallinity analysis

Profile area	*Counts*	*Amount*
Total area	7797452	100.00%
Diffraction peaks	1170364	15.01%
Background	6627088	84.99%
Instrumental background	1734077	22.24%
Amorphous phases	4893011	62.75%

Degree of crystallinity (DOC) = 19.30%
Amorphous content (weight %) =80.70%

Integrated Profile Areas

Based on calculated profile

Profile area	*Counts*	*Amount*
Overall diffraction profile	7797452	100.00%
Background radiation	6627088	84.99%
Diffraction peaks	1170364	15.01%
Peak area belonging to selected phases	821309	10.53%
Peak area of phase A (Copper Oxide Tenorite, syn)	*821309*	*10.53%*
Unidentified peak area	349055	4.48%

Peak Residuals

Peak data	*Counts*	*Amount*
Overall peak intensity	21143	100.00%
Peak intensity belonging to selected phases	18112	85.66%
Unidentified peak intensity	3031	14.34%

Figure 11: XRD match analysis report of green-synthesized CuO NPs with ICDD 00-045-0937 Figure 12 (a) (Part III)

Appendix G

Degree of crystallinity analysis

Profile area	*Counts*	*Amount*
Total area	7945252	100.00%
Diffraction peaks	1296024	16.31%
Background	6649228	83.69%
Instrumental background	1734077	21.83%
Amorphous phases	4915150	61.86%

Degree of crystallinity (DOC) = 20.87%
Amorphous content (weight %) =79.13%

Integrated Profile Areas

Based on calculated profile

Profile area	*Counts*	*Amount*
Overall diffraction profile	7945252	100.00%
Background radiation	6649228	83.69%
Diffraction peaks	1296024	16.31%
Peak area belonging to selected phases	751501	9.46%
Peak area of phase A (Copper Oxide Tenorite, syn)	*751501*	*9.46%*
Unidentified peak area	544523	6.85%

Peak Residuals

Peak data	*Counts*	*Amount*
Overall peak intensity	24521	100.00%
Peak intensity belonging to selected phases	20437	83.34%
Unidentified peak intensity	4084	16.66%

Figure 12: XRD match analysis report of green-synthesized CuO NPs with ICDD 00-045-0937 Figure 12 (a) (Part III)

Appendix H

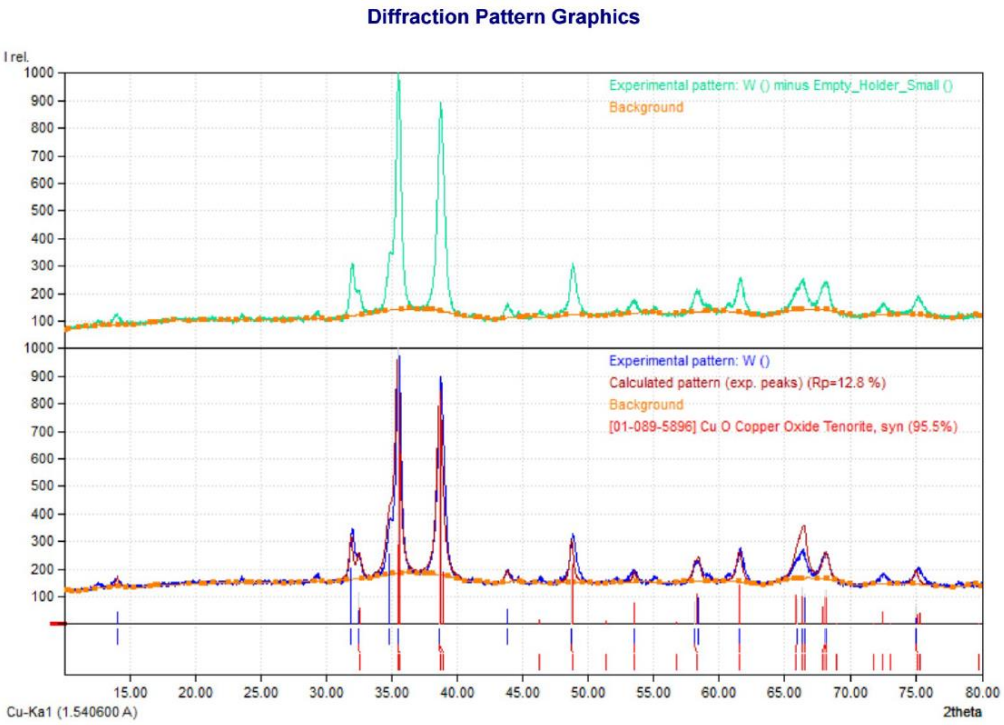

Figure 29: XRD match analysis report of green-synthesized CuO NPs with ICDD 00-045-0937 Figure 12 (a) (Part IV)

Appendix H

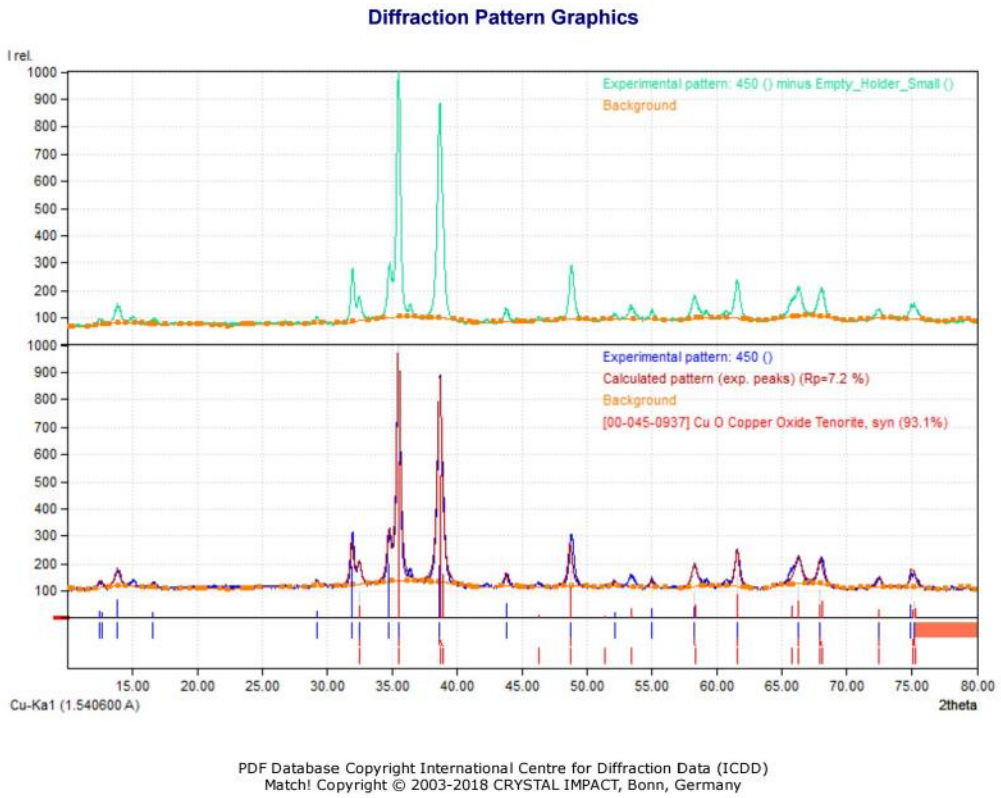

Figure 30: XRD match analysis report of green-synthesized CuO NPs with ICDD 00-045-0937 Figure 12 (a) (Part IV)

Appendix I

Calculation of bandgap energy, *Eg* used in Table 13

$$E_g = \frac{hc}{\lambda}$$

$$E_g = \frac{6.63\ x\ 10^{-84}\ \mathrm{m^2\ kg}\ s^{-1}\ \mathrm{x}\ 2.9989\ \mathrm{x}\ 10^{8}\ \mathrm{m\ s^{-1}}}{\lambda}$$

Appendix J

Calculation of degradation percentage

Percentage of RBB dye degradation = $\frac{(A_0 - A_t)}{A_0}$ x 100%

Table 1: Degradation efficiency percentage of RBB dye solution in 240minutes at 30-minute intervals

Time (min)	Initial Absorbance, A_0	Final Absorbance, A_t	Degradation efficiency (%)
0	0.700	0.700	0.00
30	0.700	0.233	66.71
60	0.700	0.116	77.43
90	0.700	0.158	83.43
120	0.700	0.091	87.00
150	0.700	0.076	89.14
180	0.700	0.071	89.86
210	0.700	0.070	90.00
240	0.700	0.061	91.29